

SELECTING THE NUMBER OF CLUSTERS, CLUSTERING MODELS, AND ALGORITHMS. A UNIFYING APPROACH BASED ON THE QUADRATIC DISCRIMINANT SCORE

Luca Coraggio*

Pietro Coretto†

Abstract

Cluster analysis requires many decisions: the clustering method and the implied reference model, the number of clusters and, often, several hyper-parameters and algorithms' tunings. In practice, one produces several partitions, and a final one is chosen based on validation or selection criteria. There exist an abundance of validation methods that, implicitly or explicitly, assume a certain clustering notion. Moreover, they are often restricted to operate on partitions obtained from a specific method. In this paper, we focus on groups that can be well separated by quadratic or linear boundaries. The reference cluster concept is defined through the quadratic discriminant score function and parameters describing clusters' size, center and scatter. We develop two cluster-quality criteria called quadratic scores. We show that these criteria are consistent with groups generated from a general class of elliptically-symmetric distributions. The quest for this type of groups is common in applications. The connection with likelihood theory for mixture models and model-based clustering is investigated. Based on bootstrap resampling of the quadratic scores, we propose a selection rule that allows choosing among many clustering solutions. The proposed method has the distinctive advantage that it can compare partitions that cannot be compared with other state-of-the-art methods. Extensive numerical experiments and the analysis of real data show that, even if some competing methods turn out to be superior in some setups, the proposed methodology achieves a better overall performance.

Keywords: validation, number of clusters, model-based clustering, mixture models.

*University of Naples "Federico II" (Italy) – E-mail: luca.coraggio@unina.it

†University of Salerno (Italy) – E-mail: pcoretto@unisa.it

1 Introduction

The typical workflow in cluster analysis is to run one or more algorithms with various settings producing several partitions, among which a researcher needs to choose a final one. There may be multiple partitions that describe the data well according to different clusters’ concepts (Von Luxburg et al., 2012). Because of the intrinsic unsupervised nature of the clustering problem, the selection of the desired cluster solution remains a long-standing and open problem (Hennig, 2015). The most significant common issue to all methods and algorithms is choosing an appropriate number of groups, K . However, K is not the only relevant decision: many clustering methods and algorithms also require hyper-parameters that control the complexity level at which the data structure is represented. Different methods with different hyper-parameters may be able to discover similar partitions of a given data set. In Section S1 of the “Supplemental Material File” (SMF), we show an example where we compare 8 partitions of the well-known Iris data set (Anderson, 1936), setting $K = 3$. The 8 partitions correspond to the solutions obtained with clustering methods pursuing somewhat different cluster concepts, all having different hyper-parameters; 4 of these partitions match completely, and 5 of them are close to the ground truth. However, the ground truth is usually not available in practice, and one needs to choose the “best” partition using unlabeled data.

There is a vast catalog of methods proposed to solve the selection problem; for a recent comprehensive overview, see Halkidi et al. (2015). Traditionally, in cluster analysis, the selection of the desired partition has been treated as a validation problem rather than a model selection problem. This is probably because many clustering methods are not derived from stochastic models, although most are built around at least some implicit model assumptions. Recently, Ullmann et al. (2021) attempted to categorize five types of validation approaches. Our proposal contributes to the literature on *internal validation methods*, which are methods using the same data used to fit the clusters. The advantage of internal methods is that they do not

require additional information that is sometimes expensive to find. Typically, new proposals are advertised claiming their universal ability to discover the data’s “true” groups. However, in pure unsupervised contexts, true groups do not exist. Furthermore, it is often overlooked that each method pursues a specific notion of clusters, which implicitly or explicitly assumes the existence of certain structures in the data. As noted in [Akhanli and Hennig \(2020\)](#), one needs to choose the validation approach that is consistent with the primary goal of the analysis. There are *method-dependent* validation methods, specifically designed to evaluate the output of a specific clustering method and *method-independent* methods that can potentially evaluate the output of any clustering methodology. However, even method-independent validation approaches privilege a certain idea of clusters.

In this paper, we take a different approach: we first define a notion of clusters that different clustering methods may retrieve and then propose a method-independent validation criterion to measure the quality of such clusters. Specifically, we look for clusters that can be well separated by quadratic boundaries or linear boundaries as a special case. These clusters are consistent with a class of elliptically-symmetric distributions (ESD), where the within-group dependence structure of the features is mainly driven by correlation. The quest for clusters of this type is rather common in applications ([Fraley and Raftery, 1998](#)).

Related literature. Model-based clustering (MBC) methods, based on ML estimation of finite mixture models of ESDs, are strong candidates for capturing the clusters mentioned above. Assuming that each of the K mixture components generates a group, the selection of the desired clustering solution is translated into a model-selection problem where, in practice, the likelihood fit is contrasted with a penalty accounting for model complexity. The most popular selection strategy is to use information criteria such as the BIC and the AIC ([McLachlan and Peel, 2000](#); [Bouveyron et al., 2019](#)).

Although information-type criteria are based on a solid theoretical background, there are

some issues with their application to cluster selection. [Keribin \(1998\)](#) showed that the BIC is consistent for the number of mixture components under somewhat restrictive assumptions, but practitioners tend to believe that this result is more general, causing some faith in it. The consistency notion of [Keribin \(1998\)](#) is for the recovery of the underlying data distribution and not for clusters. Paradoxically, these consistency results are problematic for cases where the mixture model is not meant to capture the “true” underlying distribution but rather for approximating the density regions formed by the clusters. Finite Gaussian mixtures can approximate a large class of distributions ([Nguyen et al., 2020](#)), implying that consistent criteria like the BIC will include additional components inflating K if, for example, a group that is only approximately normal is better fitted by more than one Gaussian component. The *Integrated Complete-data Likelihood* (ICL) criterion of [Biernacki et al. \(2000\)](#) (see also [Baudry, 2015](#)) modifies the BIC, adapting it to solve the clustering problem. Another model-selection approach, based on likelihood-type criteria derived from mixture models, is the cross-validation method proposed in [Smyth \(2000\)](#). An additional drawback of information-type indexes is that they are method-dependent: they only allow to compare solutions from MBC methods because their calculation is based on likelihood quantities and models’ degrees of freedom. A further issue is that, in some cases, these criteria can not be calculated for MBC methods when the effective degrees of freedom of the underlying model can not be derived (see the case of ML for Gaussian mixtures with the eigen-ratio regularization treated in [Section 4](#)).

Outside the MBC context, there are many method-independent internal validation indexes that mostly measure the within-cluster homogeneity contrasted to a measure of between-clusters heterogeneity. Notable examples are the popular CH index of [Caliński and Harabasz \(1974\)](#) and the Average Silhouette Width criteria (ASW) of [Rousseeuw and Kaufman \(1990\)](#). These are not genuinely *model-free* indexes because they pursue cluster shapes that depend on the underlying dissimilarity notion. These indexes have in common with the BIC-type criteria that they implicitly attempt to contrast the cluster fit vs. the increased complexity caused by the

increase in K .

Another idea from the literature that inspired some aspects of the present contribution is that of *stability selection* (Ben-David et al., 2006). The idea taken from this literature is not the notion of stability, which is about finding similar clusterings on similar data sets (Hennig, 2007; Fang and Wang, 2012), but the idea of exploring variations of the clusterings based on perturbations of the data set obtained by bootstrap resampling of the original data.

Contribution and organization of the paper. We develop a framework where each cluster is represented by a triplet of parameters representing the notions of size, location and scatter. This allows to map clusterings obtained with different methods in a form that is consistent with the notion previously discussed. The method-independent nature of our proposal is a major advantage over competitors from the MBC literature. These clusters' parameters and the quadratic discriminant score function, at the heart the Quadratic Discriminant Analysis (QDA), are used to develop two cluster quality criteria called *quadratic scores*. These criteria are shown to be consistent with clusters generated from a restricted class of ESDs, including the popular Gaussian model (see Sections 2.1). We show connections between the proposed criteria and likelihood-type quantities related to finite mixtures of ESDs and, in particular, Gaussian mixtures (see Section 2.2). In the same spirit of the pioneering work of Akaike (1973) on model-selection, we propose to select a clustering solution produced by a method that achieves the largest expected score across all possible partitions of data sets sampled from the data distribution. The expected score and its confidence interval are approximated via empirical bootstrap in Section 3. Finally, in Section 4, we propose an extensive numerical analysis where the proposed method is compared against some alternatives on both real and artificial data sets. Overall, the proposed methodology shows competitive performances and proves to be able to retrieve interesting clustering solutions even in adverse circumstances. Proofs of the statements, additional examples and details are given in the SMF, available online.

2 Quadratic scoring

We fix some general notation used throughout the rest of the paper. The general clustering problem is to construct a partition $\mathcal{G}_K = \{G_k, k = 1, 2, \dots, K\}$ allocating the objects $\{1, 2, \dots, n\}$ into K groups, where K is generally unknown. Let $\mathbb{X}_n = \{\mathbf{x}_i, i = 1, 2, \dots, n\}$ be an observed sample of p -dimensional feature vectors $\mathbf{x}_i \in \mathbb{R}^p$; \mathbb{X}_n is the observed version of a random sample $\mathcal{X}_n = \{X_i, i = 1, 2, \dots, n\}$, where $X_i \in \mathbb{R}^p$ is the p -dimensional random vector of features representing the i -th unit. In clustering, a typically unsupervised task, we observe the features, but we do not observe the group memberships that we want to discover. Group memberships are introduced through the random vector of 0-1 variables $Z = (Z_1, Z_2, \dots, Z_K)^\top$, where $Z_k = 1$ denotes membership to the k -th group. Define the sequence $\{Z_i, i = 1, 2, \dots, n\}$, where $Z_i = (Z_{i1}, Z_{i2}, \dots, Z_{iK})^\top$ denote the i -th object group membership as follows: $Z_{ik} = \mathbb{I}\{i \in G_k\}$.

2.1 The reference cluster concept

Assume that $X \sim F$, where F is the population distribution function producing K clustered regions of points. We assume that each cluster $k = 1, 2, \dots, K$ is meaningfully described by the triplet of parameters $\boldsymbol{\theta}_k = \{\pi_k, \boldsymbol{\mu}_k, \boldsymbol{\Sigma}_k\}$ formalizing the notions of size, center and scatter. For the k -th cluster, π_k is the expected fraction of points belonging to the k -th group, $\boldsymbol{\mu}_k \in \mathbb{R}^p$ is the vector of centers and $\boldsymbol{\Sigma}_k \in \mathbb{R}^{p \times p}$ is a positive definite scatter matrix that either coincides with or is proportional to the group's covariance matrix. A cluster configuration m of K groups is represented by the parameter vector $\boldsymbol{\theta}^{(m)}$ including all unique elements of the objects $\{(\pi_k^{(m)}, \boldsymbol{\mu}_k^{(m)}, \boldsymbol{\Sigma}_k^{(m)}), k = 1, 2, \dots, K\}$. Since different $\boldsymbol{\theta}^{(m)}$ may refer to cluster configurations with a different number of groups, depending on the context, we will often use the notation $K(\boldsymbol{\theta}^{(m)})$, or $K(m)$, to denote the number of groups described by $\boldsymbol{\theta}^{(m)}$. The superscript (m) is dropped if it is unnecessary to index more than one cluster configuration. $\boldsymbol{\theta}$ is a *parameter*

serving as a general description of the clustered region but, in general, we do not presume that F is necessarily a function of $\boldsymbol{\theta}$. Given a configuration $\boldsymbol{\theta}$, we look for clusters that form a partition of the data space into K disjoint subsets $\mathcal{Q}(\boldsymbol{\theta}) = \{Q_k(\boldsymbol{\theta}), k = 1, 2, \dots, K\}$,

$$Q_k(\boldsymbol{\theta}) := \left\{ \mathbf{x} \in \mathbb{R}^p : \text{qs}(\mathbf{x}, \boldsymbol{\theta}_k) = \max_{1 \leq j \leq K} \text{qs}(\mathbf{x}, \boldsymbol{\theta}_j) \right\}, \quad (1)$$

where $\text{qs}(\mathbf{x}, \boldsymbol{\theta}_k)$ is the quadratic discriminant score function at \mathbf{x} according to $\boldsymbol{\theta}_k$, that is

$$\text{qs}(\mathbf{x}, \boldsymbol{\theta}_k) := \log(\pi_k) - \frac{1}{2} \log(\det(\boldsymbol{\Sigma}_k)) - \frac{1}{2}(\mathbf{x} - \boldsymbol{\mu}_k)^\top \boldsymbol{\Sigma}_k^{-1}(\mathbf{x} - \boldsymbol{\mu}_k). \quad (2)$$

From now onward, we call $\mathcal{Q}(\boldsymbol{\theta})$ the *quadratic partition*. A point \mathbf{x} is defined to belong to the group for which the quadratic score is maximized. Hence, $\text{qs}(\mathbf{x}, \boldsymbol{\theta}_k)$ can generally be interpreted as a measure of the fit of \mathbf{x} into the k -th cluster according to $\boldsymbol{\theta}_k$. Note that $\exp(\text{qs}(\mathbf{x}; \boldsymbol{\mu}_k, \boldsymbol{\Sigma}_k)) \propto \pi_k \phi(\mathbf{x}; \boldsymbol{\mu}_k, \boldsymbol{\Sigma}_k)$, where $\phi(\cdot, \boldsymbol{\mu}_k, \boldsymbol{\Sigma}_k)$ is the multivariate normal density function with mean $\boldsymbol{\mu}_k$ and covariance $\boldsymbol{\Sigma}_k$. The classical interpretation of (1) is that it represents the optimal classification boundaries under the Gaussian assumption. As noted in [Hastie and Zhu \(2001\)](#), in practice, the quadratic score can effectively describe partitions well beyond Gaussianity whenever quadratic and linear boundaries can adequately separate clustered regions. The following result states that the partition in (1) is consistent with a class of elliptic-symmetric models that includes the Gaussian.

Proposition 1. *Assume $\Pr\{Z_k = 1\} = \pi_k$ and that for all $k = 1, 2, \dots, K$ the group-conditional distribution, i.e. the distribution of $X \mid Z_k = 1$, has density function*

$$f(\mathbf{x}; \boldsymbol{\mu}_k, \boldsymbol{\Sigma}_k) = \det(\boldsymbol{\Sigma}_k)^{-\frac{1}{2}} g\left((\mathbf{x} - \boldsymbol{\mu}_k)^\top \boldsymbol{\Sigma}_k^{-1}(\mathbf{x} - \boldsymbol{\mu}_k)\right), \quad (3)$$

where $g(\cdot)$ is a strictly decreasing function on $[0, +\infty)$, $\boldsymbol{\mu}_k \in \mathbb{R}^p$ is the centrality parameter and $\boldsymbol{\Sigma}_k \in \mathbb{R}^{p \times p}$ is a positive definite scatter matrix. Assume at least one of the following:

(C1) $f(\cdot)$ is the Gaussian density function (for an appropriate choice of $g(\cdot)$);

(C2) $\pi_i \det(\mathbf{\Sigma}_i)^{-\frac{1}{2}} = \pi_j \det(\mathbf{\Sigma}_j)^{-\frac{1}{2}}, i \neq j, i, j = 1, 2, \dots, K$.

Then, for any partition of the feature space $\{A_k, k = 1, 2, \dots, K\}$,

$$\Pr \left\{ \bigcup_{k=1}^K \{Z_k = 1 \cap X \in A_k\} \right\} \leq \Pr \left\{ \bigcup_{k=1}^K \{Z_k = 1 \cap X \in Q_k(\boldsymbol{\theta})\} \right\}, \quad (4)$$

where $Q_k(\boldsymbol{\theta}) \in \mathcal{Q}(\boldsymbol{\theta})$ is defined in (1).

The previous result connects and develops ideas from linear classification and its connections to elliptically-symmetric families investigated in [Velilla and Hernández \(2005\)](#).

Remark 1. The quadratic partition achieves the largest probability that its members contain points generated from the K sub-populations. The group-conditional model (3) includes popular unimodal models like the Gaussian, the Student-t, the Laplace, the multivariate logistic, etc. These models generate groups of points lying in regions that are intersections of ellipsoids described by the pairs $(\boldsymbol{\mu}_k, \mathbf{\Sigma}_k)$ and, within each group, the features are connected via their joint linear dependence. The generating mechanism assumed in Proposition 1 is consistent with data generated from finite mixtures of such elliptically-symmetric families. Outside the Gaussian case (C1), Proposition 1 is restricted to the cases where groups have a comparable square root of the generalized precision, $\det(\mathbf{\Sigma}_k)^{-\frac{1}{2}}$, after weighting by the cluster size π_k . A special case of (C2) is when groups are balanced (equal sizes π_k) and homoscedastic (equal dispersions $\mathbf{\Sigma}_k$).

2.2 Scoring cluster configurations

Given \mathbb{X}_n , we want to measure how well a cluster configuration $\boldsymbol{\theta}^{(m)}$ organizes these points within the quadratic partition. We want to select the “boxes” $\{Q_k(\boldsymbol{\theta}), k = 1, 2, \dots, K\}$ that

best represents the clustered points. Let $B_\varepsilon^k(\mathbf{x}_i; \boldsymbol{\theta})$ be a ball of radius $\varepsilon > 0$, centered at \mathbf{x}_i , such that $B_\varepsilon^k(\mathbf{x}_i; \boldsymbol{\theta}) \subset Q_k(\boldsymbol{\theta})$, i.e. $B_\varepsilon^k(\mathbf{x}_i; \boldsymbol{\theta}) := \{\mathbf{y} \in \mathbb{R}^p : \|\mathbf{y} - \mathbf{x}_i\| < \varepsilon \cap \mathbf{y} \in Q_k(\boldsymbol{\theta})\}$. For ε sufficiently small, the joint probability that all points in \mathbb{X}_n are accommodated in the quadratic partition consistently with the underlying group memberships is

$$\prod_{i=1}^n \Pr\{Z_k = 1 \cap X_i \in B_\varepsilon^k(\mathbf{x}_i; \boldsymbol{\theta})\} = \prod_{i=1}^n \Pr\{Z_k = 1\} \Pr\{X_i \in B_\varepsilon^k(\mathbf{x}_i; \boldsymbol{\theta}) \mid Z_k = 1\}. \quad (5)$$

Under the generating process of Proposition 1, taking $\varepsilon \rightarrow 0$, the probability law (5) is transformed into its density representation

$$\mathcal{L}_n(\boldsymbol{\theta}) := \prod_{i=1}^n \prod_{k=1}^{K(\boldsymbol{\theta})} (\pi_k f(\mathbf{x}_i; \boldsymbol{\mu}_k, \boldsymbol{\Sigma}_k))^{\mathbb{I}\{\mathbf{x}_i \in Q_k(\boldsymbol{\theta})\}}, \quad (6)$$

where $\mathbb{I}\{\cdot\}$ is the usual indicator function. (6) closely resembles the likelihood function for a partition model (see Fröhlich-Schnatter et al., 2019, Ch. 7). However, this is not exactly the case: for a partition model, we would have had class membership indicators replacing $\mathbb{I}\{\mathbf{x}_i \in Q_k(\boldsymbol{\theta})\}$ in (6). Taking the logarithm of (6), we would like to achieve the largest

$$L_n(\boldsymbol{\theta}) = \frac{1}{n} \sum_{i=1}^n \sum_{k=1}^{K(\boldsymbol{\theta})} \mathbb{I}\{\mathbf{x}_i \in Q_k(\boldsymbol{\theta})\} \log(\pi_k f(\mathbf{x}_i; \boldsymbol{\mu}_k, \boldsymbol{\Sigma}_k)). \quad (7)$$

Evaluation of (7) requires the knowledge of the specific group-conditional model $f(\cdot)$. However, we want to evaluate the quality of the partition even when the group-conditional distribution is not precisely known. Proposition 1 states that, for certain group-conditional distributions, point-wise maximization of the quadratic score in the feature space well captures the main clustered regions. We propose to rank cluster configurations based on the following *hard score*

criterion:

$$H_n(\boldsymbol{\theta}) = \frac{1}{n} \sum_{i=1}^n \sum_{k=1}^{K(\boldsymbol{\theta})} \mathbb{I}\{\mathbf{x}_i \in Q_k(\boldsymbol{\theta})\} \text{qs}(\mathbf{x}_i; \boldsymbol{\theta}_k). \quad (8)$$

We call it *hard* because $H_n(\cdot)$ is a weighted average of the points score with the 0–1 “hard” weights $\mathbb{I}\{\mathbf{x}_i \in Q_k(\boldsymbol{\theta})\}$. Interpreting $\text{qs}(\mathbf{x}_i; \boldsymbol{\theta}_k)$ as the strength at which the object i is assigned to the k -th group, (8) is the average strength achieved by a cluster configuration. Despite this qualitative interpretation of $H_n(\cdot)$, there is a connection between (7) and (8) at the population level, based on the fact that $\text{qs}(\mathbf{x}_i; \boldsymbol{\theta}_k)$ contains the kernel of the Gaussian density. Under regularity conditions, both sample averages (7) and (8) will asymptotically approach their population counterparts

$$L(\boldsymbol{\theta}) = \sum_{k=1}^{K(\boldsymbol{\theta})} \int_{Q_k(\boldsymbol{\theta})} \log(\pi_k f(\mathbf{x}; \boldsymbol{\theta}_k)) dF \quad \text{and} \quad H(\boldsymbol{\theta}) = \sum_{k=1}^{K(\boldsymbol{\theta})} \int_{Q_k(\boldsymbol{\theta})} \text{qs}(\mathbf{x}; \boldsymbol{\theta}_k) dF, \quad (9)$$

respectively. From now onward, $\Theta_M = \{\boldsymbol{\theta}^{(m)}, m = 1, 2, \dots, M\}$ denotes the collection of cluster configurations under comparison. The following proposition clarifies the relationship between $H(\cdot)$ and $L(\cdot)$.

Proposition 2. *Assume that the following integrals exist and that*

$$(C3) \quad \inf_{\boldsymbol{\theta}^{(m)} \in \Theta_M} \left\{ \int_{Q_k(\boldsymbol{\theta}^{(m)})} \log f(\mathbf{x}; \boldsymbol{\mu}_k^{(m)}, \boldsymbol{\Sigma}_k^{(m)}) dF - \int_{Q_k(\boldsymbol{\theta}^{(m)})} \log \phi(\mathbf{x}; \boldsymbol{\mu}_k^{(m)}, \boldsymbol{\Sigma}_k^{(m)}) dF \right\} \geq 0 \text{ for all } k = 1, 2, \dots, K(\boldsymbol{\theta}^{(m)}).$$

Then

$$H(\boldsymbol{\theta}^{(m)}) = c + L(\boldsymbol{\theta}^{(m)}) - \Lambda(\boldsymbol{\theta}^{(m)}), \quad (10)$$

where c is a positive constant, and

$$\Lambda(\boldsymbol{\theta}^{(m)}) = \sum_{k=1}^K \int_{Q_k(\boldsymbol{\theta}^{(m)})} \log \left(\frac{f(\mathbf{x}; \boldsymbol{\mu}_k^{(m)}, \boldsymbol{\Sigma}_k^{(m)})}{\phi(\mathbf{x}; \boldsymbol{\mu}_k^{(m)}, \boldsymbol{\Sigma}_k^{(m)})} \right) dF \geq 0.$$

At the population level, the hard score criterion can be interpreted as the quality of the fitting of the partition, expressed by $L(\cdot)$, minus a penalty term, $\Lambda(\boldsymbol{\theta}^{(m)}) \geq 0$, that measures the departure from the Gaussian clusters' prototype model embedded into the quadratic score function. When clusters are truly Gaussian, i.e. $f(\cdot) = \phi(\cdot)$, then $\Lambda(\boldsymbol{\theta}^{(m)}) = 0$ and $H(\boldsymbol{\theta}^{(m)}) \propto L(\boldsymbol{\theta}^{(m)})$. Condition (C3) is needed to interpret the method: it ensures that $\Lambda(\boldsymbol{\theta}^{(m)}) \geq 0$ for any possible cluster configuration $\boldsymbol{\theta}^{(m)}$ under comparison so that it works as a penalty. (C3) obeys to *the natural principle* that, whenever we pick a configuration $\boldsymbol{\theta}$, the approximating Gaussian model underlying $qs(\cdot)$ can not fit the quadratic regions better than the underlying true generating model $f(\cdot)$. Indeed, (C3) is violated if there exists a configuration $\boldsymbol{\theta}^{(m)}$ for which $\int_{Q_k(\boldsymbol{\theta}^{(m)})} \log f(X; \boldsymbol{\mu}_k^{(m)}, \boldsymbol{\Sigma}_k^{(m)}) dF < \int_{Q_k(\boldsymbol{\theta}^{(m)})} \log \phi(X; \boldsymbol{\mu}_k^{(m)}, \boldsymbol{\Sigma}_k^{(m)}) dF$, where these integrals can be seen as the expected log-likelihood contribution over the k -th members of the quadratic partition under $f(\cdot)$ and $\phi(\cdot)$, respectively.

To see how $H(\cdot)$ ranks cluster configurations in Gaussian and non-Gaussian situations, consider the following examples:

dgpG: F is a mixture of two spherical Gaussians in dimension $p = 2$ with equal sizes $\pi_1 = \pi_2 = 0.5$ and equal identity covariance matrix. The first Gaussian component is centered at $\boldsymbol{\mu}_1 = (0, 0)^\top$, while the second component has mean $\boldsymbol{\mu}_2 = (d, 0)^\top$, for some fixed $d > 0$.

dgpU: F is a mixture of two uniform distributions with equal volume in dimension $p = 2$ and $\pi_1 = \pi_2 = 0.5$. The first uniform distribution has support on the square $[-1, 1]^2$ with center at $\boldsymbol{\mu}_1 = (0, 0)^\top$. The second uniform distribution takes value on the square $[d - 1, d + 1] \times [-1, 1]$ with center at $\boldsymbol{\mu}_2 = (d, 0)^\top$, for some fixed $d > 0$.

In both cases, d is the Euclidean distance between the clusters' centers. For $d \in [0, 10]$ we have different data generating processes. The dgpU is introduced as a substantial departure from the elliptic assumption of Proposition 1. For each d , we compute $H(\cdot)$ at two alternative cluster configurations $\{\boldsymbol{\theta}^{(1)}, \boldsymbol{\theta}^{(2)}\}$ such that $K(\boldsymbol{\theta}^{(1)}) = 1$ and $K(\boldsymbol{\theta}^{(2)}) = 2$. In each case, the pair

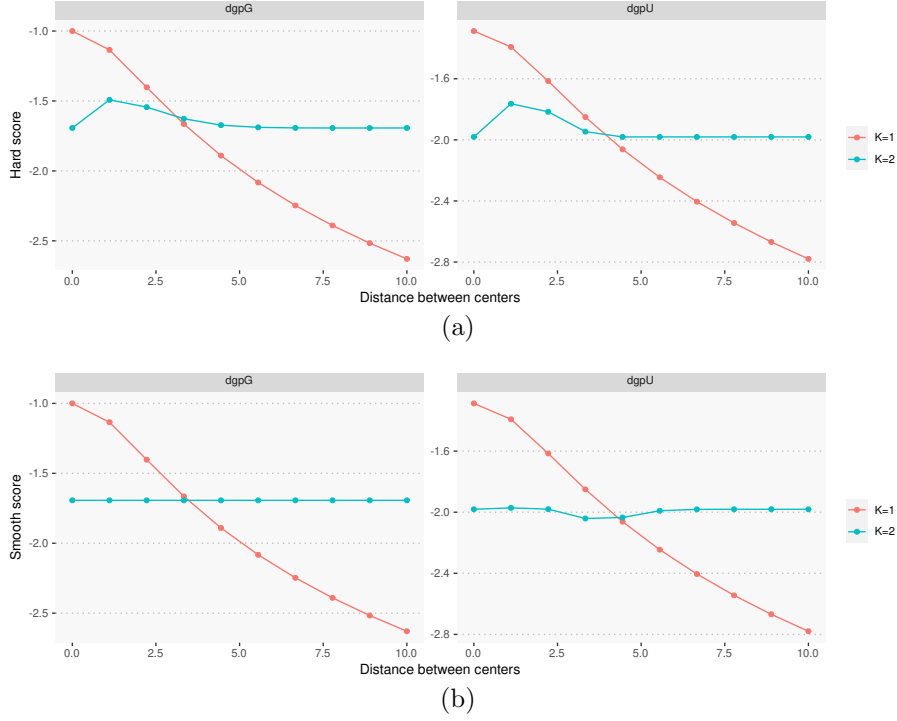


Figure 1: Population score vs within-cluster distance for the dgpG and dgpU example. Figure 1a: plots of $H(\cdot)$. Figure 1b: plots of $S(\cdot)$.

$\{\theta^{(1)}, \theta^{(2)}\}$ is defined to reflect the underlying true distribution F at the specific d . A detailed description of the setup, including details about the calculations, is given in Section S2-(SMF). Figure 1a reports $H(\cdot)$ vs. d . For both dgpG and dgpU, the hard score prefers a single cluster for low values of d . The two clusters are split at $d = 3.173$ for dgpG and $d = 3.694$ for dgpU (in the SMF, we show examples of data sets for values of d around the split point). The general behavior of $H(\cdot)$ is similar for both sampling designs. Under $K = 2$, for both dgpG and dgpU, there is evidence of a non-monotonic behavior of the criterion due to the hard weighting nature of $H(\cdot)$. Taking dgpG with $K = 2$, d only changes the position of the second group, and this is precisely reflected in the definition of $\theta^{(2)}$. We have the same quadratic regions accommodating data points in the same manner. The only difference introduced by d is their location. Therefore, one may expect a monotonic behavior of $H(\cdot)$. However, when d increases

to a value where the tails of the two distributions start to separate, both the quadratic regions $\{Q_1(\boldsymbol{\theta}^{(2)}), Q_2(\boldsymbol{\theta}^{(2)})\}$ start to lose tail points in favor of more central points where $\text{qs}(\cdot)$ is larger. This causes the tendency to split overlapped regions of points that one would not qualify as separate clusters. This may be problematic in cases of strong overlap as for the Olive data set studied in Section 4.

Since $\text{qs}(\cdot)$ measures the strength at which a point is assigned to a cluster, a smooth weighting is obtained by normalizing the quadratic scores. We propose to use the softmax transformation, that is the i -th point's weight into the k -th cluster is

$$\tau_k(\mathbf{x}_i; \boldsymbol{\theta}) = \frac{\exp(\text{qs}(\mathbf{x}_i; \boldsymbol{\theta}_k))}{\sum_{i=1}^n \exp(\text{qs}(\mathbf{x}_i; \boldsymbol{\theta}_k))}. \quad (11)$$

The corresponding *smooth score criterion* is defined as

$$T_n(\boldsymbol{\theta}) = \frac{1}{n} \sum_{i=1}^n \sum_{k=1}^{K(\boldsymbol{\theta})} \tau_k(\mathbf{x}_i; \boldsymbol{\theta}) \text{qs}(\mathbf{x}_i; \boldsymbol{\theta}_k). \quad (12)$$

Other weighting schemes are possible, but the choice of the softmax transformation is because it guarantees some form of optimality for Gaussian clusters (see the following proposition). Under regularity conditions, for sufficiently large n , (12) will approach its population counterpart

$$T(\boldsymbol{\theta}) = \sum_{k=1}^{K(\boldsymbol{\theta})} \int \tau_k(\mathbf{x}; \boldsymbol{\theta}) \text{qs}(\mathbf{x}; \boldsymbol{\theta}_k) dF. \quad (13)$$

Figure 1b shows the behavior of $T(\cdot)$ for the dgpG and dgpU examples. For $K = 2$, $T(\cdot)$ is flat for dgpG and almost flat for dgpU. $T(\cdot)$ splits the two groups at slightly larger separation now: $d = 3.47$ for dgpG and $d = 4.05$ for dgpU. $T(\cdot)$ does not attempt to split close clusters and is more appropriate to handle overlapped groups. Scatter plots of data sets around the transition are shown in Figure S4-(SMF).

Under the generating mechanism of Proposition 1, the unconditional distribution of X has the finite mixture density

$$\psi_f(\mathbf{x}; \boldsymbol{\theta}) := \sum_{k=1}^{K(\boldsymbol{\theta})} \pi_k f(\mathbf{x}; \boldsymbol{\mu}_k, \boldsymbol{\Sigma}_k). \quad (14)$$

For a sample point $\mathbf{x}_i \in \mathbb{X}_n$, under (14) define the *posterior weights*

$$\omega_{f,k}(\mathbf{x}_i; \boldsymbol{\theta}) = \Pr\{Z_{ik} = 1 \mid \mathbb{X}_n\} = \frac{\pi_k f(\mathbf{x}_i; \boldsymbol{\mu}_k, \boldsymbol{\Sigma}_k)}{\psi_f(\mathbf{x}_i; \boldsymbol{\theta})}. \quad (15)$$

The ratios defined in (15) are central in MBC methods where the i -th object is assigned to the k -th component by the following rule

$$\hat{z}_k(\mathbf{x}_i; \boldsymbol{\theta}) = \mathbb{I} \left\{ k = \arg \max_{1 \leq j \leq K(\boldsymbol{\theta})} \omega_{f,j}(\mathbf{x}_i; \boldsymbol{\theta}) \right\}; \quad (16)$$

in practice, $\boldsymbol{\theta}$ is replaced with an estimate. Typically, $\boldsymbol{\theta}$ is fitted based on an ML-type estimator, numerically approximated with the EM-algorithm (McLachlan and Peel, 2000). The rule (16), called MAP, retrieves the unobservable membership variables $\{Z_{ik}\}$ and coincides with the optimal Bayes classifier if the group-conditional model holds. The MAP rule produces a hard assignment from the smooth (also called fuzzy) membership weights in (15). The overall uncertainty of the assignment (16) reflecting (15) is captured by

$$\text{ent}(X; \boldsymbol{\theta}) = - \sum_{k=1}^{K(\boldsymbol{\theta})} \omega_{f,k}(X; \boldsymbol{\theta}) \log \omega_{f,k}(X; \boldsymbol{\theta}), \quad (17)$$

which is the entropy of the conditional distribution of $Z \mid X$. In situations where clusters are strongly separated the posteriors weights (15) will be close to either 1 or 0 for most points, and the MAP assignment will produce “clear clusters”, reflecting the low entropy of $Z \mid X$. On the other hand, cluster configurations with substantial overlap will exhibit large entropy. Let ψ_ϕ be the mixture model (14) when the group-conditional model is the Gaussian density $\phi(\cdot)$, and let

$\text{ent}_\phi(\cdot)$ be the corresponding entropy. Moreover, let $d_{\text{KL}}(f_0||g)$ the Kullback-Leibler discrepancy from the approximating model g to the “true” model f_0 .

Proposition 3. *Let f_0 be the density function corresponding to the “true” underlying population distribution function F . Then*

$$\arg \max_{1 \leq m \leq M} T(\boldsymbol{\theta}^{(m)}) = \arg \min_{1 \leq m \leq M} \left\{ d_{\text{KL}}(f_0 || \psi_\phi(\cdot; \boldsymbol{\theta}^{(m)})) + E_F[\text{ent}_\phi(X; \boldsymbol{\theta}^{(m)})] \right\}, \quad (18)$$

where all expectations are assumed to exist and $E_F[\cdot]$ denotes the expectation under F .

Proposition 3 clarifies that $T(\cdot)$ looks for a compromise between the best approximation of f_0 , in the sense of ψ_ϕ , and the lowest entropy of the resulting assignment under the Gaussian prototype model. The entropy term discourages the criteria from focusing on too complex clustering structures. The term $d_{\text{KL}}(f_0 || \psi_\phi(\cdot; \boldsymbol{\theta}^{(m)}))$ can be made arbitrarily small if $\boldsymbol{\theta}^{(m)}$ is an overly rich description of the density regions produced by F . Indeed, finite Gaussian mixtures can approximate any continuous distribution in a nonparametric sense (Nguyen et al., 2020). However, an overly complex $\boldsymbol{\theta}^{(m)}$ (e.g. $K(\boldsymbol{\theta}^{(m)})$ is large) that describes the density regions too locally would imply a strong overlap and therefore a large $\text{ent}_\phi(\cdot)$.

Remark 2. Baudry (2015) formulated a parameter estimation criterion based on the right-hand side of (18) to perform MBC. However, the mathematical formulation and the framework here is different. $H(\cdot)$ and $T(\cdot)$ are not meant to be estimation criteria to be optimized at the sample level. Propositions 2 and 3 are only meant to clarify the type of model reference-concept driving the proposed score selection. Both $H(\cdot)$ and $T(\cdot)$ are meant to recover certain clustering structures and not a “true” underlying generating model F , which may well be not a function of the $\boldsymbol{\theta}^{(m)} \in \Theta_M$. For instance, in the previous dgpG/dgpU example, for all d , the true underlying model corresponds to $K = 2$, but both scores will prefer $K = 1$ for low values of d . The latter implies that the maximum score can not identify the true underlying distribution even in the Gaussian case.

Under the Gaussian assumption, there is a further connection between the sample scores $H_n(\cdot)$ and $T_n(\cdot)$ and what is called observed *complete data log-likelihood* into the MBC literature. For details, we refer the reader to Section S4-(SMF).

3 Score selection via resampling

The following discussion applies to both hard and smooth score criteria, therefore we unify the notation. Rewrite both (8) and (12) as the average

$$S_n(\boldsymbol{\theta}) = \frac{1}{n} \sum_{i=1}^n s(\mathbf{x}_i; \boldsymbol{\theta}), \quad \text{where} \quad s(\mathbf{x}; \boldsymbol{\theta}) := \sum_{k=1}^{K(\boldsymbol{\theta})} w_k(\mathbf{x}; \boldsymbol{\theta}) \text{qs}(\mathbf{x}; \boldsymbol{\theta}) \quad (19)$$

is the cluster-weighted point-score. With $w_k(\mathbf{x}; \boldsymbol{\theta}) = \mathbb{I}\{\mathbf{x} \in Q_k(\boldsymbol{\theta})\}$ we obtain the hard scoring, while $w_k(\mathbf{x}; \boldsymbol{\theta}) = \tau_k(\mathbf{x}; \boldsymbol{\theta})$ returns the smooth score. In Section 2, we assumed a fixed list of candidate configurations Θ_M . In practice, we work with a list of solutions obtained from applying different algorithms (and their various settings) to the only available data set \mathbb{X}_n . Let $\hat{\boldsymbol{\theta}}_n = \text{Clust}(\mathbb{X}_n)$ be a cluster configuration obtained by running a certain algorithm on \mathbb{X}_n ; $\hat{\boldsymbol{\theta}}_n$ reflects the sampling variability, the fitting method's variance and often an error equal to the difference between the method's true solution and its algorithmic approximation. Computing both $\hat{\boldsymbol{\theta}}_n$ and $S_n(\cdot)$ using the same observed sample is not a good idea because it will lead to an over-optimistic estimate. As noted in Section 1, the clustering problem is affected by a bias-variance trade-off mechanism. Increasing K , or setting the algorithm's hyper-parameters to accommodate complex structures, increases the fit on the observed data but does not guarantee a more coherent representation of the underlying clustering structure.

One way to overcome the previous issue is to make the fitting step independent of the validation step. Assume that $\hat{\boldsymbol{\theta}}_n \sim G$, where G reflects the randomness of the clustering output. Assuming that $\hat{\boldsymbol{\theta}}_n$ is independent of X , we want to construct a selection criterion that,

Algorithm 1: bootstrap estimation

Input: observed sample \mathbb{X}_n , $\alpha \in (0, 1)$

Output: $\widetilde{W}_n, \widetilde{L}_n, \widetilde{U}_n$.

for $b = 1, \dots, B$ **do**

 (step 1.1) $\mathbb{X}_n^{*(b)} \leftarrow \{x_i^{*(b)}; i = 1, 2, \dots, n\} \stackrel{\text{iid}}{\sim} \mathbb{F}_n$
 (step 1.2) $\hat{\boldsymbol{\theta}}_n^{*(b)} \leftarrow \text{Clust}(\mathbb{X}_n^{*(b)})$
 (step 1.3) $S_n^{*(b)} \leftarrow S_n(\hat{\boldsymbol{\theta}}_n^{*(b)}) = n^{-1} \sum_{i=1}^n s(x_i; \hat{\boldsymbol{\theta}}_n^{*(b)})$

(step 2) $\widetilde{W}_n \leftarrow \frac{1}{B} \sum_{b=1}^B S_n^{*(b)}$

(step 3) Let $R_n^{*(b)} = \sqrt{n} (S_n^{*(b)} - \widetilde{W}_n)$, compute

$$\widetilde{L}_n \leftarrow \inf_t \left\{ t : \frac{1}{B} \sum_{b=1}^B \mathbb{I} \{ R_n^{*(b)} \leq t \} \geq \frac{\alpha}{2} \right\}$$

$$\widetilde{U}_n \leftarrow \inf_t \left\{ t : \frac{1}{B} \sum_{b=1}^B \mathbb{I} \{ R_n^{*(b)} \leq t \} \geq 1 - \frac{\alpha}{2} \right\}$$

at the population level, targets the quantity $W = \mathbb{E}_G[\mathbb{E}_F[s(X; \hat{\boldsymbol{\theta}}_n)]]$. W is the expectation over all possible realization of $\hat{\boldsymbol{\theta}}_n$ of the expected cluster-weighted point score (19). This approach is inspired by the seminal work of Akaike (1973) on model selection. Indeed, at the population level, AIC is defined as the expected Kullback-Leibler information loss over all possible estimates of the unknown parameter. In practical situations, G is not available, but the variations induced by $\hat{\boldsymbol{\theta}}_n$ can be reproduced by repeating the clustering step on resampled versions of the data. Let \mathbb{F}_n be the ecdf of the sample; we propose to approximate W using multiple independent samples obtained from \mathbb{F}_n . The proposed estimation procedure is described in Algorithm 1, and it is based on the classical Efron's empirical bootstrap idea. In steps (1.1)–(1.2) of Algorithm 1, independent bootstrap samples from the original data are used to reproduce the variations of $\hat{\boldsymbol{\theta}}_n$. In step (1.3), the original sample is used to compute the empirical approximation of the inner expectation of W at the specific $\hat{\boldsymbol{\theta}}_n^{*(b)}$. Step (2) of Algorithm 1 computes an estimate \widetilde{W}_n of W obtained as the expectation of the Monte Carlo approximation of the bootstrap distribution

of $S_n^{*(b)}$. Step (3) corresponds to the percentile method calculation of an approximate $(1 - \alpha)$ -confidence interval for W . Calculation of a confidence interval for W can be used to consider the uncertainty about W , reflecting both the sample variations and the variance of $\hat{\theta}_n$. Let $W^{(m)}$ be the value of the expected score, W , produced by the m -th method/algorithm under comparison. Instead of selecting the cluster configurations achieving the largest estimated $\widetilde{W}^{(m)}$, we propose to select the clustering corresponding to $\hat{\theta}_n^{(m^*)}$ where, for a fixed level of $\alpha \in (0, 1)$,

$$m^* = \arg \max_{1 \leq m \leq M} \widetilde{L}_n^{(m)}. \quad (20)$$

The main drawback of Algorithm 1 is that it requires refitting the clusters B times for each clustering configuration $m \in \Theta_M$. This may be problematic if the set \mathcal{M} of candidate solutions is large. In principle, one should fix B large enough. In the large experiment shown in Section 4, we set $B = 1000$. In the SMF, we also provide evidence that even choosing $B = 100$ did not change results substantially.

Remark 3 (Bootstrap vs. cross-validation). Cross-validation (CV) is probably the most popular resampling method to perform model selection by separating the fitting and the testing step. CV has been proposed to estimate K in the MBC framework by Smyth (2000). Fu and Perry (2020) proposed the CV to select K with the k-means algorithm. However, the application of the CV approach to the clustering framework is problematic. CV is designed to estimate the prediction error of a model conditional on the training set, although Bates et al. (2021) recently proved that CV does not achieve the previous goal in general. However, clustering is not a prediction problem. Here we want to assess the extent by which a certain $\theta^{(m)}$ describes the clustered structure produced by the underlying F . Therefore, we need that both the fitted $\hat{\theta}_n^{(m)}$ and the sample on which the score is computed convey the same information about the underlying F . This is achieved by Algorithm 1, where the ecdf drives all the independent samples. In contrast, in the CV, the aim is to estimate a conditional prediction error, requiring

that the train and the test set do not overlap, which often causes the two subsamples' structure to differ substantially in finite samples. Bootstrap is shown to perform better than CV in Section 4.

Remark 4 (Bootstrap consistency). We do not investigate the theoretical properties of the bootstrap procedure. Algorithm 1 is meant as a simple (and possibly brute force) approximation of the desired W . However, the reader may wonder whether the bootstrap estimate \widetilde{W}_n converges in some sense to the desired W or whether the calculated confidence interval is valid. It is well known that bootstrap theory can be technically involved depending on the statistical object that is resampled, that here is $\hat{\theta}_n$ (see Efron and Hastie, 2016, and references therein). Formal guarantees for the Algorithm 1 would essentially require certain strong regularity conditions on the mapping $\text{Clust} : \mathbb{X}_n^{*(b)} \rightarrow \hat{\theta}_n^{*(b)}$ involved in step (1.2). It is undoubtedly of interest to check whether popular clustering algorithms lead to formal guarantees for the bootstrap. However, this would involve extensive technical developments that are postponed to future research.

4 Experimental analysis

In this section, we present an extensive experimental analysis of the selection problem. The complexity of the following setting aims at offering a neutral comparison, where each competing method is expected to perform well in certain scenarios. This is of utmost importance to achieve scientific progress in unsupervised learning, where global theoretical guarantees are rare, and most of the performances are shown via experimental studies (Mechelen et al., 2018). Here, we describe the general aspects that are applied to all data sets in the experiments.

Clustering methods and algorithms. For each data set, we obtain several clustering solutions, indexed with $m \in \mathcal{M}$. In practice, each member $m \in \mathcal{M}$ is the output of an algorithm that implements a specific method, configured with a certain number of clusters $K(m)$ plus

other hyper-parameters of the method and the algorithm. For some clustering methods, we also consider configurations where the initialization is considered part of the tuning. \mathcal{M} denotes the set of all cluster configurations obtained from a fixed input data set, and we want to select one of them. We consider a set of 440 cluster configurations, i.e. $|\mathcal{M}| = 440$, obtained with algorithms that implement: K-means and K-medoids partitioning methods; ML for Gaussian and Student-t mixtures with several covariance matrix models (as implemented in the popular `mclust` software of [Scrucca et al. \(2016\)](#) and in the `EMMIXskew` software of [Wang et al. \(2018\)](#)); ML for the more general class of Skew Student-t mixture models; ML for Gaussian mixtures with the eigen-ratio regularization (implemented in the `otrimle` software of [Coretto and Hennig \(2021, 2017\)](#)). The co-existence of three MBC methods is because we want to show cases when classical information criteria are not adequate (see below). The 440 configurations are obtained running the previous methods with $K = 1, 2, \dots, 10$ and setting each of these methods with different hyper-parameters' specifications. In what follows, we occasionally refer to subsets of solutions in \mathcal{M} , named after the implementing software: K-MEANS, K-MEDOIDS, MCLUST, RIMLE and EMMIX. The detailed description of \mathcal{M} is given in Section S5.1-(SMF).

Selection methods. For each data set, we select the desired solution from \mathcal{M} using 13 different selection methods. As stressed in Section 1, the list of existing methods is vast, and we restrict the comparison to classical internal validation criteria routinely used by practitioners or those criteria rooted into the MBC literature that are more appropriate for pursuing the notion of cluster of interest. Among the classical method-independent internal validation criteria, we consider the CH and ASW indexes based on Euclidean distances. Note that these indexes are not designed to pursue the cluster's notion investigated in this paper, but they are rather popular, and practitioners use them in various settings. The second group of methods includes the information criteria: AIC, BIC, and ICL. In tandem with MBC methods based on ESD mixture models, these criteria constitute the strongest candidate to discover the cluster concept

of interest. However, note that information criteria can not be computed for all members of \mathcal{M} . For instance, they cannot be computed for K-MEANS or K-MEDOIDS solutions or solutions obtained with ML for Gaussian mixtures with the eigen-ratio constraint (see the SMF for more details). Within the context of likelihood-type methods, we also consider the cross-validation methodology of [Smyth \(2000\)](#), labeled as CVLK. The latter consists in using cross-validation to estimate a risk measure that equals minus the expected log-likelihood of the underlying mixture model. The target risk in CVLK is the predicted Kullback–Leibler information loss. CVLK requires the definition of an underlying probability model, and it is applied to members of \mathcal{M} corresponding to MBC methods (i.e. MCLUST, RIMLE and EMMIX). The bootstrap stability method of [Fang and Wang \(2012\)](#), labeled as FW, is introduced in the comparison as another bootstrap-based alternative. FW is a method-independent validation method that pursues a stability notion rather than the validation philosophy developed here. However, stability recently gained wide popularity in applications, so that it is interesting to see its performance in the following applications. Section S5.2-(SMF) describes all the selection methods mentioned above more formally and in greater detail.

Finally, the experiments include the scoring methodology proposed in this paper plus additional variants to show some motivations underlying the bootstrap approach. The methods’ labeled as BQH and BQS correspond to the bootstrap-based selection method defined in (20). BQH refers to the hard scoring version, while BQS refers to the smooth version. We set $B = 1000$; this may be a demanding computing load for large data sets but, in practice, setting a much lower $B = 100$ left the results almost unaltered (see SMF). In order to show the drawbacks of estimating the quadratic score criteria using in-sample information only, we introduce two additional variants labeled QH and QS. QH and QS select the $m^* \in \mathcal{M}$ such that (8) and (12) are maximized, respectively. These are the *in-sample* versions of the quadratic score because, in this case, both (8) and (12) are computed on the same observed data set used to fit $\theta^{(m)}$. In Remark 3, we discussed the conceptual issues of treating the score estimation within

the prediction-based paradigm. As a robust check for such a claim, we introduce the CVQH and CVQS variants, in which we apply 10-fold cross-validation to estimate (8) and (12) on test data not seen by the clustering algorithm. CVQH is for the hard score, while CVQS refers to the smooth version. The detailed cross-validation algorithm is given in the SMF.

Performance measures. For each data set and method, we measure two types of performance: (i) agreement with respect to true clusters’ memberships; (ii) selection of the number of clusters compared to the ground truth. Point (i), which is the similarity between true and fitted groups, is measured using the Adjusted Rand Index (ARI) of [Hubert and Arabie \(1985\)](#) and the Variation of Information Criterion (VIC) of [Meilă \(2007\)](#). The $\text{ARI} \in [0, 1]$, where $\text{ARI}=1$ means perfect agreement. Originally, $\text{VIC} \in [0, \infty)$; however, we compute and report the negative of the VIC, so that a larger value means better agreement as for the ARI. ARI and VIC are not only different in scales, but they capture the similarity differently. The data sets present different challenges in retrieving the true classes. We design situations where, even for some artificial data, the “true clustering” is not obvious and none of the 440 methods in \mathcal{M} is able to reach near-to-perfect performances (e.g. $\text{ARI} \approx 1$ and/or $\text{VIC} \approx 0$). Nevertheless, here we do not compare clustering methods. In contrast, we study the problem of selecting the best available partition. For this reason, besides comparing with the ground truth, we benchmark the 13 selection methods against the “two best feasible partitions”, labeled as BEST ARI and BEST VIC. These are obtained running the 440 methods’ configurations on a data set and choosing the partitions achieving the best ARI and VIC, respectively. Note that for some data sets, there are multiple members of \mathcal{M} that give the same best feasible partition.

4.1 Analysis of real data sets

The three real data sets analyzed in this study are: the Iris data set of [Anderson \(1936\)](#) and [Fisher \(1936\)](#) with $n = 150$, $p = 4$ features measuring physical parameters of Iris flowers and

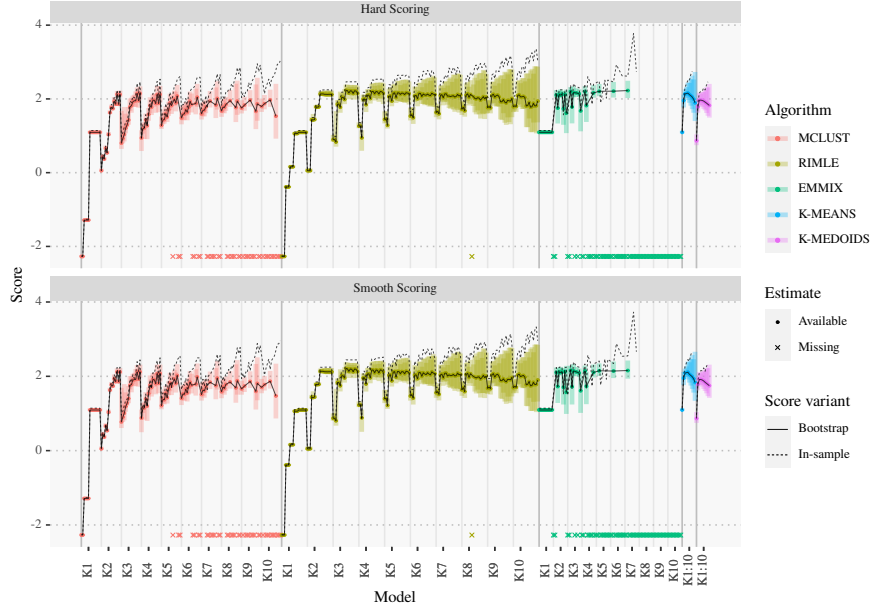


Figure 2: Results for the quadratic score criteria (QH, QS, BQH, BQS) computed on the Iris data set. Top panel: hard scoring; Bottom panel: smooth scoring.

$K = 3$ groups that identify Iris species; the Banknote data set (Flury and Riedwyl, 1988) with $n = 200$ and $p = 6$ features measuring aspects of Swiss banknotes, split in $K = 2$ groups of “counterfeit” and “genuine” banknotes; the Olive data set (Forina et al., 1983) with $n = 572$ and $p = 8$ features measuring chemical contents in olive oils from Italy. There are two possible true partitions for this data set: a coarser one with 3 classes corresponding to Italian geographical macro-regions; a finer classification with 9 narrower geographical regions. The Olive data set is a truly challenging case due to strong overlap, discrepancies in the between-clusters shapes and some features’ discreteness. Additional information and data visualizations are given into the SMF.

Figure 2 provides a graphical representation of the results for the proposed methodology applied to the Iris case. On the horizontal axis of each plot we list all the 440 members of \mathcal{M} , hierarchically sorted on: the clustering algorithm; increasing K (reported in the plot’s labels); the increasing complexity of the underlying clustering model (see SMF). The method behind

each member of \mathcal{M} is denoted with colors. For some of the algorithms, some settings produced missing solutions for the in-sample estimates and/or an excessive amount of missing solutions across bootstrap repetitions; these cases are discarded and denoted with a (\times)-symbol (see the SMF). In both plots: dashed lines are the in-sample QH and QS scores; the solid lines represent the expectation W estimated by \widetilde{W}_n using the bootstrap; color-filled bands around solid lines are the estimated confidence intervals for W at 95%-level. The difference between BQH and BQS is not clear-cut. On the other hand, for all the clustering methods, there is remarkable evidence that both in-sample estimates of the score (QH and QS) become overly optimistic as the complexity of the clustering solutions increases. Indeed, for $K > 3$ (true number of groups) and increased model complexity, both QH and QS leave the scores' confidence intervals. Moreover, as soon as $K(m)$ exceeds the true $K = 3$, the more complex members of \mathcal{M} also produce wider confidence bands, confirming the well-known pattern in the model selection that unnecessary additional model complexity introduces additional uncertainty. For the sake of space, we report the same visualization for the Banknote and the Olive data sets in Figure S7(b)-(SMF) and Figure S7(c)-(SMF), respectively. We have a pattern similar to that found for Iris for both data sets, although for the Olive data set the plot in Figure S7(c)-(SMF) is less clear due to its vertical scale. The SMF also reports the same summary plots for each data set, derived using only the first $B = 100$ bootstrap replicates out of the original 1000. The latter shows that the proposed method is pretty robust to the bootstrap-induced variability and that a low value of B does not produce dramatically different results.

Table 1 reports the selected solutions for all the clustering selection criteria on the three data sets. First, note that the best feasible partitions available from \mathcal{M} (BEST ARI and BEST VIC) do not always retrieve the underlying clusters perfectly, although they catch the true K but for the Olive data with 9 classes. In this case, the best feasible solution corresponds to a configuration fitted by the `mclust` software with $K = 8$ groups (Table 1-(d)). For the Iris data, the selected solutions include partitions with a K ranging from 2 to 6. The true $K = 3$

Table 1: Clustering solutions selected by the 13 selection criteria under comparison on the three real data sets. First two rows in each table indicate the two best feasible solutions: BEST ARI and BEST VIC partitions. The column “K” reports the number of groups discovered by the selected solution. The “Algorithm” and “Configuration” columns identify the specific member of \mathcal{M} that is selected. The nomenclature used in the previous columns is defined in Section S5-(SMF). Finally, the ARI and the VIC columns measure the agreement of the selected partition with respect to the ground truth.

(a) Iris dataset

Criterion	K	Algorithm	Configuration	ARI	VIC
BEST ARI	3	Mclust	EEE	0.94	-0.26
BEST VIC	3	Mclust	EEE	0.94	-0.26
AIC	6	Emmix	mvt; ncov = 3	0.57	-1.52
BIC	2	Mclust	VEV	0.57	-0.67
ICL	2	Mclust	VEV	0.57	-0.67
QH	7	Emmix	mvt; ncov = 4	0.42	-1.56
QS	7	Emmix	mvt; ncov = 4	0.42	-1.56
CH	3	Mclust	EII	0.73	-0.76
ASW	2	Mclust	EVV	0.57	-0.67
FW	2	Mclust	VII	0.57	-0.67
CVLK	4	Rimle	$\gamma = 10000$; InitClust	0.81	-0.57
CVQH	4	Rimle	$\gamma = 10000$; InitClust	0.81	-0.57
CVQS	4	Rimle	$\gamma = 1000$; InitClust	0.81	-0.58
BQH	3	Rimle	$\gamma = 100$; pam	0.9	-0.32
BQS	3	Rimle	$\gamma = 100$; pam	0.9	-0.32

(b) Banknote dataset

Criterion	K	Algorithm	Configuration	ARI	VIC
BEST ARI	2	Mclust	EII	1	0
BEST VIC	2	Mclust	EII	1	0
AIC	6	Emmix	mvt; ncov = 3	0.6	-1.16
BIC	3	Mclust	VVE	0.84	-0.43
ICL	3	Mclust	VVE	0.84	-0.43
QH	10	Rimle	$\gamma = 10000$; pam	0.26	-2.14
QS	10	Rimle	$\gamma = 10000$; pam	0.26	-2.14
CH	2	Rimle	$\gamma = 1$; pam	1	0
ASW	2	Rimle	$\gamma = 1$; kmeans	1	0
FW	2	Rimle	$\gamma = 100$; kmeans	0.98	-0.08
CVLK	3	Rimle	$\gamma = 10$; InitClust	0.85	-0.42
CVQH	3	Mclust	VEV	0.78	-0.62
CVQS	3	Mclust	VEV	0.78	-0.62
BQH	3	Rimle	$\gamma = 10$; kmeans	0.86	-0.37
BQS	3	Rimle	$\gamma = 10$; kmeans	0.86	-0.37

(c) Olive dataset (3 classes)

Criterion	K	Algorithm	Configuration	ARI	VIC
BEST ARI	3	Emmix	mvt; ncov = 3	1	-0.03
BEST VIC	3	Emmix	mvt; ncov = 3	1	-0.03
AIC	10	Emmix	mvt; ncov = 3	0.33	-1.74
BIC	6	Emmix	mvt; ncov = 3	0.52	-1.42
ICL	6	Emmix	mvt; ncov = 3	0.52	-1.42
QH	10	Mclust	VVV	0.29	-1.84
QS	10	Mclust	VVV	0.29	-1.84
CH	3	K-Means		0.32	-1.88
ASW	2	Emmix	mvt; ncov = 5	0.39	-1.28
FW	2	Emmix	mvt; ncov = 3	0.82	-0.42
CVLK	10	Rimle	$\gamma = 10000$; InitClust	0.3	-1.81
CVQH	7	Emmix	mvt; ncov = 3	0.28	-2.04
CVQS	7	Emmix	mvt; ncov = 3	0.28	-2.04
BQH	8	Mclust	VVV	0.49	-1.28
BQS	8	Mclust	VVV	0.49	-1.28

(d) Olive dataset (9 classes)

Criterion	K	Algorithm	Configuration	ARI	VIC
BEST ARI	8	Mclust	EVE	0.88	-0.65
BEST VIC	8	Mclust	EVE	0.88	-0.65
AIC	10	Emmix	mvt; ncov = 3	0.47	-1.77
BIC	6	Emmix	mvt; ncov = 3	0.76	-1.32
ICL	6	Emmix	mvt; ncov = 3	0.76	-1.32
QH	10	Mclust	VVV	0.54	-1.26
QS	10	Mclust	VVV	0.54	-1.26
CH	3	K-Means		0.42	-2.28
ASW	2	Emmix	mvt; ncov = 5	0.29	-2.28
FW	2	Emmix	mvt; ncov = 3	0.36	-1.84
CVLK	10	Rimle	$\gamma = 10000$; InitClust	0.58	-1.18
CVQH	7	Emmix	mvt; ncov = 3	0.44	-1.96
CVQS	7	Emmix	mvt; ncov = 3	0.44	-1.96
BQH	8	Mclust	VVV	0.86	-0.74
BQS	8	Mclust	VVV	0.86	-0.74

is detected by BQH, BQS and CH. However, only BQH and BQS selected partition is very close to the best available. For the Banknote data, the top performers are CH and ASW that can discover the true partition exactly, with FW reporting a close performance. In this case, some methods, including BQH, BQS and ICL, provided a second-best performance fitting $K = 3$ groups. This is due to the inhomogeneity of the “counterfeit” class, which a single ESD component can not adequately capture (see Figure S5-(SMF)). For the Olive data set assuming $K = 9$ classes, none of the selection methods discovers 9 groups (Table 1-(d)): BQH and BQS retrieve two partitions that are close to the best available in \mathcal{M} , while all other methods select solutions that are far away from the ground truth. On the other hand, assuming the 3-classes version of the data set (Table 1-(c)), only CH discovers 3 groups, but these are unrelated to the ground truth. In this case, FW reports the best, reasonably good ARI and VIC, with 2 groups mixing some of the underlying 3 classes. The overall conclusion across the three data set are: (i) BQH and BQS offer a similar performance, finding the best feasible partition or a partition close to it; (ii) the in-sample versions of the quadratic score criteria, QH and QS, dramatically over-estimate K in all situations; (iii) all cross-validation alternatives showed a poor performance; (iv) information-based criteria showed a mixed evidence. AIC tends to select too complex solutions, while both BIC and the ICL select less complex solutions as expected. BIC and ICL show the same performance, selecting a reasonable partition only in the case of the Banknote data. However, the following section shows that ICL does much better with simulated data.

4.2 Monte Carlo experiments

In this section, we present experiments with data simulated from 5 different data generating processes (DGP), shown in Figure 3. The DGPs are labeled as: *Pentagon5*, *T52D*, *T510D*, *Flower2* and *Uniform*. All DGPs produce data in dimension $p = 2$ except for T10D, where $p = 10$. The Uniform design generates points drawn from a single 2-dimensional uniform distribution

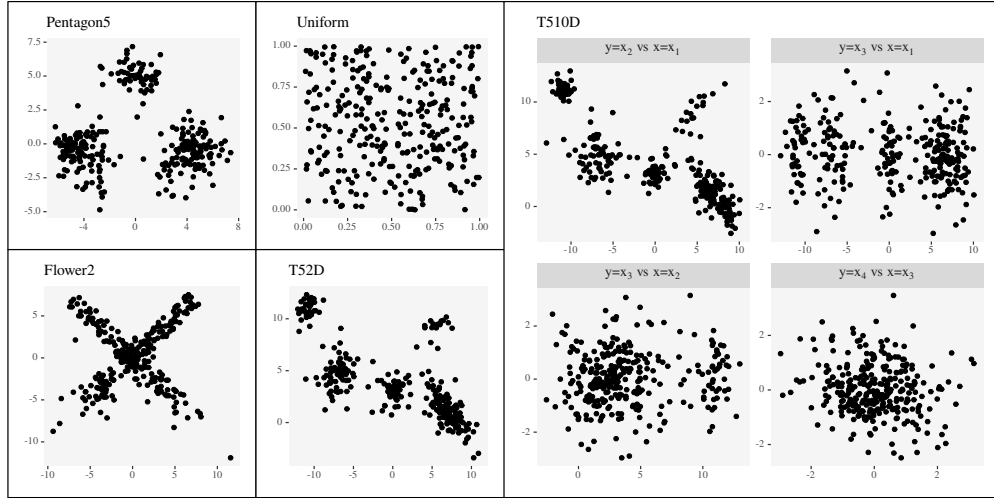


Figure 3: Scatters produced by the 5 DGPs with $n = 300$ in each case. For T510D (right) we plot the first two marginals (x_1 and x_2), a combination of them with an uninformative marginal (x_3) and two uninformative marginals (x_3 and x_4).

to test the behavior with unclustered data. For all other DGPs, points are drawn from finite mixtures with 5 components. Pentagon5 generates points from Gaussian components, some of which are strongly overlapped and unbalanced. T52D generates points from reasonably separated Student-t components. T510D generates the same clusters as T52D on the first two coordinates while the remaining 8 dimensions are “noisy features” with a joint spherical distribution that does not carry any clustering information. Finally, Flower2 generates points from both uniform and ESD components. A detailed description of the DGPs and additional data visualizations are available in the SMF. The “true” cluster membership of a point is identified with the corresponding mixture component generating it. However, some DGPs produce situations that are not always in line with this ground truth definition. For example, one may want to look for 3 clusters in Pentagon5, while 5 groups may not be necessarily the only appropriate description of Flower2’s structure. Some DGPs contain substantial departures from elliptic shapes, unbalanced groups and strong between-scatter discrepancies. This is for testing the robustness of the proposed method in situations where the assumptions in Proposition 1

are not exactly fulfilled. Moreover, we fix $n = 300$ for all simulated data sets. The latter choice challenges some resampling criteria due to the strong stress it imposes on bootstrap resampling. Indeed, empirical bootstrap may fail to replicate the distribution of small clusters when n is small. The resampling-based selection methods require multiple fits of the clusters for each data set. Due to the demanding computing power required by these experiments, we consider 100 Monte Carlo replicates for each data set. All the following performance summary measures refer to the corresponding Monte Carlo distribution. Additional details on the DGPs, data visualizations and summaries are available in the SMF.

Results for all the designs are summarized in Figure 4, showing boxplots of the Monte Carlo distribution of the ARI and the VIC (top and bottom panel of each subplot). The ARI and the VIC compare the selected partition to the ground truth previously defined. The dashed line in each plot indicates the average best feasible ARI and VIC available in \mathcal{M} (achieved by the BEST ARI and BEST VIC solutions), together with bands (shaded area) ranging from the first to the third quartiles of the scores' empirical distributions. Figure S9-(SMF) adds barplots representing the frequencies for the corresponding selection of the number of clusters.

For Pentagon5 all methods do well. The AIC and the BIC selected 5 groups in roughly 50% of the experiments. This confirms the tendency of such criteria to recover the underlying true DGP rather than the clustering structure. In fact, for this DGP, 3 groups are what one would suggest by visual inspection of the scatter plot in Figure 3. The other well-performing criteria typically prefer the 3-clusters solution. Looking at the barplots in Figure S9(a)-(SMF), BQH, BQS, ICL, ASW, CH and FW also excelled for the stability of the results.

For the T52D case, the top performers are BIC, ICL, ASW, BQH and BQS. All of these criteria fit 5 clusters, on average, selecting partitions of \mathcal{M} that are close to the best available in the set. This is not surprising given the strong between-cluster separation. BQH and BQS do marginally better, showing the most stable selection (see Figure S9(b)-(SMF)). It is worth noting that ASW does well, even if it is not specifically designed to handle DGPs of this type.

Whenever clusters are well separated, the intuition is that a distance-based index like ASW can retrieve the true clusters if it uses an appropriate metric.

The addition of uninformative noisy features in T510D changes the results dramatically: only ICL and BQS maintain excellent performances, with BQS doing slightly better overall in terms of ARI and VIC. Figure S9(c)-(SMF) shows that ICL has a slightly better stability. However, it is worth noting that information-type criteria select over a smaller subset of \mathcal{M} , not including K-MEANS, K-MEDOIDS and RIMLE solutions, which may produce less variability in the selection.

Flower2 is probably the most challenging case. The best feasible solutions in \mathcal{M} achieve modest levels of average ARI and VIC. A 5 cluster solution achieves the best ARI and VIC roughly 77% of the time, and the methods identifying 5 clusters more often are ASW, FW, BQH, and BQS. BQH does only marginally better than its competitors in terms of ARI and VIC, but we can say that the performance of BQS, ASW, and FW are equally good.

The Uniform sampling design is more of a clear-cut: ICL, BQS, and CVQS are all able to correctly identify no clustering structure. In this case, the clear winner is BQS, selecting a single cluster in 96% of the replicates compared to the 85% of CVQS and 77% of ICL (see Table S8(e)-(SMF)). All the other methods wrongly identify clustering structures in the data (note that FW can not be directly used to handle the unclustered case). Here, we can see that the AIC looks for the best distribution fit rather than accommodating clustered regions. Indeed, AIC prefers a large number of mixture components to fit the highly unstructured uniform scatter. The BIC mitigates this tendency, but it is not enough. It is also remarkable to see the difference between the top performer, BQS, and its close cousin BQH failing miserably. The explanation of such a bad performance is the tendency of the hard scoring approach to split close groups of points; this was shown in the example of Section 2.2. In this case, with a small $n = 300$, the uniform DGP (see Figure 3) creates many small groups of data points with minimal within-distance, which encourages the hard score to identify many groups.

Based on the experimental evidence provided in this work, we draw the following conclusions. BQS has shown a top or a second-best performance in all cases, while the BQH suffers in situations with strong overlap between clusters. For this reason, we advocate the use of BQS version of our proposal. ICL is undoubtedly the strongest competitor, although its performance is far from optimal on some occasions. Method-independent methods like the ASW and the CH, which practitioners routinely use, sometimes completely miss the underlying structure. However, they selected meaningful solutions occasionally, depending on the underlying clustering structure. As already noted for the real data sets, the in-sample estimates QH and QS show a strong selection bias and variance for all data sets. All the methods based on cross-validation exhibit disappointing performances.

5 Conclusions and final remarks

We propose a novel method for selecting an appropriate clustering for a given data set, which is based on the notion of the quadratic score and pursues a general class of clusters. The proposed method allows selecting over a set of candidate partitions obtained with different clustering methods. An extensive comparative study showed that the proposed methodology is capable of a competing performance with respect to alternative existing methodologies. The main drawback of the proposed method is that it requires to fit the clusters on multiple bootstrap resamples, which can be computationally demanding for large data sets and/or when the collection of candidate partitions is large. Future research needs to tackle this issue and the study of theoretical guarantees for the bootstrap estimation not treated in the present contribution.

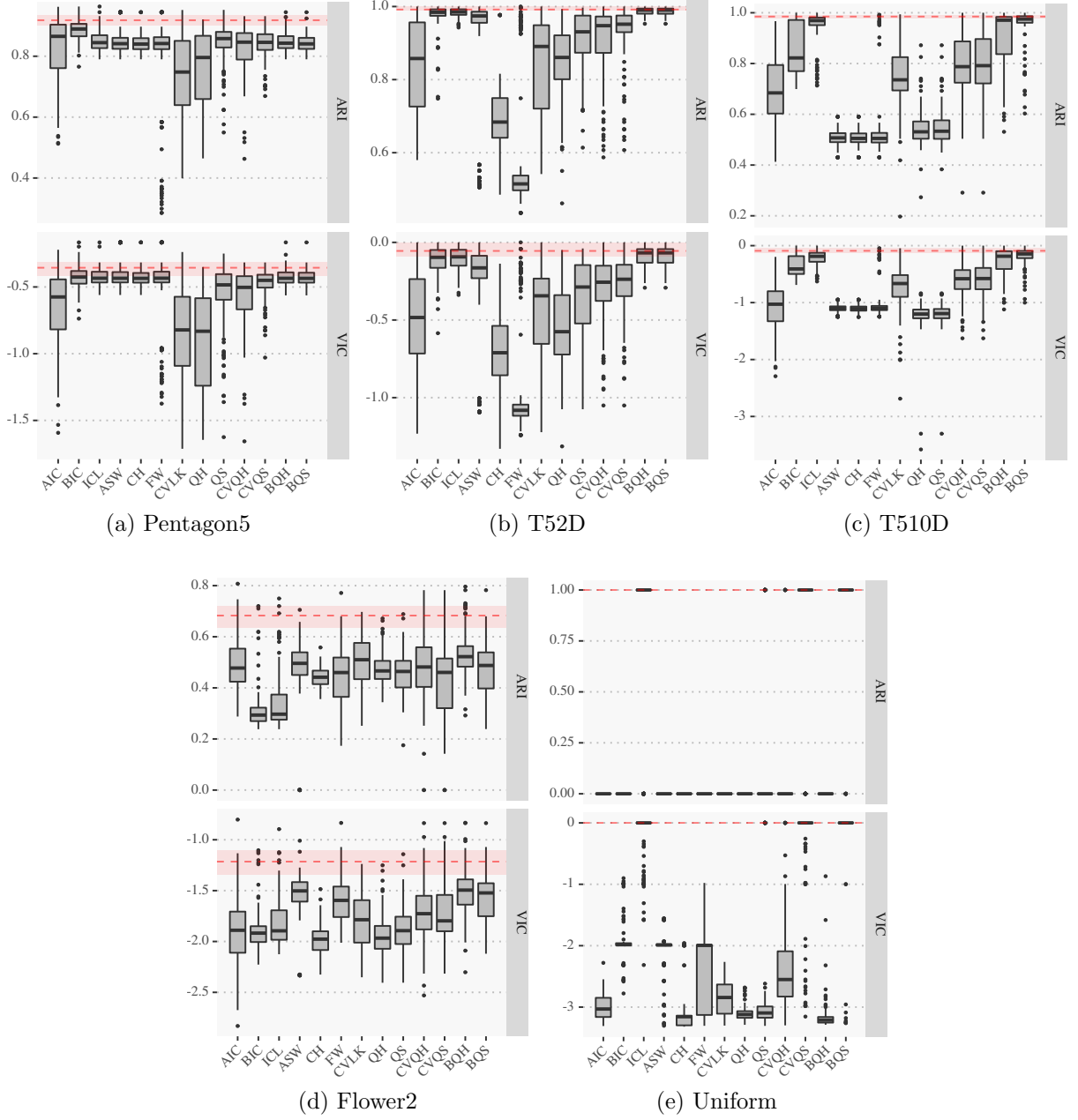


Figure 4: Boxplots of Monte Carlo distribution of ARI and VIC performance measures.

References

- Akaike, H. (1973). Information theory and an extension of the maximum likelihood principle. In *Second International Symposium on Information Theory (Tsahkadsor, 1971)*, pp. 267–281.
- Akhanli, S. E. and C. Hennig (2020). Comparing clusterings and numbers of clusters by aggregation of calibrated clustering validity indexes. *Statistics and Computing* 30(5), 1523–1544.
- Anderson, E. (1936). The Species Problem in Iris. *Annals of the Missouri Botanical Garden Vol.* 23(No. 3), 471–483.
- Bates, S., T. Hastie, and R. Tibshirani (2021). Cross-validation: what does it estimate and how well does it do it? ArXiv:2104.00673. Available at <https://arxiv.org/abs/2104.00673> (Accessed: 2021-05-31).
- Baudry, J.-P. (2015). Estimation and model selection for model-based clustering with the conditional classification likelihood. *Electronic Journal of Statistics* 9(1), 1041–1077.
- Ben-David, S., U. von Luxburg, and D. Pál (2006). A sober look at clustering stability. In G. Lugosi and H. U. Simon (Eds.), *Learning Theory*, Berlin, Heidelberg, pp. 5–19. Springer Berlin Heidelberg.
- Biernacki, C., G. Celeux, and G. Govaert (2000). Assessing a mixture model for clustering with the integrated completed likelihood. *IEEE transactions on pattern analysis and machine intelligence* 22(7), 719–725.
- Bouveyron, C., G. Celeux, T. B. Murphy, and A. E. Raftery (2019). *Model-based clustering and classification for data science*. Cambridge Series in Statistical and Probabilistic Mathematics. Cambridge University Press, Cambridge. With applications in R.

- Caliński, T. and J. Harabasz (1974). A dendrite method for cluster analysis. *Communications in Statistics-theory and Methods* 3(1), 1–27.
- Coretto, P. and C. Hennig (2017). Consistency, breakdown robustness, and algorithms for robust improper maximum likelihood clustering. *Journal of Machine Learning Research* 18(142), 1–39.
- Coretto, P. and C. Hennig (2021). *otrimle: Robust Model-Based Clustering*. R package version 2.0.
- Efron, B. and T. Hastie (2016). *Computer age statistical inference*, Volume 5 of *Institute of Mathematical Statistics (IMS) Monographs*. Cambridge University Press, New York. Algorithms, evidence, and data science.
- Fang, Y. and J. Wang (2012). Selection of the number of clusters via the bootstrap method. *Computational Statistics & Data Analysis* 56(3), 468–477.
- Fisher, R. A. (1936). The use of Multiple Measurements in Taxonomic Problems. *Annals of Eugenics*.
- Flury, B. and H. Riedwyl (1988). *Multivariate Statistics. A practical approach*. Chapman and Hall.
- Forina, M., C. Armanino, S. Lanteri, and E. Tiscornia (1983). Classification of olive oils from their fatty acid composition. *Food Research and Data Analysis* (January 1983), 189–214.
- Fraley, C. and A. E. Raftery (1998). How many clusters? which clustering method? answers via model-based cluster analysis. *The computer journal* 41(8), 578–588.
- Frühwirth-Schnatter, S., G. Celeux, and C. P. Robert (Eds.) (2019). *Handbook of mixture analysis*. Chapman & Hall/CRC Handbooks of Modern Statistical Methods. CRC Press, Boca Raton, FL.

- Fu, W. and P. O. Perry (2020). Estimating the number of clusters using cross-validation. *Journal of Computational and Graphical Statistics* 29(1), 162–173.
- Halkidi, M., M. Vazirgiannis, and C. Hennig (2015). Method-independent indices for cluster validation and estimating the number of clusters. In *Handbook of Cluster Analysis*, pp. 616–639. Chapman and Hall/CRC.
- Hastie, T. J. and M. Zhu (2001). Discussion of dimension reduction and visualization in discriminant analysis (with discussion), by Cook and Yin. *Australian & New Zealand Journal of Statistics* 43(2), 147–199.
- Hennig, C. (2007). Cluster-wise assessment of cluster stability. *Computational Statistics & Data Analysis* 52(1), 258–271.
- Hennig, C. (2015). Clustering strategy and method selection. In C. Hennig, M. Meila, F. Murtagh, and R. Rocci (Eds.), *Handbook of Cluster Analysis*, pp. 703–730. CRC Press.
- Hubert, L. and P. Arabie (1985). Comparing partitions. *Journal of classification* 2(1), 193–218.
- Keribin, C. (1998). Consistent estimate of the order of mixture models. *Comptes Rendus De L Academie Des Sciences Serie I-Mathematique* 326(2), 243–248.
- McLachlan, G. J. and D. Peel (2000). *Finite Mixture Models*. John Wiley & Sons, Inc.
- Mechelen, I. V., A.-L. Boulesteix, R. Dangl, N. Dean, I. Guyon, C. Hennig, F. Leisch, and D. Steinley (2018). Benchmarking in cluster analysis: A white paper. arXiv:1809.10496, available at <https://arxiv.org/abs/1809.10496>.
- Meilă, M. (2007). Comparing clusterings—an information based distance. *Journal of Multivariate Analysis* 98(5), 873–895.

- Nguyen, T. T., H. D. Nguyen, F. Chamroukhi, and G. J. McLachlan (2020). Approximation by finite mixtures of continuous density functions that vanish at infinity. *Cogent Mathematics & Statistics* 7(1), 1750861.
- Rousseeuw, P. J. and L. Kaufman (1990). Finding groups in data. *Hoboken: Wiley Online Library*.
- Scrucca, L., M. Fop, T. B. Murphy, and A. E. Raftery (2016). mclust 5: clustering, classification and density estimation using Gaussian finite mixture models. *The R Journal* 8(1), 205–233.
- Smyth, P. (2000). Model selection for probabilistic clustering using cross-validated likelihood. *Statistics and computing* 10(1), 63–72.
- Ullmann, T., C. Hennig, and A.-L. Boulesteix (2021). Validation of cluster analysis results on validation data: A systematic framework. arXiv:2103.01281. Preprint available at <https://arxiv.org/abs/2103.01281>.
- Velilla, S. and A. Hernández (2005). On the consistency properties of linear and quadratic discriminant analyses. *Journal of Multivariate Analysis* 96(2), 219–236.
- Von Luxburg, U., R. C. Williamson, and I. Guyon (2012). Clustering: Science or art? In *Proceedings of ICML workshop on unsupervised and transfer learning*, pp. 65–79. JMLR Workshop and Conference Proceedings.
- Wang, K., A. Ng, and G. J. McLachlan (2018). *EMMIXskew: The EM Algorithm and Skew Mixture Distribution*. R package version 1.0.3.

Supplemental Material

SELECTING THE NUMBER OF CLUSTERS, CLUSTERING MODELS, AND ALGORITHMS. A UNIFYING APPROACH BASED ON THE QUADRATIC DISCRIMINANT SCORE

Luca Coraggio*

Pietro Coretto†

Unless otherwise stated, the notation refers to the main paper file (PF). All cross-references to parts (sections, equations, etc.) in this file are prefixed with an “S”. Furthermore, all cross-references to elements defined in the paper file are postfixed with “-(PF)”.

Contents

S1 Iris data example	2
S2 Examples of Section 2.2-(PF)	5
S3 Proofs of statements of Section 2-(PF)	8
S4 Connections between sample scores and the Gaussian complete data likelihood	10
S5 Further details on the experimental analysis	11
S5.1 Clustering methods and algorithms	11
S5.2 Selection methods	15
S5.3 Data	20
S5.4 Real data sets	21
S5.5 Results for real data sets	21
S5.6 Sampling designs producing artificial data sets	28
S5.7 Monte Carlo experiments	30

*University of Naples “Federico II” (Italy) – E-mail: luca.coraggio@unina.it

†University of Salerno (Italy) – E-mail: pcoretto@unisa.it

S1 Iris data example

This section expands the description of the Iris example introduced in Section 1-(PF). The well-known Iris data set, first studied in [Anderson \(1936\)](#) and [Fisher \(1936\)](#), contains 50 samples from each of three species of Iris flowers, for a total of 150 samples; 4 numerical (continuous) features were measured on each sample. Figure [S1](#) shows the observed features and “true clusters” defined in terms of the Iris species. In Figure [S1b](#), true clusters are adequately captured by normal ellipsoids. The true groups can be captured by different methods, where not all of them are genuinely designed for discovering this type of cluster. In order to show that the number of groups, K , is not the only relevant choice to make, we set $K = 3$ (true value) for all of the following methods.

- k-means:** this partition is obtained with the classical algorithm of [Hartigan and Wong \(1979\)](#) approximating the K-means partition. The solution is calculated using the R-base package of [R Core Team \(2021\)](#).
- pam:** solution corresponding to the K-medoids partition with Euclidean dissimilarity. The partition is approximated with the PAM algorithm of [Kaufman and Rousseeuw \(1987\)](#) implemented in the `cluster` software of [Maechler et al. \(2019\)](#).
- gm-s:** clustering based on Maximum Likelihood (ML) estimation of finite Gaussian mixture models with covariance regularization based on the so-called eigen-ratio constraint. The eigen-ratio constraint is a constant $\gamma \in [1, +\infty)$ that bounds the maximum ratio between eigenvalues of all clusters’ covariance matrices. It controls the relative discrepancy between clusters’ scatters and ensures the existence and the consistency of the ML estimator (see [Coretto and Hennig, 2017](#)). Here we set $\gamma = 1$, which corresponds to the simplest model in terms of γ as it imposes spherical scatters for all clusters. Additional details on these methods are given in Section [S5](#). The numerical solution is obtained using the `otrimle` software of [Coretto and Hennig \(2021\)](#) implementing the ECM algorithm studied in [Coretto and Hennig \(2017\)](#).
- gm-c:** this setting is exactly equal to **gm-s**, except that $\gamma = 10^6$. Such a large value of γ produces little regularization allowing the covariance matrix parameters of the model to vary almost freely. This extremely large value of γ determines a model that is more flexible than **gm-s**; however, it exposes the algorithm to the risk of finding spurious clusters that are close to having a singular covariance matrix.
- tm-s:** clustering based on Maximum Likelihood (ML) estimation of Student-t mixture models with the possibility of choosing among several clusters’ covariance models ([Peel and McLachlan, 2000](#)). In this case, we choose the simplest covariance model: clusters’ covariance matrices are restricted to be equal and spherical. Computations are performed using the `EMMIXskew` software of [Wang et al. \(2018\)](#).

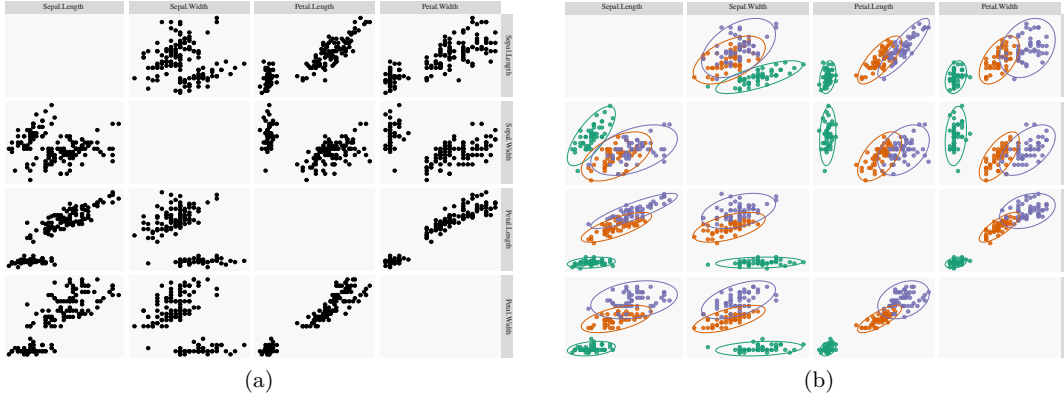


Figure S1: pairwise scatter plots of the Iris data. Panel (a): raw data scatters that does not use groups’ information. Panel (b): scatters with colors and 95%-normal ellipses identifying “true clusters” coinciding with the 3 Iris species. Normal ellipses are computed based on the within-group empirical mean and covariance matrix.

- tm-c:** this setting is exactly equal to **tm-s**, except that covariance matrices are not restricted to any model. As in the case of **gm-c**, this corresponds to a flexible parametrization that causes the risk of finding spurious singular groups.
- cfsfdp:** solution obtained with the “clustering by fast search and find of density peaks” (CFSFDP) algorithm of [Rodriguez and Laio \(2014\)](#) implemented into the densityClust software of [Pedersen et al. \(2017\)](#). The CFSFDP is a density-based algorithm. It requires two hyper-parameters used by the algorithm to determine K ; we followed the guidelines provided in [Rodriguez and Laio \(2014\)](#), setting the hyper-parameters to obtain three groups.
- dbscan:** this solution is obtained with the dbscan package of [Hahsler et al. \(2019\)](#) implementing the popular dbscan clustering algorithm of [Ester et al. \(1996\)](#). As in for the **cfsfdp**, dbscan also requires choosing two bandwidth-type hyper-parameters and a kernel function. The number of clusters K is determined by the algorithm which additionally may identify some data-points as noise. As for the **cfsfdp**, we set **dbscan** to obtain the best solution with $K = 3$.

The comparison involves 6 algorithms with a total of 8 different settings. Each of the two MBC algorithms are set up in order to pursue a simple (spherical solution) vs. a richer solution where cluster covariances are left free. Table S1 reports the agreement between all pairs of partitions including the true one. **kmean**, **pam**, **gm-s**, and **tm-s** produce the same partition shown in Figure S2a. Another partition that is rather close to the previous one is that produced by the **cfsfdp** method (see Figure S2b). The two partitions achieve the best agreement with the true partition (**cfsfdp** does marginally better).

Although **gm-c** and **tm-c** are methods that are specifically designed to capture elliptically-shaped clusters, their flexible covariance parametrization drives the algorithms towards excessive fitting in some regions of the data, completely missing the overall structure. The solution corresponding to **tm-c** can be seen in Figure S3a: one of the mixture components is almost singular, representing a single point so that the software ignores it. **gm-c** in Figure S3b does a better job because it returns three groups, but one of the mixture

Table S1: Agreement between pairs of partitions produced in the Iris example. The agreement is expressed as the percentage of data points assigned to the same group by both the row and the column method. For each pair, the agreement is computed with respect to the permutation of cluster labels resulting in the best match. The *Truth* column/row represents the partition corresponding to the true Iris species.

	Truth	k-means	pam	gm-s	gm-c	tm-s	tm-c	cfsfdp	dbscan
Truth		89.3%	89.3%	89.3%	66.7%	89.3%	66.7%	90.7%	68.7%
k-means	89.3%		100.0%	100.0%	74.7%	100.0%	74.7%	98.7%	75.3%
pam	89.3%	100.0%		100.0%	74.7%	100.0%	74.7%	98.7%	75.3%
gm-s	89.3%	100.0%	100.0%		74.7%	100.0%	74.7%	98.7%	75.3%
gm-c	66.7%	74.7%	74.7%	74.7%		74.7%	86.0%	76.0%	86.0%
tm-s	89.3%	100.0%	100.0%	100.0%	74.7%		74.7%	98.7%	75.3%
tm-c	66.7%	74.7%	74.7%	74.7%	86.0%	74.7%		76.0%	88.7%
cfsfdp	90.7%	98.7%	98.7%	98.7%	76.0%	98.7%	76.0%		76.7%
dbscan	68.7%	75.3%	75.3%	75.3%	86.0%	75.3%	88.7%	76.7%	

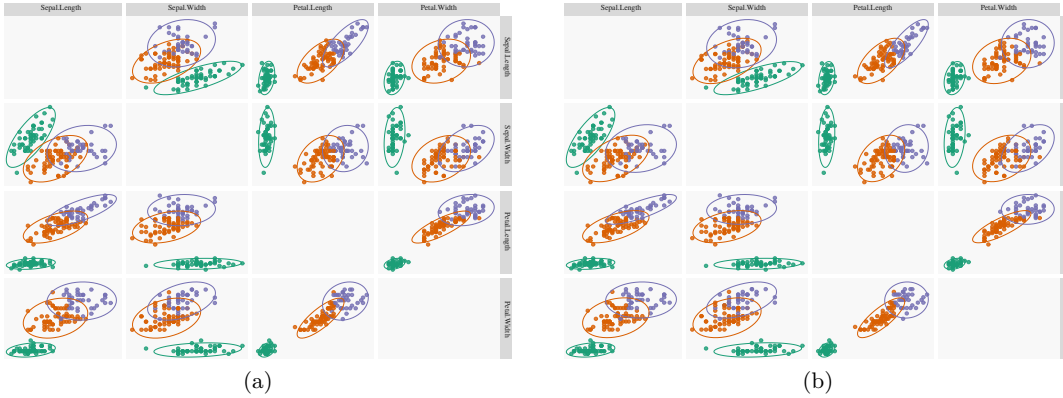


Figure S2: Iris data clustering. Panel (a): clustering solutions obtained from **k-mean**, **pam**, **gm-s**, and **tm-s** methods. Panel (b): clustering solution obtained from the **cfsfdb** method.

components fits a concentrated portion of points in the center of one of the original clusters, splitting it into two clusters, and merges the remaining two original clusters. The **dbscan** solution finds a large proportion of noise, messing all the clusters.

We draw two important conclusions from this example.

- Different algorithms can lead to the same partition. This is not surprising because algorithms built around different principles can target similar cluster notions. For example, **kmean** and **pam** (with Euclidean dissimilarity) are very similar, and they tempt to pursue balanced spherical clusters. Since the Student-t model includes the Gaussian model, **tm-s** can be seen as more general version of **gm-s**. Both **tm-s** and **gm-s** pursue spherical groups, although not necessarily balanced groups. Generally, the K-means partition is formalized as the solution to a partitioning problem but has a strong connection with model-based methods. The seminal paper of [Pollard \(1981\)](#) showed that the K-means partition solves the ML problem for a population probability model with homoscedastic equally weighted Gaussian groups. In general,

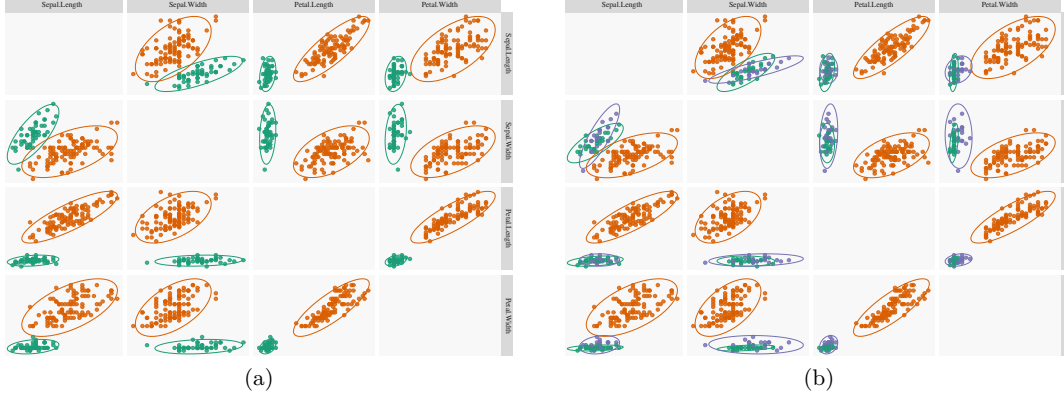


Figure S3: Iris data clustering. Panel (a): clustering solutions obtained from **tm-c** method. Panel (b): clustering solution obtained from the **gm-c** method.

what **kmean**, **pam**, **tm-s** and **gm-s** have in common is that they are able to find groups that can be separated by linear shapes. Nevertheless, these groups form dense regions that can also be found with the completely different **cfsfdp** method.

- The second conclusion is that methods' flexibility in representing the data structure is a key factor. In principle, **gm-c** and **tm-c** are the strongest candidates to capture the true clusters in the example: as shown in Figure S1b, true clusters are well described by elliptical regions, and both **gm-c** and **tm-c** are specifically designed to capture these kind of structures. However, the high flexibility of the clusters' covariance matrix models in **gm-c** and **tm-c** produced an excessive fitting in some regions of the data. For some of these methods, there is a clear notion of flexibility because this is mapped into the underlying model complexity. However, for methods that are not genuinely formalized in terms of a generating model, it is not straightforward to think about the complexity of the data structures that a certain method can handle. The complexity is usually tuned by the methods' hyper-parameters. This happens for example for the two density-based algorithms considered here, namely **cfsfdp** and **dbscan**. In clustering problems, K is certainly the major source of the complexity level at which we are willing to describe the data; however, most methods have additional hyper-parameters that can strongly interact with K for obtaining a certain result.

S2 Examples of Section 2.2-(PF)

In this section, we give more details about the definitions and the calculations of $H(\cdot)$ and $T(\cdot)$ for the dgpG and dgpU examples in Section 2.2-(PF).

For each value of d , we have a different generating distribution function, F_d , that is a mixture of: two Gaussian components in dgpG; two uniform components in dgpU. At each d , we compare the population version of the score for two alternative cluster configurations $\{\theta^{(1)}, \theta^{(2)}\}$, where $K(\theta^{(1)}) = 1$ and $K(\theta^{(2)}) = 2$. The number of possible choices of such configurations is infinite. Hence, we compare two possible specifications, $\theta^{(1)}$ and $\theta^{(2)}$, that try to reflect the group-conditional distributions corresponding to F_d .

The problem here is that the two types of F_d considered in the example are not always a function of cluster configuration parameters as defined in Section 2.1-(PF). In the dgpG case with $K = 2$, the generating distribution F_d is exactly specified in terms of proportion, mean and covariance parameters of the two Gaussian components. However, for all the remaining cases, this is not true. For example, in the dgpG case with $K = 1$, we need to define $\boldsymbol{\theta}^{(1)} = (\pi^{(m)}, \boldsymbol{\mu}^{(m)}, \boldsymbol{\Sigma}^{(m)})$ that does not coincide with the parameters of the corresponding F_d . In each case, we defined competing cluster configuration parameters to provide the best description of the group-conditional distributions.

- **Cases dgpG and dgpU with $K = 1$.** We set $\boldsymbol{\theta}^{(1)} = (\pi_1^{(1)}, \boldsymbol{\mu}^{(1)}, \boldsymbol{\Sigma}^{(1)})$ as follows

$$\begin{aligned}\pi_1^{(1)} &= 1, \\ \boldsymbol{\mu}^{(1)} &= \int \mathbf{x} dF_d, \\ \boldsymbol{\Sigma}^{(1)} &= \int (\mathbf{x} - \boldsymbol{\mu}^{(1)}) (\mathbf{x} - \boldsymbol{\mu}^{(1)})^\top dF_d.\end{aligned}\tag{S1}$$

- **Case dgpG when $K = 2$.** This is the easiest case, because as previously noted, the parameters of F_d coincides with the parameters of the two groups. In this case, $\boldsymbol{\theta}^{(2)}$ is defined as follows

$$\begin{aligned}\pi_1^{(2)} &= \pi_2^{(2)} = 0.5, \\ \boldsymbol{\mu}_1^{(2)} &= (0, 0)^\top, \\ \boldsymbol{\mu}_2^{(2)} &= (d, 0)^\top, \\ \boldsymbol{\Sigma}_1^{(2)} &= \boldsymbol{\Sigma}_2^{(2)} = \begin{pmatrix} 1 & 0 \\ 0 & 1 \end{pmatrix}.\end{aligned}\tag{S2}$$

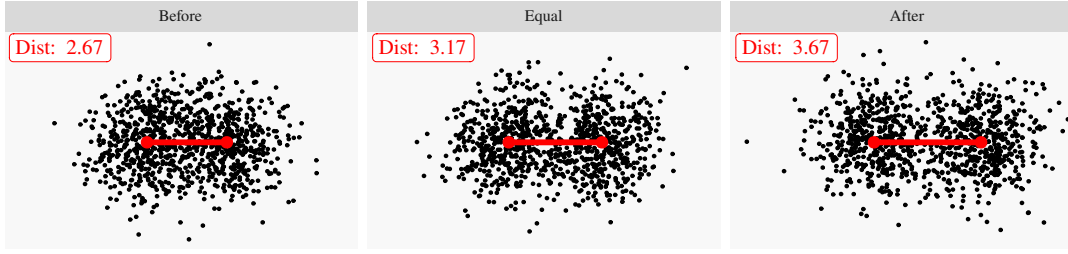
- **Case dgpU when $K = 2$.** The main problem for this case is that a uniform distribution is not a function of a scatter parameter. Both uniform components in dgpU have the same volume and, apart from their center, they would produce the same scatter of points. First, we computed

$$\mathbf{V}_U = \int \mathbf{x} \mathbf{x}^\top dU,$$

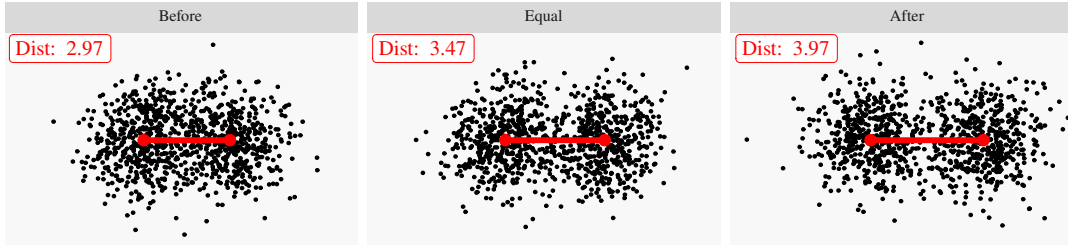
where U is the distribution function of a random variable X uniformly distributed on the square $[-1, 1]^2$. \mathbf{V}_U would be the covariance of such X . The parameter $\boldsymbol{\theta}^{(2)}$ is set as follows

$$\begin{aligned}\pi_1^{(2)} &= \pi_2^{(2)} = 0.5, \\ \boldsymbol{\mu}_1^{(2)} &= (0, 0)^\top, \\ \boldsymbol{\mu}_2^{(2)} &= (d, 0)^\top, \\ \boldsymbol{\Sigma}_1^{(2)} &= \boldsymbol{\Sigma}_2^{(2)} = \mathbf{V}_U.\end{aligned}\tag{S3}$$

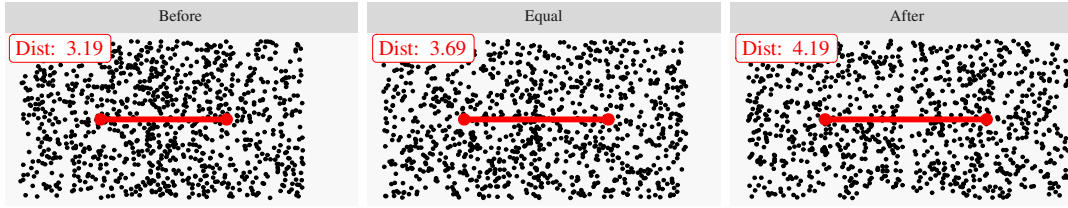
Since some of the previous integrals, including those defining $H(\cdot)$ and $T(\cdot)$, can not be calculated analytically we computed their approximation (for each value of d) using Monte Carlo integration; all the integrals involved in the example are computed on completely independent experiments with 10^6 random draws. Each integral has been computed 100 times, and the results were averaged to obtain a Monte Carlo standard error consistently



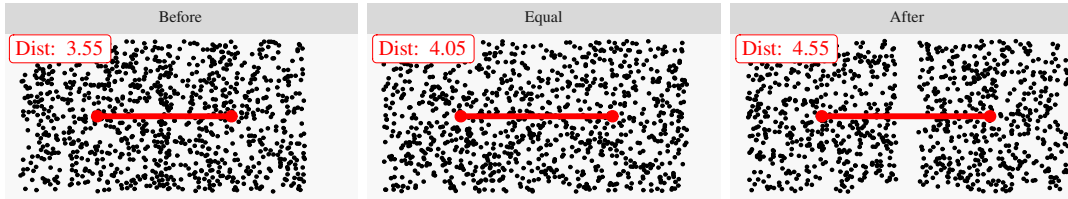
(a) dgpG; Hard Score



(b) dgpG; Smooth Score



(c) dgpU; Hard Score



(d) dgpU; Smooth Score

Figure S4: Scatter plots of data sampled under the dgpG and dgpU sampling designs of the example in Section 2.2-(PF). In each of the four row panels (a)–(d), we show the same sample design for three different values of d : the center plot refers to a value of d such that the criterion ($H(\cdot)$ or $T(\cdot)$) values both cases (i.e. $K = 1$ and $K = 2$) equally; the left plot refers to a value of d , where the criterion prefers $K = 1$; the right plot refers to a value of d , where the criterion prefers $K = 2$. Panels (a) and (b) represents the dgpG design, while panels (c) and (d) represent the dgpU design. The behavior of the hard scoring is shown in panels (a) and (c). Panels (b) and (d) refer to the smooth score criterion.

below 10^{-5} . Figure S4 shows examples of data produced by the two sampling designs around the point d where each of the two criteria splits a single cluster into two clusters. For each case, we calculated the value d at which a scoring criterion is indifferent between $K = 1$ and $K = 2$; each raw panel of Figure S4 shows data examples slightly before this point, where the criteria prefer $K = 1$, and just after this point, where the criteria prefer $K = 2$.

S3 Proofs of statements of Section 2-(PF)

Proof of Proposition 1. The problem is the analogue of showing the optimality of the Bayes classifier. However, this is conceptually different due to the unsupervised nature of the clustering problem, where a natural notion of loss does not exist. Consider any partition $\{A_k, k = 1, 2, \dots, K\}$, then

$$\begin{aligned} \Pr\left\{\bigcup_{k=1}^K \{Z_k = 1 \cap X \in A_k\}\right\} &= \sum_{k=1}^K \Pr\{Z_k = 1\} \Pr\{X \in A_k \mid Z_k = 1\}, \\ &= \sum_{k=1}^K \int_{A_k} \pi_k f(\mathbf{x}; \boldsymbol{\mu}_k, \boldsymbol{\Sigma}_k) d\mathbf{x}. \end{aligned} \quad (\text{S4})$$

In order to maximize (S4) it suffices to choose the partition $\{A_k^*, k = 1, 2, \dots, K\}$

$$A_k^* = \left\{ \mathbf{x} \in \mathbb{R}^p : \pi_k f(\mathbf{x}; \boldsymbol{\mu}_k, \boldsymbol{\Sigma}_k) = \max_{1 \leq j \leq K} \pi_j f(\mathbf{x}; \boldsymbol{\mu}_j, \boldsymbol{\Sigma}_j) \right\}.$$

Under (C1), $\pi_k f(\mathbf{x}; \boldsymbol{\mu}_k, \boldsymbol{\Sigma}_k) = \pi_k \phi(\mathbf{x}; \boldsymbol{\mu}_k, \boldsymbol{\Sigma}_k)$, and it is immediate to see that A_k^* coincides with Q_k , proving (4)-(PF). Denote $\delta_k = (\mathbf{x} - \boldsymbol{\mu}_k)^\top \boldsymbol{\Sigma}_k^{-1} (\mathbf{x} - \boldsymbol{\mu}_k)$. Since both $g(t)$ and $\exp(-t/2)$ are monotonically decreasing for $t \in [0, +\infty)$, under (C2), for any $\mathbf{x} \in \mathbb{R}^p$,

$$\begin{aligned} \pi_k f(\mathbf{x}; \boldsymbol{\mu}_k, \boldsymbol{\Sigma}_k) \geq \max_{1 \leq j \leq K} \pi_j f(\mathbf{x}; \boldsymbol{\mu}_j, \boldsymbol{\Sigma}_j) &\iff g(\delta_k) \geq \max_{1 \leq j \leq K} \{g(\delta_j)\}, \\ &\iff \exp(-\delta_k/2) \geq \max_{1 \leq j \leq K} \{\exp(-\delta_j/2)\}, \\ &\iff \text{qs}(\mathbf{x}, \boldsymbol{\theta}_k^{(m)}) \geq \max_{1 \leq j \leq K} \{\text{qs}(\mathbf{x}, \boldsymbol{\theta}_j^{(m)})\}. \end{aligned}$$

Which means that $A_k^* = Q_k(\boldsymbol{\theta}) \in \mathcal{Q}(\boldsymbol{\theta})$ for all $k \in 1, 2, \dots, K$. \square

Proof of Proposition 2. First, note that

$$\text{qs}(\mathbf{x}, \boldsymbol{\theta}_k^{(m)}) = c + \log(\pi_k^{(m)} \phi(\mathbf{x}; \boldsymbol{\mu}_k^{(m)}, \boldsymbol{\Sigma}_k^{(m)})),$$

where $c = p \log(\sqrt{2\pi})/2$, with π here being the mathematical constant. Since $\sum_{k=1}^{K(\boldsymbol{\theta}^{(m)})} \int_{Q_k(\boldsymbol{\theta}^{(m)})} c dF = c$, then

$$H(\boldsymbol{\theta}^{(m)}) = c + \sum_{k=1}^{K(\boldsymbol{\theta}^{(m)})} \int_{Q_k(\boldsymbol{\theta}^{(m)})} \log(\pi_k^{(m)}) dF + \sum_{k=1}^{K(\boldsymbol{\theta}^{(m)})} \int_{Q_k(\boldsymbol{\theta}^{(m)})} \log(\phi(\mathbf{x}; \boldsymbol{\mu}_k^{(m)}, \boldsymbol{\Sigma}_k^{(m)})) dF. \quad (\text{S5})$$

Using the first expression in (9)-(PF) we can write

$$\sum_{k=1}^{K(\boldsymbol{\theta}^{(m)})} \int_{Q_k(\boldsymbol{\theta}^{(m)})} \log(\pi_k^{(m)}) dF = L(\boldsymbol{\theta}^{(m)}) - \sum_{k=1}^{K(\boldsymbol{\theta}^{(m)})} \int_{Q_k(\boldsymbol{\theta}^{(m)})} \log(f(\mathbf{x}; \boldsymbol{\mu}_k^{(m)}, \boldsymbol{\Sigma}_k^{(m)})) dF.$$

Replace the right-hand side of the previous equation into (S5) to obtain (10)-(PF). Under (C3), for any choice of $\boldsymbol{\theta}^{(m)}$ and k ,

$$\int_{Q_k(\boldsymbol{\theta}^{(m)})} \log \left(\frac{f(\mathbf{x}; \boldsymbol{\mu}_k^{(m)}, \boldsymbol{\Sigma}_k^{(m)})}{\phi(\mathbf{x}; \boldsymbol{\mu}_k^{(m)}, \boldsymbol{\Sigma}_k^{(m)})} \right) dF \geq 0,$$

which proves that $\Lambda(\boldsymbol{\theta}^{(m)}) \geq 0$. \square

Proof of Proposition 3. The posterior weights (15)-(PF) under the Gaussian group-conditional model coincide with the smooth score weights, in fact

$$\omega_{\phi,k}(\mathbf{x}; \boldsymbol{\theta}^{(m)}) = \frac{\pi_k^{(m)} \phi(\mathbf{x}; \boldsymbol{\mu}_k^{(m)}, \boldsymbol{\Sigma}_k^{(m)})}{\sum_{k=1}^{K(\boldsymbol{\theta}^{(m)})} \pi_k^{(m)} \phi(\mathbf{x}; \boldsymbol{\mu}_k^{(m)}, \boldsymbol{\Sigma}_k^{(m)})} = \tau_k(\mathbf{x}; \boldsymbol{\theta}^{(m)})$$

for all k . Use the same arguments as in the proof of Proposition 2 and write

$$T(\boldsymbol{\theta}^{(m)}) = c + \sum_{k=1}^{K(\boldsymbol{\theta}^{(m)})} \int \omega_{\phi,k}(\mathbf{x}; \boldsymbol{\theta}^{(m)}) \log(\pi_k^{(m)} \phi(\mathbf{x}; \boldsymbol{\mu}_k^{(m)}, \boldsymbol{\Sigma}_k^{(m)})) dF, \quad (\text{S6})$$

for an appropriate constant c that does not depend on $\boldsymbol{\theta}^{(m)}$. Since $\sum_{k=1}^{K(\boldsymbol{\theta}^{(m)})} \omega_{\phi,k}(\mathbf{x}; \boldsymbol{\theta}^{(m)}) = 1$, the right-hand-side of (S6), neglecting the constant term, can be expressed as

$$\sum_{k=1}^{K(\boldsymbol{\theta}^{(m)})} \int \omega_{\phi,k}(\mathbf{x}; \boldsymbol{\theta}^{(m)}) \log(\pi_k^{(m)} \phi(\mathbf{x}; \boldsymbol{\mu}_k^{(m)}, \boldsymbol{\Sigma}_k^{(m)})) dF = A(\boldsymbol{\theta}^{(m)}) - B(\boldsymbol{\theta}^{(m)}), \quad (\text{S7})$$

where

$$A(\boldsymbol{\theta}^{(m)}) = \int \log(\psi_\phi(\mathbf{x}; \boldsymbol{\theta}^{(m)})) dF = \int \log \left(\sum_{k=1}^{K(\boldsymbol{\theta}^{(m)})} \pi_k^{(m)} \phi(\mathbf{x}; \boldsymbol{\mu}_k^{(m)}, \boldsymbol{\Sigma}_k^{(m)}) \right) dF, \quad (\text{S8})$$

and

$$B(\boldsymbol{\theta}^{(m)}) = - \sum_{k=1}^{K(\boldsymbol{\theta}^{(m)})} \int \omega_{\phi,k}(\mathbf{x}; \boldsymbol{\theta}^{(m)}) \log \omega_{\phi,k}(\mathbf{x}; \boldsymbol{\theta}^{(m)}) dF. \quad (\text{S9})$$

The term $A(\boldsymbol{\theta}^{(m)})$ is the expected log-likelihood under the Gaussian mixture model. Since f_0 by assumption is the density of F , then

$$A(\boldsymbol{\theta}^{(m)}) = -\text{d}_{\text{KL}}(f_0 \parallel \psi(\cdot; \boldsymbol{\theta}^{(m)})) + \int \log(f_0(\mathbf{x})) dF,$$

where the last integral depends only on unknown population objects, and therefore does not depend on $\boldsymbol{\theta}^{(m)}$. (S9) is the expectation under F of

$$\text{ent}_\phi(Z \mid X; \boldsymbol{\theta}^{(m)}) = - \sum_{k=1}^{K(\boldsymbol{\theta}^{(m)})} \omega_{\phi,k}(X; \boldsymbol{\theta}^{(m)}) \log \left(\omega_{\phi,k}(X; \boldsymbol{\theta}^{(m)}) \right).$$

We can now conclude that

$$\begin{aligned} \arg \max_{1 \leq m \leq M} S(\boldsymbol{\theta}^{(m)}) &= \arg \max_{1 \leq m \leq M} A(\boldsymbol{\theta}^{(m)}) - B(\boldsymbol{\theta}^{(m)}), \\ &= \arg \min_{1 \leq m \leq M} \text{d}_{\text{KL}}(f_0 \parallel \psi(\cdot; \boldsymbol{\theta}^{(m)})) + \mathbb{E}_F[\text{ent}_\phi(\boldsymbol{\theta}^{(m)})]. \end{aligned}$$

The latter proves the desired result (S10). \square

S4 Connections between sample scores and the Gaussian complete data likelihood

In model-based clustering, there are two approaches to fit the unknown mixture parameters of a model like (14)-(PF). These approaches correspond to the maximization of one of the following log-likelihood functions:

$$\text{lik}_{f,n}(\boldsymbol{\theta}) = \sum_{i=1}^n \log(\psi_f(\mathbf{x}_i; \boldsymbol{\theta})), \quad \text{klik}_{f,n}(\boldsymbol{\theta}) = \sum_{i=1}^n \sum_{k=1}^K Z_{ik} \log(\pi_k f(\mathbf{x}_i; \boldsymbol{\theta}_k)). \quad (\text{S10})$$

$\text{lik}_{f,n}(\cdot)$ is the log-likelihood function for the mixture model $\psi_f(\cdot)$; $\text{klik}_{f,n}(\cdot)$ is the so-called *complete-data* log-likelihood function where, in practice, the memberships indicators $\{Z_{ik}\}$ are treated as missing data and replaced with (16)-(PF). Maximization of $\text{klik}_{f,n}(\cdot)$ leads to inconsistent mixture parameters estimates but, as expected, produces more separated groups (see Fröhlich-Schnatter et al., 2019, and references therein).

Proposition 4. *Let $\text{lik}_{\phi,n}(\cdot)$ and $\text{klik}_{\phi,n}(\cdot)$ be respectively the log-likelihood and the complete-data log-likelihood function under the Gaussian group-conditional model. The following hold*

$$\arg \max_{1 \leq m \leq M} H_n(\boldsymbol{\theta}^{(m)}) = \arg \max_{1 \leq m \leq M} \max_{\{Z_{ik}\}} \text{klik}_{\phi,n}(\boldsymbol{\theta}^{(m)}), \quad (\text{S11})$$

$$\arg \max_{1 \leq m \leq M} T_n(\boldsymbol{\theta}^{(m)}) = \arg \max_{1 \leq m \leq M} \mathbb{E}[\text{klik}_{\phi,n}(\boldsymbol{\theta}^{(m)}) \mid \mathbb{X}_n], \quad (\text{S12})$$

Proof. The optimal replacement of $\{Z_{ik}\}$ is given by the MAP assignment (16)-(PF), that is

$$\max_{\{Z_{ik}\}} \text{klik}_{\phi,n}(\boldsymbol{\theta}^{(m)}) = \sum_{i=1}^n \sum_{k=1}^{K(\boldsymbol{\theta}^{(m)})} \hat{z}_k(\mathbf{x}_i; \boldsymbol{\theta}^{(m)}) \log \left(\pi_k^{(m)} \phi(\mathbf{x}_i; \boldsymbol{\mu}_k^{(m)}, \boldsymbol{\Sigma}_k^{(m)}) \right);$$

the latter is at the basis of the EM algorithm for the maximization of the classification likelihood (McLachlan and Krishnan, 2007). Under the Gaussian group-conditional model, $\hat{z}_k(\mathbf{x}_i; \boldsymbol{\theta}^{(m)}) = \mathbb{I}\{\mathbf{x}_i \in Q_k(\boldsymbol{\theta})\}$. Using the fact that $\text{qs}(\mathbf{x}_i; \boldsymbol{\theta}_k^{(m)}) = c + \log(\pi_k \phi(\mathbf{x}_i; \boldsymbol{\mu}_k, \boldsymbol{\Sigma}_k))$

with $c = p \log(\sqrt{2\pi})/2$, we obtain

$$\begin{aligned} \max_{\{Z_{ik}\}} \text{clik}_{\phi,n}(\boldsymbol{\theta}^{(m)}) &= \sum_{i=1}^n \sum_{k=1}^{K(\boldsymbol{\theta}^{(m)})} \hat{z}_k(\mathbf{x}_i; \boldsymbol{\theta}^{(m)}) \log \left(\pi_k^{(m)} \phi(\mathbf{x}_i; \boldsymbol{\mu}_k^{(m)}, \boldsymbol{\Sigma}_k^{(m)}) \right), \\ &= \sum_{i=1}^n \sum_{k=1}^{K(\boldsymbol{\theta}^{(m)})} \mathbb{I}\{\mathbf{x}_i \in Q_k(\boldsymbol{\theta})\} \left(\text{qs}(\mathbf{x}_i; \boldsymbol{\theta}_k^{(m)}) - c \right), \\ &= H_n(\boldsymbol{\theta}^{(m)}) - nc. \end{aligned}$$

The previous expression proves (S11). Now observe that under the Gaussian assumption the posterior weights, $\omega(\cdot)$, would coincide with the $\tau(\cdot)$ weights, therefore

$$\begin{aligned} \mathbb{E} \left[\text{clik}_{\phi,n}(\boldsymbol{\theta}^{(m)}) \mid \mathbb{X}_n \right] &= \sum_{i=1}^n \sum_{k=1}^{K(\boldsymbol{\theta}^{(m)})} \mathbb{E}[Z_{ik} | \mathbb{X}_n] \log \left(\pi_k^{(m)} \phi(\mathbf{x}_i; \boldsymbol{\mu}_k^{(m)}, \boldsymbol{\Sigma}_k^{(m)}) \right), \\ &= \sum_{i=1}^n \sum_{k=1}^{K(\boldsymbol{\theta}^{(m)})} \tau_k(\mathbf{x}_i; \boldsymbol{\theta}^{(m)}) \log \left(\pi_k^{(m)} \phi(\mathbf{x}_i; \boldsymbol{\mu}_k^{(m)}, \boldsymbol{\Sigma}_k^{(m)}) \right), \\ &= \sum_{i=1}^n \sum_{k=1}^{K(\boldsymbol{\theta}^{(m)})} \tau_k(\mathbf{x}_i; \boldsymbol{\theta}^{(m)}) \left(\text{qs}(\mathbf{x}_i; \boldsymbol{\theta}_k^{(m)}) - c \right) \\ &= T_n(\boldsymbol{\theta}^{(m)}) - nc, \end{aligned}$$

which proves (S12). □

S5 Further details on the experimental analysis

In this section, we provide additional details on the experimental setting presented in Section 4-(PF).

S5.1 Clustering methods and algorithms

The 440 clustering configurations under comparison are obtained using two main approaches: distance-based clustering and model-based clustering. A clustering method, $m \in \mathcal{M}$, specifies the clustering algorithm together with its required settings: number of clusters $K(m)$, the m -th method's hyper-parameters and, eventually, its algorithmic tunings. Table S2 summarizes the clustering methods aggregated by algorithms and credits the software via which they are implemented. In what follows, we describe used methods in greater details.

Distance-based clustering. We consider the two most popular partitioning distance-based methods: K-means and K-medoids. In the K-means problem, the target cost function coincides with the total within-cluster dissimilarity defined in terms of squared Euclidean distance. The K-medoids allows specifying different notions of dissimilarity and,

Table S2: Clustering methods in the experimental analysis. The total number of models (“#Models”) for each algorithm is obtained combining “#K” and “Other configurations”.

Algorithm	Clustering strategy	#Models	#K	Other configurations	Software
K-means	Distance-based	10	1-10		R Core Team (2021)
K-medoids	Distance-based	10	1-10		Maechler et al. (2019)
Mclust	Gaussian mixtures	140	1-10	14 Covariance parametrizations (Celeux and Govaert (1995))	Scrucca et al. (2016)
Rimle	Gaussian mixtures	180	1-10	$\gamma \in \{1, 5, 10, 100, 1000, 10000\}$; 3 initialization methods.	Coretto and Hennig (2017) , Coretto and Hennig (2016) , Coretto and Hennig (2021) .
Emmix	t-student mixtures	100	1-10	5 Covariance parametrizations; skewed and not-skewed t-distributions	Wang et al. (2018)

for this study, we choose the squared Euclidean distance. The solutions corresponding to K-mean and K-medoids are obtained with the same software implementation used for the Iris example in Section S1. For these two algorithms only $K \in \{1, 2, \dots, 10\}$ varies across each configuration, therefore we have 10 solutions for each of them.

Model-based clustering (MBC). The remaining methods use an MBC approach. We briefly review the main MBC’s ideas and methodologies. It is assumed that X_i has a finite mixture distribution with density function (14)-(PF). The idea is to fit the unknown parameter θ and to assign observed points to the clusters using the MAP rule (16)-(PF). The rationale behind the MAP rule is that if the model specification is correct, then the MAP assignment ensures the best possible misclassification rate. The most popular method to fit θ is the ML method, where one maximizes a likelihood function as those in (S10). The MBC methods in \mathcal{M} all maximize a log-likelihood function $\text{lik}_n(\cdot)$.

The centrality of ML estimation into the MBC methodology is probably because the maximization of (S10) can be conveniently solved by numerical procedures from the general class of Expectation-Maximization (EM) algorithms of [Dempster et al. \(1977\)](#). Solutions corresponding to MBC methods considered here are based on the Gaussian and Student-t group-conditional model. In both cases, there are two main issues with the ML estimation:

- *Unboundedness of the likelihood:* [Kiefer and Wolfowitz \(1956\)](#) discovered that, for one-dimensional Gaussian mixtures, the likelihood function could be made arbitrarily large by taking one or more components’ variances arbitrarily small. The same issue extends to the multivariate case for a large class of location-scale families, including the Gaussian and the Student-t distribution. The ML optimization requires constraints that prevent the groups’ covariance matrix from degenerating. Several approaches have been proposed in the literature, and the three MBC methods considered here tackle this problem from different perspectives. The unbounded likelihood is essentially a mathematical problem that requires a fix to develop a well-working optimization software. However, all the fixes proposed in the literature result in covariance matrix constraints that, in practice, control the complexity of the underlying model with a significant impact on the clustering.
- *Excessive number of free parameters:* for both Gaussian and Student-t mixtures, the number of free parameters to be estimated grows rather quickly for increasing p and K . This is essentially due to the large number of parameters needed to fill each of the covariances matrices. Indeed, each Σ_k contains $(p^2 + p)/2$ parameters. Let $\nu(\theta)$ be the number of mixture parameters. When the ratio $n/\nu(\theta)$ is small, the ML esti-

mator becomes highly variable, increasing the chance to fit spurious clusters. There exist MBC implementations that allow a choice between parsimonious parametrization of the covariance matrices. These parametrizations imply constraints on the between-clusters shapes that strongly affect the clustering. As for the solution of the unboundedness problem above, although the motivation for these constraints is to solve a technical problem, they modify the underlying model complexity.

The MBC configurations considered in \mathcal{M} correspond to three different MBC strategies that we name after the software implementing them; these are: MCLUST, RIMLE and EMMIX.

Mclust. The popular `mclust` software of [Scrucca et al. \(2016\)](#) performs MBC based on ML estimation of Gaussian mixtures. Regarding the unboundedness of the likelihood function, `Mclust` does not allow the user to tune the covariance regularization. The underlying EM algorithm includes a step where a lower bound for the minimum determinant across the covariance matrices is determined from the data using the Bayes regularization method proposed in [Fraley and Raftery \(2007\)](#). On the other hand, `Mclust` allows the user to specify a covariance matrix model from a list of 14 available models proposed in [Celeux and Govaert \(1995\)](#). The covariance matrix of the k -th mixture component is decomposed as

$$\Sigma_k = \lambda_k \mathbf{D}_k \mathbf{A}_k \mathbf{D}_k^T, \quad (\text{S13})$$

where $\lambda_k = \det(\Sigma_k)^{1/p}$, \mathbf{A}_k is the diagonal matrix of the normalized eigenvalues sorted in decreasing order and \mathbf{D}_k is the matrix of the corresponding eigenvectors. The factors of the decomposition model control geometrical aspects of the k -th within-cluster scatter: volume, orientation and shape. The parametrizations available in `Mclust` are reported in Table S3; they range from the strongest restriction $\Sigma_k = \lambda \mathbf{I}$ for all $k = 1, 2, \dots, K$, implying the same spherical scatter for all groups, to the unrestricted case where all members of the decomposition (S13) vary unrestricted across clusters. Note that each model in Table S3 assumes a certain restriction for the between-cluster scatter discrepancy (except for the *full* model corresponding to the last row of the table). `Mclust` does not allow to control the initial partition, and the members of \mathcal{M} corresponding to the MCLUST configurations varies for K and the covariance model. The combination of $K \in \{1, 2, \dots, 10\}$ and the 14 covariance models leads to a total of 140 MCLUST specifications. The naming of the MCLUST configurations in the Table 1-(PF) uses the short nomenclature in the last column of Table S3.

Rimle. As an alternative way of restricting the scatter parameters of mixtures of Gaussians, we introduce solutions computed using the `rimle` function from the `otrimle` software of [Coretto and Hennig \(2021\)](#). This setup was already considered for the Iris data example in Section S1. The `otrimle` software performs robust cluster analysis for data sets affected by outliers and noise, and it implements the methods developed in [Coretto and Hennig \(2016\)](#) and [Coretto and Hennig \(2017\)](#). The data are modeled by a mixture of Gaussian distributions and a noise component: an improper uniform distribution over the Euclidean space. Setting the parameter $\delta = 0$ in [Coretto and Hennig \(2017\)](#) (corresponding to `logicd = -Inf` into the `rimle` software), one can fit a plain Gaussian mixture where the unboundedness of the likelihood function is regularized based on the so-called eigen-ratio constraint (ERC).

Table S3: Covariance matrix models available in `Mclust`. If a member of the right-hand side of (S13) has a subscript k , it means that it is allowed to vary across clusters. Elements of Σ_k not having a subscript k are restricted to be equal across the K groups. p is data dimensionality. α counts the number of parameters other than those in covariance matrices, i.e. means μ 's and mixing proportions π 's; $\alpha = Kp + K - 1$; if mixing proportions are restricted to be equal, $\alpha = Kp$. β counts the number of parameters in a covariance matrix; $\beta = p(p + 1)/2$.

Σ_k	# parameters to estimate	Cluster' geometry	Clusters' Volume	Clusters' Shape	Clusters' Orientation	Configuration Short name
$\lambda \mathbf{I}$	$\alpha + 1$	Spherical	Equal	Equal	–	EII
$\lambda_k \mathbf{I}$	$\alpha + p$	Spherical	Variable	Equal	–	VII
$\lambda \mathbf{A}$	$\alpha + p$	Diagonal	Equal	Equal	Coord. Axes	EEI
$\lambda_k \mathbf{A}$	$\alpha + p + K - 1$	Diagonal	Variable	Equal	Coord. Axes	VEI
$\lambda \mathbf{A}_k$	$\alpha + Kp - K + 1$	Diagonal	Equal	Variable	Coord. Axes	EVI
$\lambda_k \mathbf{A}_k$	$\alpha + Kp$	Diagonal	Variable	Variable	Coord. Axes	VVI
$\lambda \mathbf{DAD}^\top$	$\alpha + \beta$	Ellipsoidal	Equal	Equal	Equal	EEE
$\lambda \mathbf{DA}_k \mathbf{D}^\top$	$\alpha + \beta + K - 1$	Ellipsoidal	Equal	Variable	Equal	EVE
$\lambda_k \mathbf{DAD}^\top$	$\alpha + \beta + (K - 1)(p - 1)$	Ellipsoidal	Variable	Equal	Equal	VEE
$\lambda_k \mathbf{DA}_k \mathbf{D}^\top$	$\alpha + \beta + (K - 1)p$	Ellipsoidal	Variable	Variable	Equal	VVE
$\lambda \mathbf{D}_k \mathbf{AD}_k^\top$	$\alpha + K\beta - (K - 1)p$	Ellipsoidal	Equal	Equal	Variable	EEV
$\lambda_k \mathbf{D}_k \mathbf{AD}_k^\top$	$\alpha + K\beta - (K - 1)(p - 1)$	Ellipsoidal	Variable	Equal	Variable	VEV
$\lambda \mathbf{D}_k \mathbf{A}_k \mathbf{D}_k^\top$	$\alpha + K\beta - (K - 1)$	Ellipsoidal	Equal	Variable	Variable	EVV
$\lambda_k \mathbf{D}_k \mathbf{A}_k \mathbf{D}_k^\top$	$\alpha + K\beta$	Ellipsoidal	Variable	Variable	Variable	VVV

For convenience, we label members of \mathcal{M} computed with `rimle` as RIMLE configurations. The ERC bounds the maximum spread between all eigenvalues of all mixture components' covariance matrices by a fixed constant $1 \leq \gamma$, that is

$$\max_{s,t=1,2,\dots,K} \frac{\lambda_{\max}(\Sigma_s)}{\lambda_{\min}(\Sigma_t)} \leq \gamma, \quad (\text{S14})$$

where $\lambda_{\max}(\Sigma_k)$ and $\lambda_{\min}(\Sigma_k)$ are the minimum and the maximum eigenvalue of Σ_k , respectively. The idea of the ERC dates back to the seminal contribution of [Hathaway \(1985\)](#) (for a recent overview, see [García-Escudero et al., 2017](#)). [Coretto and Hennig \(2017\)](#) showed consistency results for the ML estimator under the ERC, and they developed the EM-type algorithm with convergence guarantees implemented through the `rimle` software.

For any $\gamma \in [1, +\infty)$ the resulting estimated covariance matrices are guaranteed to be positive definite whatever large are p and K compared to n . As found in [Coretto and Hennig \(2017\)](#), although the ERC fixes an otherwise ill-posed optimization problem, it strongly affects the complexity of the underlying model, significantly impacting the final clustering. In fact, γ bounds the relative discrepancy between clusters' scatters: γ close to one is the same as imposing spherical groups; $\gamma \rightarrow +\infty$ completely frees the clusters' shape, allowing to discover more complex structures. In some sense, the ERC tunes the complexity of the covariance structure as the 14 `mclust` parametrizations do, but the tuning provided by the ERC is *continuous* in the sense that increasing γ enriches the model structure continuously. For any fixed γ , the number of parameters to be estimated does not change, but different values of γ correspond to the clusters' different levels of complexity. In the following section, we will see that the latter has implications for applying classical estimators of the information criteria.

Additional to K and γ , the `rimle` implementation allows to control the initialization strategy. The RIMLE members of \mathcal{M} combine: number of groups $K \in \{1, 2, \dots, 10\}$,

$\gamma \in \{1, 5, 10, 100, 1000, 10000\}$ and 3 different initialization methods. The three type of initial partitions are based on K-means, K-medoids partitioning and agglomerative hierarchical clustering based on likelihood criteria of Fraley (1998). The total number of RIMLE configuration is 180.

Emmix. Lastly, we consider ML for mixture models of Student-t and Skew Student-t distributions. EMMIX configurations are computed using the EMMIXskew R package of Wang et al. (2018). Details of the algorithms are given in Wang et al. (2009). The Skew Student-t models contain the Student-t model as a special case and the latter, in turns, contains the Gaussian model. The skew version of the Student-t model does not fulfill the assumptions of Proposition 1, but its more flexible structure allows fitting elliptically shaped and spherical clusters as special cases. Thus, it is introduced to assess whether the selection methods under study tempt to select configurations corresponding to models that have more chances to overfit the data because of their extra flexibility. The **tm-s** and **tm-c** settings in Section S1 also correspond to EMMIXskew configurations. Similar to Mclust, EMMIXskew allows choosing between a smaller set of 5 covariance models: (1) homoscedastic groups, that is $\Sigma_k = \Sigma$ for all $k = 1, 2, \dots, K$; (2) homoscedastic diagonal model: $\Sigma_k = \text{diag}(\sigma_1^2, \sigma_2^2, \dots, \sigma_p^2)$ for all $k = 1, 2, \dots, K$; (3) fully heteroskedastic model (called general variance in EMMIXskew): Σ_k are free to vary across groups; (4) heteroskedastic diagonal model: $\Sigma_k = \text{diag}(\sigma_{k1}^2, \sigma_{k2}^2, \dots, \sigma_{kp}^2)$; (5) heteroskedastic spherical model: $\Sigma_k = \sigma_k^2 \mathbf{I}_p$. For the skew version of the Student-t model, these covariances are combined with a skew parameter to obtain non-elliptical shapes. As for Mclust, EMMIXskew also applies covariance regularization to prevent spurious degenerate solutions, but this is done internally and it can not be controlled by the user. EMMIX configurations are obtained combining: the 2 group-conditional models (Student-t vs. Skew Student-t), $K \in \{1, 2, \dots, 10\}$ and 5 covariance models. The total number of EMMIX configurations is 100.

S5.2 Selection methods

In this section we give additional information and definitions for the selection methods introduced in Section 4-(PF). These are

ASW:	Average Silhouettes Width criterion;
CH:	Calinski-Harabasz criterion;
AIC:	Akaike Information Criterion;
BIC:	Bayesian Information Criterion;
ICL:	Integrated Complete-data Likelihood criterion;
FW:	bootstrap stability selection of Fang and Wang (2012);
CVLK:	cross-validation of likelihood risk of Smyth (2000);
BQH:	bootstrap selection with the Quadratic Hard Score criterion;
BQS:	bootstrap selection with the Quadratic Smooth Score criterion;
QH:	in-sample Quadratic Hard Score criterion;
QS:	in-sample Quadratic Smooth Score criterion;
CVQH:	cross-validation with the Quadratic Hard Score criterion;
CVQS:	cross-validation with the Quadratic Smooth Score criterion;

In Table S4 we classify these selection methods into 4 groups. Each of the previous

methods is set to maximize the corresponding criterion over the members of \mathcal{M} , and in case of ties, we apply random selection between equally good members of \mathcal{M} . Note that not all selection methods in the list above can be computed for all members of \mathcal{M} ; this is summarized in Table S5 and discussed below. Therefore, some of the selection methods are compared on a subset of the 440 members of \mathcal{M} . QH, QS, BQH, and BQS criteria are explained in detail in PF, here we give a more detailed description of the remaining methods.

Table S4: Selection methods classified as: *method-independent* vs. *method-dependent* criteria; methods using *in-sample* estimates vs. methods that use *resampling* of the original data.

	Method-independent	Method-dependent
In-sample	CH, ASW, QH, QS	AIC, BIC, ICL
Resampling	FW, CVQH, CVQS BQH, BQS	CVLK

Table S5: Possibility to compute clustering quality criteria (columns) for each type of configuration in \mathcal{M} .

Configuration	AIC	BIC	ICL	ASW	CH	FW	CVLK	QH	QS	CVQH	CVQS	BQH	BQS
K-MEANS				✓	✓	✓		✓	✓	✓	✓	✓	✓
K-MEDOIDS				✓	✓	✓		✓	✓	✓	✓	✓	✓
MCLUST	✓	✓	✓	✓	✓	✓	✓	✓	✓	✓	✓	✓	✓
RIMLE				✓	✓	✓	✓	✓	✓	✓	✓	✓	✓
EMMIX	✓	✓	✓	✓	✓	✓	✓	✓	✓	✓	✓	✓	✓

Method-independent criteria using in-sample information. Many validation methods look for partitions minimizing within-clusters dissimilarity assumed as the driving notion of internal homogeneity. Let $D(\mathbf{x}_i, \mathbf{x}_j)$ be the pairwise dissimilarity between units i and j . [Caliński and Harabasz \(1974\)](#) proposed to measure the quality of clustering achieved by a partition \mathcal{G}_K in terms of the ratio

$$\text{CH}(\mathcal{G}_K) := \frac{\mathbf{B}(\mathcal{G}_K)(n - K)}{\mathbf{W}(\mathcal{G}_K)(K - 1)} \quad (\text{S15})$$

where $\mathbf{B}(\cdot)$ and $\mathbf{W}(\cdot)$ are respectively the between and within point scatter measured as

$$\mathbf{W}(\mathcal{G}_K) := \sum_{k=1}^K \frac{1}{\# \{G_k\}} \sum_{i,j \in G_k} D(\mathbf{x}_i, \mathbf{x}_j), \quad \mathbf{B}(\mathcal{G}_K) := \frac{1}{n} \sum_{i,j=1}^n D(\mathbf{x}_i, \mathbf{x}_j) - \mathbf{W}(\mathcal{G}_K).$$

Calculation of $\text{CH}(\cdot)$ only requires the clusters' labels and dissimilarities computed on the observed data set. Originally, (S15) was proposed for $D(\cdot)$ being the squared Euclidean distance within the k-means framework, but later [Milligan and Cooper \(1985\)](#) showed that the $\text{CH}(\cdot)$ criteria performed well for more general dissimilarity measures. It is preferred a clustering with large $\text{CH}(\cdot)$. The ratio $\mathbf{W}(\mathcal{G}_K)/\mathbf{B}(\mathcal{G}_K)$ can be improved simply by increasing K : this would fit the data more locally, reducing the within dissimilarity. The previous mechanism is tamed by introducing the correction factor $(n - K)/(K - 1)$.

The *Average Silhouette Width* criteria (ASW) of [Rousseeuw and Kaufman \(1990\)](#) is an-

other popular index. Let $i \in G_k$ and define

$$a(i) := \frac{1}{\#\{G_k\} - 1} \sum_{j \in G_k \setminus \{i\}} D(i, j), \quad b(i) := \min_{G_k: i \notin G_k} \left\{ \frac{1}{\#\{G_k\}} \sum_{j \in G_k} D(i, j) \right\}.$$

The ASW index averages the point's *silhouette* $s(i)$ as follows

$$\text{ASW}(\mathcal{G}_K) = \frac{1}{n} \sum_{i=1}^n s(i), \quad \text{where } s(i) = \frac{b(i) - a(i)}{\max\{a(i), b(i)\}}. \quad (\text{S16})$$

The silhouette $s(\cdot)$ measures how tightly a point is connected to its cluster compared to the remaining clusters. One desires partitions with large $\text{ASW}(\cdot)$. As for (S15), the computation of (S16) only requires clusters' label and a reference dissimilarity notion.

We use ASW and CH as in-sample criteria by estimating the clustering solution \mathcal{G}_k on the full sample, and re-using the same sample to compute both criteria; we set D to be the Euclidean distance.

Method-independent criteria using resampling. The stability criterion proposed by Fang and Wang (2012) (FW) performs method-independent selection based on bootstrap resampling. FW looks for stable clustering solutions, i.e. partitions that are robust against changes due to the randomness in the sample, and this is assessed using bootstrap resampling. Multiple independent pairs of bootstrap samples are drawn. For each pair, the given clustering method, m , is fit on both resamples, obtaining two clustering solutions; then, a clustering distance is computed using the assignment of points from the original sample into $K(m)$ clusters, made by the two solutions. The distance is averaged across the pairs to obtain the clustering instability. Algorithm S1 shows the exact implementation. FW can not be used for configurations with $K(m) = 1$ because, in this case, it would always obtain a trivial instability score of 0. Therefore, FW is not performed for members of $m \in \mathcal{M}$ with $K(m) = 1$. For the sake of consistency with the other selection methods, we report the negative clustering instability so that we maximize $-FW$; however, to ease notation, we drop the minus sign.

CVQH and CVQS are also method-independent selection procedures that use resampling. They are the cross-validation variants of BQH and BQS introduced to check the intuition behind Remark 3-(PF). The two methods are defined in Algorithm S2. The procedure closely mimics BQH and BQS, except that the bootstrap resampling scheme is replaced with the cross-validation, and percentile calculation is done using the usual normal approximation. First, the data set is partitioned into 10 equally-sized data folds. Then, each of them is used in turn to compute the quadratic score using the triplets $\hat{\theta}_n$ estimated on the remaining 9 data folds. Finally, the cross-validated score corresponds to the lower limit of the 95%-confidence interval of the average score calculated using the normal approximation. CVQH (or CVQS) selects $m \in \mathcal{M}$ achieving the largest \widetilde{CV}_n .

Method-dependent criteria using in-sample information. The first group of method-dependent criteria are those based on information-type criteria derived within the MBC setting. These would be better called “model-dependent” methods, because in reality they are strictly connected to an underlying model rather than a fitting method. In the

Algorithm S1: [Fang and Wang \(2012\)](#) stability criterion (FW)

Input: observed sample \mathbb{X}_n , integer B .

Output: FW .

for $b = 1, \dots, B$ **do**

(step 1) $(\mathbb{X}_n^*, \mathbb{Y}_n^*) \leftarrow$ couple of independent, non-parametric bootstrap resamples form \mathbb{X}_n .

(step 2) Fit clustering on bootstrap resamples, obtaining mapping functions:

$$\psi_{\mathbb{X}_n^*} \leftarrow \text{Clust}(\mathbb{X}_n^*); \quad \psi_{\mathbb{Y}_n^*} \leftarrow \text{Clust}(\mathbb{Y}_n^*)$$

(note: $\psi_{\mathbb{X}} : \mathcal{X} \rightarrow \{1, \dots, K(m)\}$)

(step 3) Compute clustering distance (on original sample \mathbb{X}_n):

$$d_b \leftarrow \frac{1}{n^2} \sum_{i=1}^n \sum_{j=1}^n |\mathbb{I}\{\psi_{\mathbb{X}_n^*}(x_i) = \psi_{\mathbb{X}_n^*}(x_j)\} - \mathbb{I}\{\psi_{\mathbb{Y}_n^*}(x_i) = \psi_{\mathbb{Y}_n^*}(x_j)\}|$$

(step 4) Obtain clustering instability

$$FW \leftarrow \frac{1}{B} \sum_{b=1}^B d_b$$

Algorithm S2: 10-fold cross-validation of quadratic scores (CVQH, CVQS)

Input: observed sample \mathbb{X}_n

Output: \widetilde{CVQH} or \widetilde{CVQS} .

(step 1) randomly partition \mathbb{X}_n into 10 folds $\{\mathbb{X}^{(t)}, t = 1, \dots, 10\}$, each with (approximately) $n/10$ data points.

for $t = 1, \dots, 10$ **do**

(step 2.1) $\widehat{\mathbb{X}} \leftarrow \bigcup_{j \neq t} \mathbb{X}^{(j)}$

(step 2.2) $\widehat{\boldsymbol{\theta}}^{(t)} \leftarrow \text{Clust}(\widehat{\mathbb{X}})$

(step 2.3) $S^{(t)} \leftarrow \frac{1}{\#\mathbb{X}^{(t)}} \sum_{\mathbf{y} \in \mathbb{X}^{(t)}} s(\mathbf{y}; \widehat{\boldsymbol{\theta}}^{(t)})$

(step 3.1) $\bar{S} \leftarrow \frac{1}{10} \sum_{t=1}^{10} S^{(t)}$

(step 3.2) $\hat{\sigma}_S \leftarrow \frac{1}{9} \sum_{t=1}^{10} (S^{(t)} - \bar{S})^2$

(step 3.3) Compute

$$\widetilde{CV} \leftarrow \bar{S} - 1.96 \frac{\hat{\sigma}_S}{\sqrt{10}}$$

$\widetilde{CVQH} = \widetilde{CV}$ when $s(\cdot)$ corresponds to the hard quadratic score

$\widetilde{CVQS} = \widetilde{CV}$ when $s(\cdot)$ corresponds to the smooth quadratic score

following definitions, $\boldsymbol{\theta}$ is meant to be the unknown parameter vector of a mixture model like (14)-(PF). The classical estimators of the AIC ([Akaike, 1973](#)) and the BIC ([Schwarz,](#)

1978) are defined as

$$\text{AIC} = 2 \text{lik}_n(\boldsymbol{\theta}_n^{\text{ml}}) - 2\nu(\boldsymbol{\theta}) \quad \text{and} \quad \text{BIC} = 2 \text{lik}_n(\boldsymbol{\theta}_n^{\text{ml}}) - \log(n)\nu(\boldsymbol{\theta}),$$

where $\nu(\boldsymbol{\theta})$ is the number of free parameters of the mixture distribution (14)-(PF) and $\boldsymbol{\theta}_n^{\text{ml}}$ is the corresponding ML estimate. The *Integrated Complete-data Likelihood* (ICL) of Biernacki et al. (2000) is an alternative information-type criteria that focuses on the clustering structure rather than the distribution fit. The definition of the ICL replaces the log-likelihood function with the conditional expected complete log-likelihood within the BIC's construction:

$$\text{ICL} = 2\text{E}[\text{clik}_n(\boldsymbol{\theta}_n^{\text{ml}}) \mid \mathbb{X}_n] - \log(n)\nu(\boldsymbol{\theta}). \quad (\text{S17})$$

Because of the relationship between the $\text{lik}_n(\cdot)$, $\text{clik}_n(\cdot)$ and the entropy term defined in (17)-(PF), it turns out that $\text{ICL} = \text{BIC} - \overline{\text{ent}}_n(\boldsymbol{\theta}_n^{\text{ml}})$, where $\overline{\text{ent}}_n(\boldsymbol{\theta}_n^{\text{ml}})$ is the empirical average of the entropy in (17)-(PF) computed at the ML estimate $\boldsymbol{\theta}_n^{\text{ml}}$. Thus, the ICL puts an extra penalty on the BIC for the uncertainty of the overall clustering, quantified by $\overline{\text{ent}}_n(\boldsymbol{\theta}_n^{\text{ml}})$. The ICL recently gained a strong popularity, and it is now included in most software packages. Baudry (2015) investigates the theoretical foundations of the ICL.

The calculations of the AIC, BIC and the ICL require:

- (i) the precise definition of a clustering probability model so that the likelihood term can be defined and calculated;
- (ii) that the parameter vector is fitted by ML;
- (iii) that the effective degrees of freedom of the competing models can be approximated in terms of model's dimension $\nu(\boldsymbol{\theta})$.

The requirements (i)-(ii) do not allow comparing clustering solutions obtained with methods that, despite being able to retrieve the clusters of interest, are not based on a generating probability model. For example, it is not hard to construct examples where the K-Medoids method based on the Euclidean distance discovers clusters similar to those found with Gaussian mixtures. However, it is not clear how to compute the BIC-type index for a K-Medoid solution. Also, (iii) is not always possible in the model-based framework. An example is the subset of RIMLE configurations in \mathcal{M} : any $1 \leq \gamma < +\infty$ changes the model complexity without changing the number of estimated parameters. Therefore, in the case of ML for Gaussian mixture models with ERC constraints, the penalty term of both the BIC and the ICL would not reflect the change in the model complexity introduced by different specifications of γ . The previous issue also affects other types of scale constraints that have been proposed to ensure the existence of the ML for mixtures of more general location-scale families.

Method-dependent criteria using resampling. In the work of Smyth (2000) the selection problem is solved by using cross-validation and defining the risk as minus the average log-likelihood function of an underlying mixture model; here, it is implemented as the CVLK method. The risk function defined by Smyth (2000) coincides with a quantity that is proportional to the expected Kullback-Leibler information loss over a test set when the true underlying generating distribution is approximated by the mixture model (14)-(PF). To some extent, the method mimics the rationale of the AIC criteria and

Algorithm S3: 10-Fold cross-validation of the likelihood risk (CVLK)

Input: observed sample \mathbb{X}_n

Output: \widetilde{CVLK} .

(step 1) randomly partition \mathbb{X}_n into 10 folds $\{\mathbb{X}^{(t)}, t = 1, \dots, 10\}$, each with (approximately) $n/10$ data points.

for $t = 1, \dots, 10$ **do**

 (step 2.1) $\widehat{\mathbb{X}} \leftarrow \bigcup_{j \neq t} \mathbb{X}^{(j)}$,
 (step 2.2) $\boldsymbol{\theta}_{(t)}^{\text{ml}} \leftarrow \arg \max_{\boldsymbol{\theta}} \sum_{\mathbf{y} \in \widehat{\mathbb{X}}} \log(\psi_f(\mathbf{y}; \boldsymbol{\theta}))$
 (step 2.3) $\ell_{(t)} \leftarrow \frac{1}{\#\mathbb{X}^{(t)}} \sum_{\mathbf{y} \in \mathbb{X}^{(t)}} \log(\psi_f(\mathbf{y}; \boldsymbol{\theta}_{(t)}^{\text{ml}}))$

(step 3) Obtain

$$\widetilde{CVLK} \leftarrow \frac{1}{10} \sum_{t=1}^{10} \ell_{(t)}$$

therefore looks for models that best fit the data distribution on unseen data. The precise implementation of the CVLK method is given in Algorithm S3. In our experiments, CVLK selects a cluster configuration that maximizes \widetilde{CVLK} . Algorithm S3 differs from the original proposal for two reasons:

1. Smyth (2000) defined the risk as “minus the average log-likelihood”, minimizing this criterion. In step 2.1 we compute “average log-likelihood” values over the test sets to maximize the final criterion, consistently with all its competitors.
2. Smyth (2000) proposed to use random cross-validation with both training and testing data sets containing half of the data points. After having implemented the original proposal, we compared it with alternative cross-validation sampling schemes, discovering that 10-fold cross-validation does a better job. Therefore, in the final experiments, we only considered the 10-fold cross-validation.

The application of the CVLK method requires a probability model to define the likelihood risk. For this reason, we classified it as method-dependent but, in fact, it would be better qualified as “model-dependent” as for the AIC, BIC and ICL. The difference with AIC, BIC and ICL is that, in this case, an approximation of degrees of freedom in terms of the number of free parameters to be estimated is not necessary. For this reason, we apply the CVLK to RIMLE configurations also, for which information criteria do not make much sense.

S5.3 Data

Real and artificial data sets are summarized in Table S6.

Table S6: Summary of the main characteristics of real and artificial data sets: number of data points (n), dimensionality (p), true number of clusters (K) and brief description of each data set.

Data/Sample Design	n	d	K	Short Description
Iris	150	4	3	Measurements on Iris flowers; two classes show substantial overlap.
Banknote	200	6	2	Measurements on original and counterfeit bills; the latter class is usually split in more groups due to the high variability of the measurements.
Olive	572	8	3/9	Measurements on olive oils' fatty acids, having two different classifications; some classes scatters are concentrated on lower dimensional hyperplanes and show substantial overlap.
Pentagon5	300	2	5	Mixture of uneven Gaussian distributions; strong pairwise overlap of 4 of the 5 components.
Uniform	300	2	1	Two-dimensional uniform distribution; many criteria are not able to identify the unclustered case.
Flower2	300	2	5	Mixture of 2 Student-t, 2 uniform and 1 spherical Gaussian component; features regions of strong clusters' overlap.
T52D	300	2	5	Mixture of 5 equal-proportions Student-t distributions.
T510D	300	10	5	Adds 8 unclustered dimensions to the T52D design to increase dimensionality without adding new clustering information.

S5.4 Real data sets

The famous Iris data set was introduced by [Anderson \(1936\)](#) and [Fisher \(1936\)](#). It collects equally split measurements on three Iris flower species: *Versicolor*, *Virginica* and *Setosa* (see Figure S5, left panel). Two of the classes, Versicolor and Virginica, show a substantial overlap, making it generally difficult to tell them apart for clustering algorithms.

The Banknote data set was introduced in [Flury and Riedwyl \(1988\)](#) and collects observations on Swiss 1000-franc banknotes, evenly split between two classes: *counterfeit* and *genuine* notes. It collects measurements on the bill: width of the note measured along the left and right sides; bottom and top margins' width; diagonal image length; bill's length. Figure S5, right panel shows data pairs plot. The two classes show a moderate overlap; the higher variability of the characteristics of the counterfeit notes may induce algorithms to split the class into two different groups.

The Olive data set, first appeared in [Forina and Tiscornia \(1982\)](#) and [Forina et al. \(1983\)](#), collects measurements on olive oils' fatty acids. The data features two levels of classification, based on oils' origins: a coarser one consisting of 3 macro-regions and a finer one identifying 9 regions. Figure S6 shows pairs plot for both classification levels. While some areas are better separated (e.g. West Liguria, Costal Sardinia and Inland Sardinia), others show larger similarities (e.g. Sicily, Calabria and South Apulia). As can be noted from the graphs, data comes with a high amount of discreteness. Moreover, for some areas, the scatters are highly concentrated along certain directions. These aspects make it particularly difficult to retrieve the true partitions.

S5.5 Results for real data sets

Table S7 mimics the Table 1-(PF). However, here results are obtained with $B = 100$ instead of $B = 1000$. This allows to assess how a smaller B affects the quality of the Monte Carlo approximation of the Bootstrap distribution. This is important because,

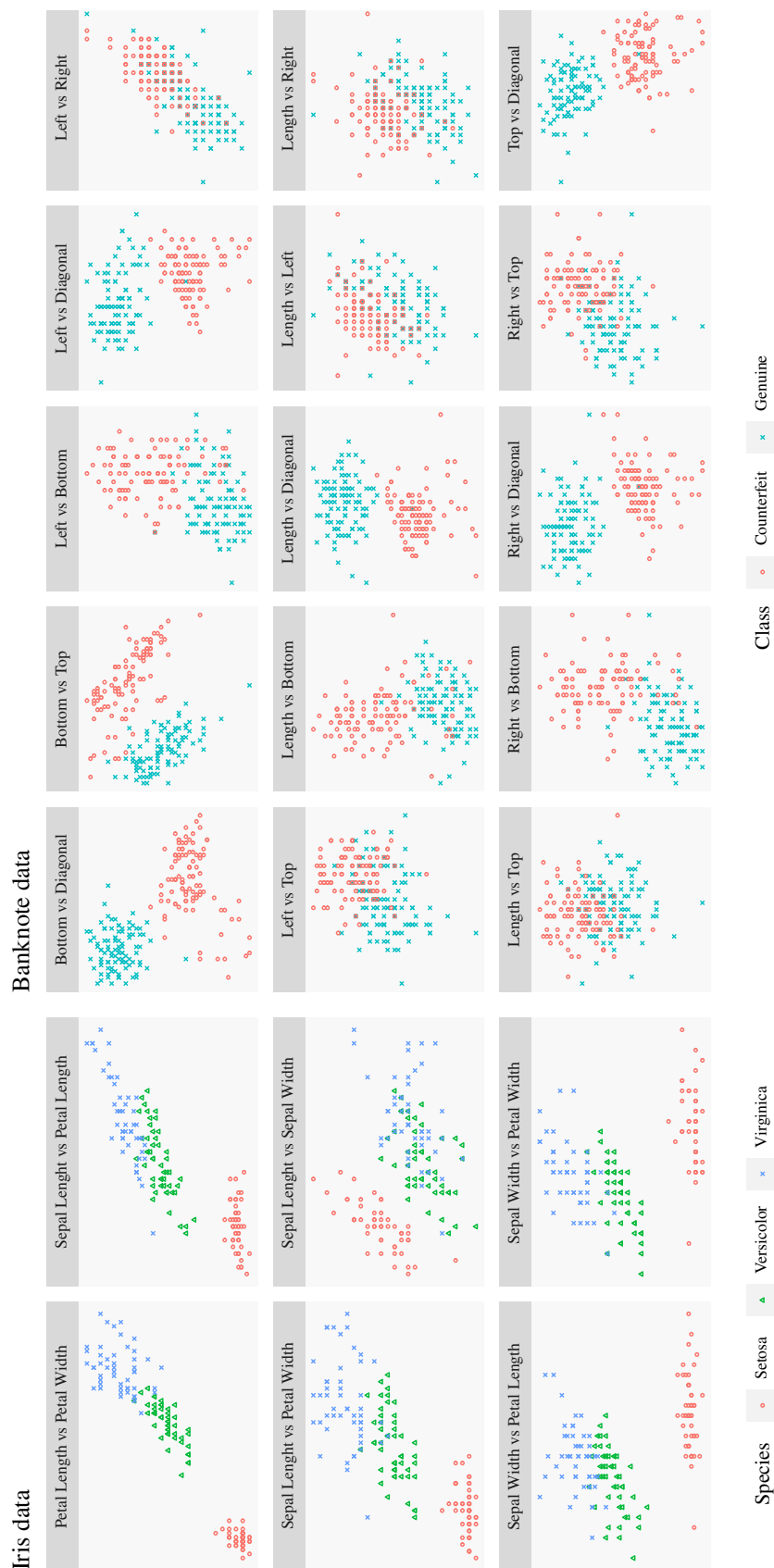


Figure S5: Pairs plots for the Iris data (left) and Banknote data (right).

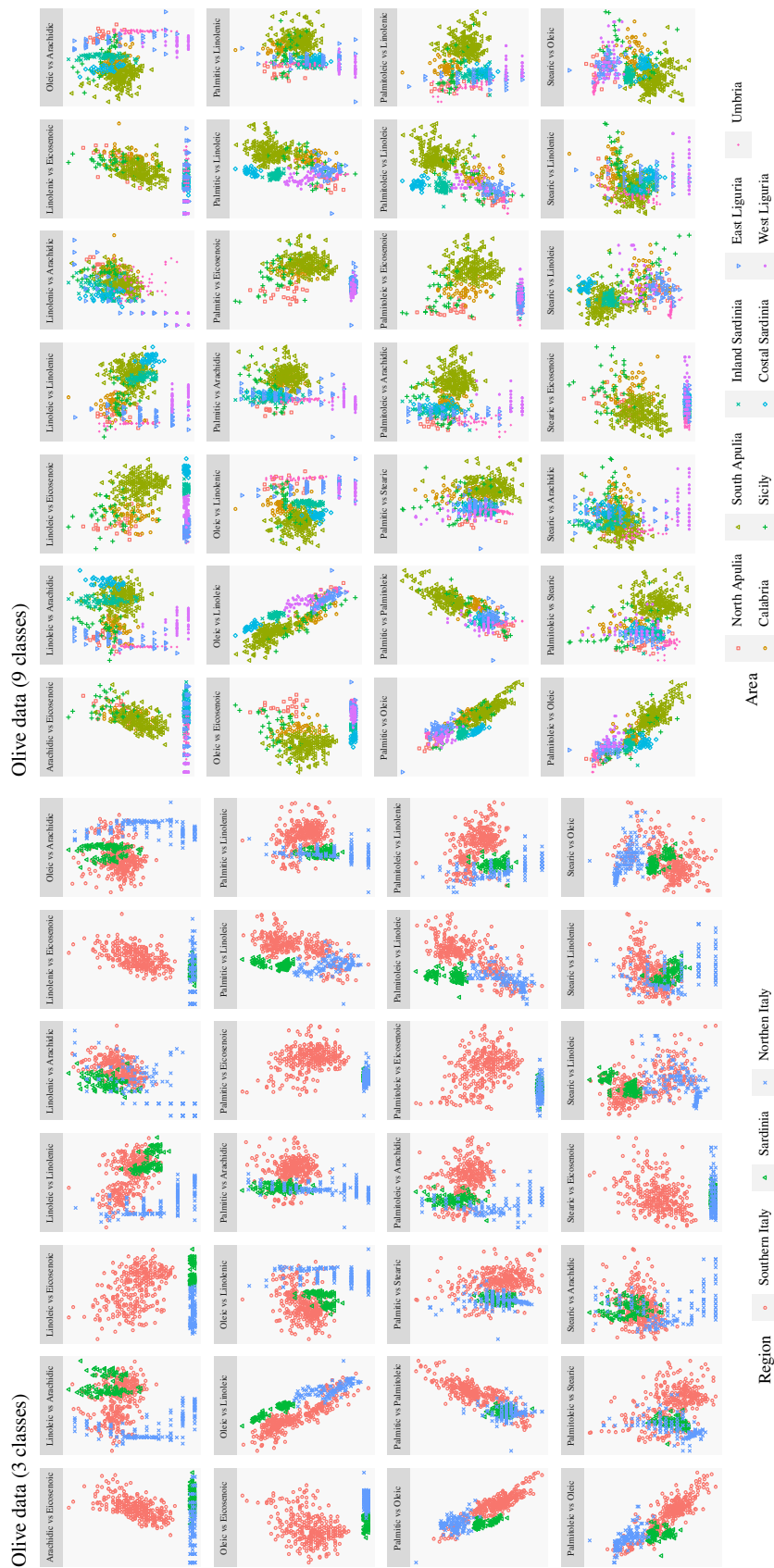


Figure S6: Pair plots for Olive data, with coarser (left) and finer (right) classifications.

when the computational cost of refitting the clusters B times is large, one may consider a low value of B . Results are qualitatively the same but for BQH and BQS for the Banknote data. In the latter case, the two methods show a better performance with $B = 1000$.

In Figure S7 we report graphs for BQH and BQS in analogy with Figure 2-(PF). Each sub-figure illustrates the two criteria on a single data set; top and bottom panels show results with $B = 100$ and $B = 1000$ bootstrap resamples, respectively. Considerations are qualitatively the same as those provided in the PF. There is no striking difference comparing the 100 and 1000 bootstrap resamples. On the Iris data, one can notice that the uncertainty around the mean quadratic scores (both hard and smooth) tends to reduce slightly when 1000 resamples are used; this is especially visible for RIMLE configurations. For Banknote data, this result seems to hold for configuration of medium complexity (e.g. RIMLE with $K = 5, 6$), while for higher complexity (RIMLE with $K = 9, 10$ and ERC = 10000) variability seems to increase, if anything. For the Olive data set, the graphs are dominated by the changes in the mean scores, making it challenging to appreciate differences in the uncertainty. Nonetheless, it can be noticed that uncertainty grows with complexity.

The overfitting pattern described in PF can be observed in all the three graphs. It is less evident in the Olive case, where it seems that more complex models are still capturing genuine characteristics of the data. This data set represents a difficult case due to the high amount of class unbalancedness, overlap and substantial variations in the within-group scatter across groups.

Table S7: Clustering solutions selected by the 13 selection criteria under comparison on the three real data sets, using 100 bootstrap resamples for FW, BQH and BQS criteria (compare with Table 1-(PF)). First two rows in each table indicate the two best feasible solutions: the BEST ARI and the BEST VIC partitions. The column “K” reports the number of groups discovered by the selected solution. The “Algorithm” and “Configuration” columns identify the specific member of \mathcal{M} that is selected. ARI and the VIC columns measure the agreement of the selected partition with respect to the ground truth.

(a) Iris data set						(b) Banknote data set					
Criterion	K	Algorithm	Configuration	ARI	VIC	Criterion	K	Algorithm	Configuration	ARI	VIC
BEST ARI	3	Mclust	EEE	0.94	-0.26	BEST ARI	2	Rimle	$\gamma = 1$; InitClust	1	0
BEST VIC	3	Mclust	EEE	0.94	-0.26	BEST VIC	2	Rimle	$\gamma = 1$; InitClust	1	0
AIC	6	Emmix	mvt; ncov = 3	0.57	-1.52	AIC	6	Emmix	mvt; ncov = 3	0.6	-1.16
BIC	2	Mclust	VEV	0.57	-0.87	BIC	3	Mclust	VVE	0.84	-0.43
ICL	2	Mclust	VEV	0.57	-0.87	ICL	3	Mclust	VVE	0.84	-0.43
QH	7	Emmix	mvt; ncov = 4	0.42	-1.56	QH	10	Rimle	$\gamma = 10000$; pam	0.26	-2.14
QS	7	Emmix	mvt; ncov = 4	0.42	-1.56	QS	10	Rimle	$\gamma = 10000$; pam	0.26	-2.14
CH	3	Rimle	$\gamma = 1$; kneans	0.73	-0.76	CH	2	Mclust	EH	1	0
ASW	2	Rimle	$\gamma = 5$; InitClust	0.57	-0.67	ASW	2	Rimle	$\gamma = 1$; pam	1	0
FW	4	Rimle	$\gamma = 10$; InitClust	0.57	-0.67	FW	2	Rimle	$\gamma = 10000$; kneans	0.98	-0.08
CVLK	4	Rimle	$\gamma = 10000$; InitClust	0.81	-0.57	CVLK	3	Rimle	$\gamma = 10$; InitClust	0.85	-0.42
CVQH	4	Rimle	$\gamma = 10000$; InitClust	0.81	-0.57	CVQH	3	Mclust	VEV	0.78	-0.62
CVQS	4	Rimle	$\gamma = 1000$; InitClust	0.81	-0.58	CVQS	3	Mclust	VEV	0.78	-0.62
BQH	3	Rimle	$\gamma = 100$; pam	0.9	-0.32	BQH	4	Rimle	$\gamma = 10$; InitClust	0.67	-0.84
BQS	3	Rimle	$\gamma = 100$; pam	0.9	-0.32	BQS	4	Rimle	$\gamma = 10$; InitClust	0.67	-0.84

(c) Olive data set (3 classes)						(d) Olive data set (9 classes)					
Criterion	K	Algorithm	Configuration	ARI	VIC	Criterion	K	Algorithm	Configuration	ARI	VIC
BEST ARI	3	Emmix	mvt; ncov = 3	1	-0.03	BEST ARI	8	Mclust	EVE	0.88	-0.65
BEST VIC	3	Emmix	mvt; ncov = 3	1	-0.03	BEST VIC	8	Mclust	EVE	0.88	-0.65
AIC	10	Emmix	mvt; ncov = 3	0.33	-1.74	AIC	10	Emmix	mvt; ncov = 3	0.47	-1.77
BIC	6	Emmix	mvt; ncov = 3	0.52	-1.42	BIC	6	Emmix	mvt; ncov = 3	0.76	-1.32
ICL	6	Emmix	mvt; ncov = 3	0.52	-1.42	ICL	6	Emmix	mvt; ncov = 3	0.76	-1.32
QH	10	Mclust	VVV	0.29	-1.84	QH	10	Mclust	VVV	0.54	-1.26
QS	10	Mclust	VVV	0.29	-1.84	QS	10	Mclust	VVV	0.54	-1.26
CH	3	K-Means	mvt; ncov = 5	0.32	-1.88	CH	3	K-Means	mvt; ncov = 5	0.42	-2.28
ASW	2	Emmix	mvt; ncov = 5	0.39	-1.28	ASW	2	Emmix	mvt; ncov = 5	0.29	-2.28
FW	2	Emmix	mvt; ncov = 3	0.82	-0.42	FW	2	Emmix	mvt; ncov = 3	0.36	-1.84
CVLK	10	Rimle	$\gamma = 1000$; InitClust	0.3	-1.81	CVLK	10	Rimle	$\gamma = 1000$; InitClust	0.58	-1.18
CVQH	7	Emmix	mvt; ncov = 3	0.28	-2.04	CVQH	7	Emmix	mvt; ncov = 3	0.44	-1.96
CVQS	7	Emmix	mvt; ncov = 3	0.28	-2.04	CVQS	7	Emmix	mvt; ncov = 3	0.44	-1.96
BQH	8	Emmix	mvt; ncov = 4	0.43	-1.32	BQH	8	Emmix	mvt; ncov = 4	0.62	-1.28
BQS	8	Mclust	VVV	0.49	-1.28	BQS	8	Mclust	VVV	0.86	-0.74

Figure S7: In-sample (dashed line) and bootstrap versions (solid line) of the Hard Scoring and Smooth Scoring for real data sets. Dashed lines correspond to QH and QS criteria. Bootstrap scores are shown for 100 and 1000 bootstrap replicates. Confidence bounds around bootstrap scores are represented by shaded areas; lower confidence bounds correspond to BQH and BQS criteria.

(a) Iris data

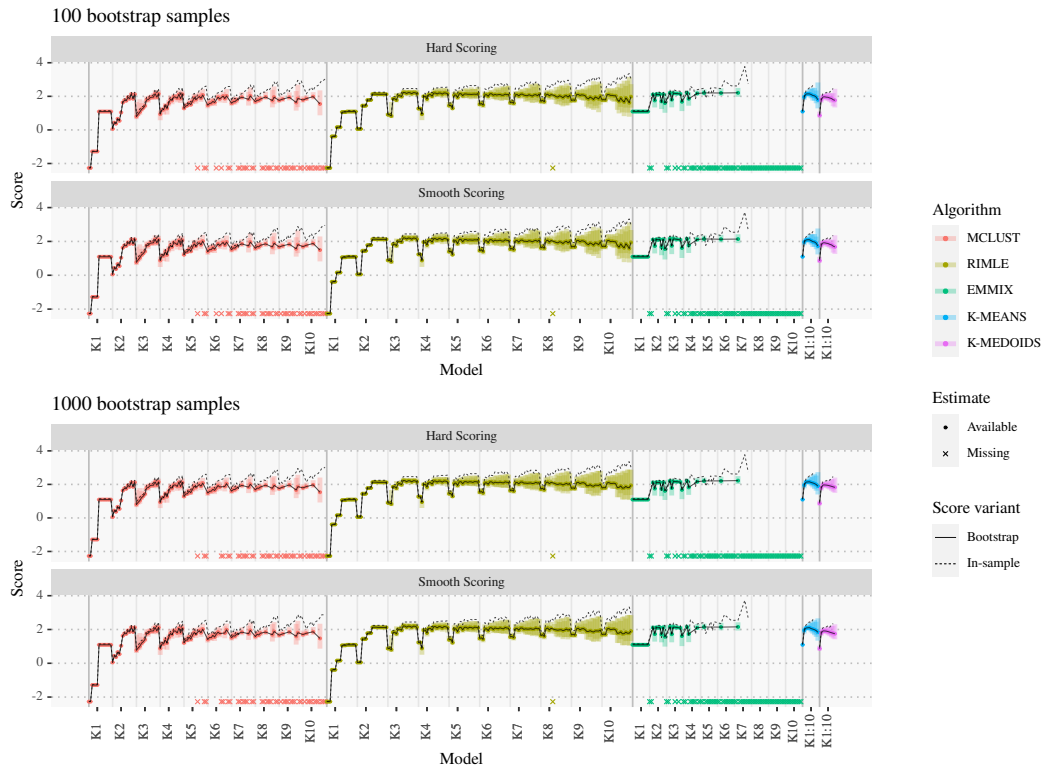
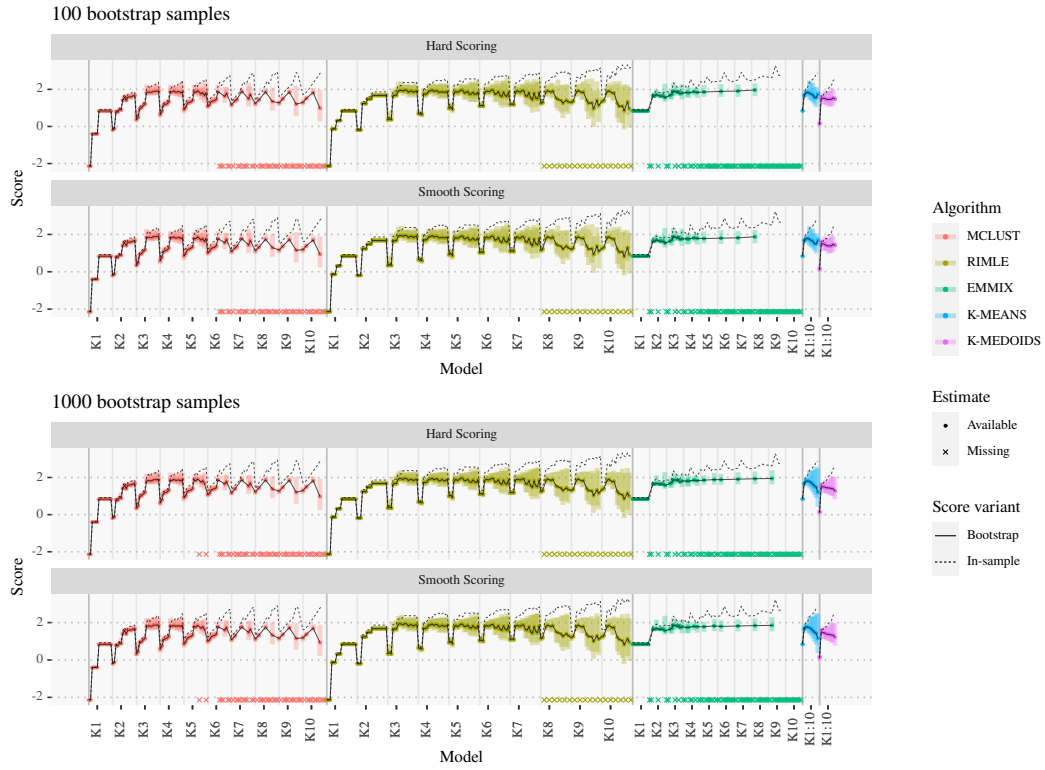
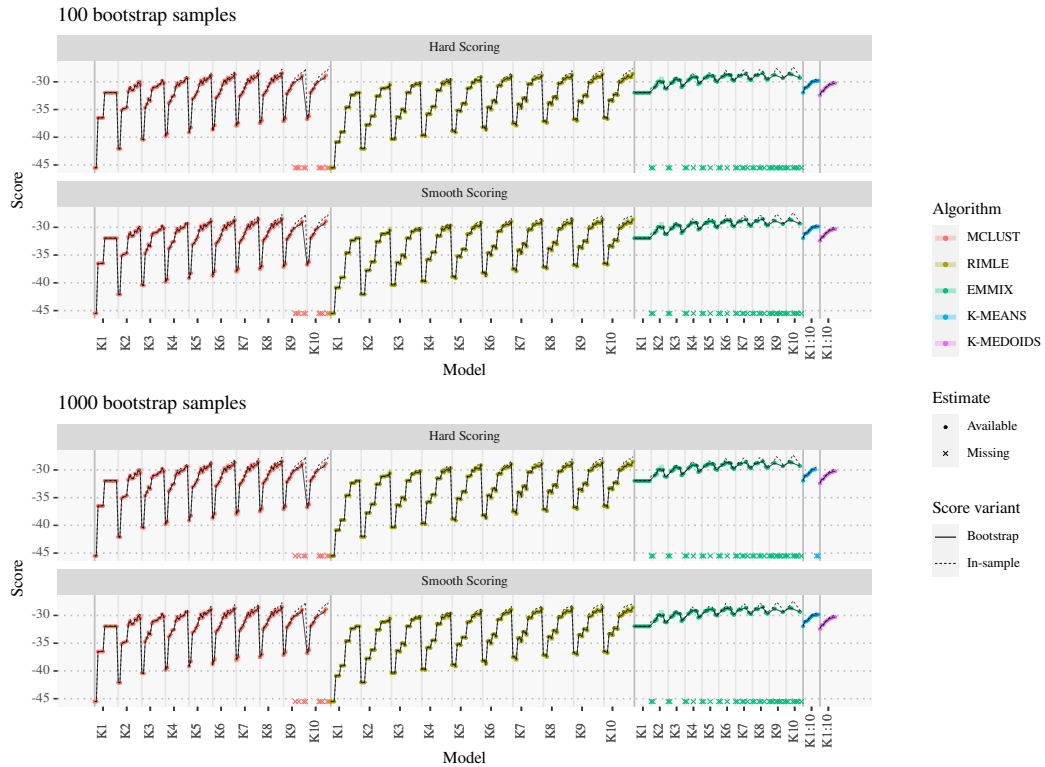


Figure S7

(b) Banknote data



(c) Olive data



S5.6 Sampling designs producing artificial data sets

Analogously to Figure 3-(PF), Figure S8 shows a sample from each of the sampling designs, adding class membership. In what follows, we explain in detail the construction of the data generating processes (DGP).

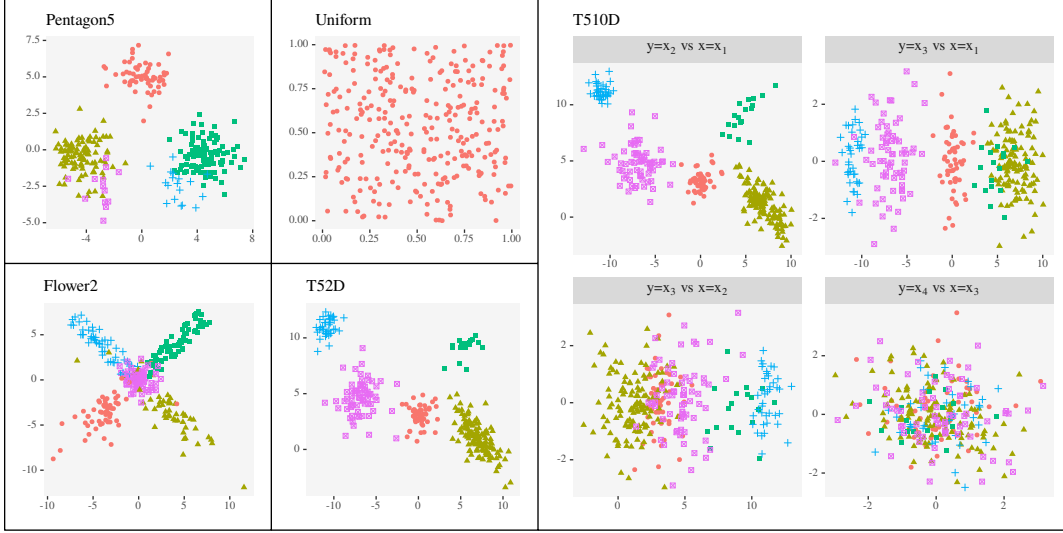


Figure S8: Scatters produced by the 5 DGPs with $n = 300$ in each case. For T510D (rightmost panel) we plot the first two marginals (x_1 and x_2), a combination of the them with an uninformative marginal (x_3) and two uninformative marginals (x_3 and x_4). Colors and points' shape represent cluster membership.

Pentagon5. The DGP is a mixture of 5 spherical Gaussian components in a two-dimensional space. The Gaussian components are centered along the sides of a pentagon centered at the origin. The underlying density function is

$$f(\mathbf{x}) = \sum_{k=1}^5 \pi_k \phi(\mathbf{x}; \boldsymbol{\mu}_k; \boldsymbol{\Sigma}_k)$$

where $\phi(\cdot; \boldsymbol{\mu}, \boldsymbol{\Sigma})$ is the Gaussian density with parameters $\boldsymbol{\mu}$ and $\boldsymbol{\Sigma}$. Components parameters are set at the following values:

- $\pi_1 = 0.2; \pi_2 = 0.35; \pi_3 = 0.35; \pi_4 = 0.05; \pi_5 = 0.05;$
- $\mu_1 = [0, 5]; \mu_2 = [-4.5, -0.5]; \mu_3 = [4.5, -0.5]; \mu_4 = [3, -2.5]; \mu_5 = [-3, -2.5];$
- $\Sigma_k = \begin{bmatrix} 1 & 0 \\ 0 & 1 \end{bmatrix}, \quad k = 1 \dots 5.$

Assuming the definition of ground truth that each mixture component generates a cluster, here we have $K = 5$. However, due to the highly unbalanced components' proportions, a 3 cluster solution may also be reasonable (see Figure 3-(PF)). If within-group homogeneity

is pursued, with small sample sizes (such as the one we consider), it may be preferable to have 3 groups rather than 5.

T52D. This is a two-dimensional design, where the DGP is a mixture of Student-t distributions, with density

$$f(x) = \sum_{k=1}^5 \pi_k t(x; \nu_k, \boldsymbol{\mu}_k, \boldsymbol{\Sigma}_k);$$

$t(\cdot)$ is the multivariate Student-t density. For the k -th component, ν_k are degrees of freedom, $\boldsymbol{\mu}_k$ is the mean vector and $\boldsymbol{\Sigma}_k$ is covariance matrix. Note that for a Student-t distribution with $\nu_k > 2$, $\boldsymbol{\Sigma}_k = (\nu_k - 2)/\nu_k \mathbf{V}_k$, where \mathbf{V}_k is a positive-definite and symmetric matrix called the *scatter (or scale) matrix*. For convenience, we parameterize the Student-t distribution in terms of the covariance matrices since we always consider $\nu_k > 2$. Components' parameters are set at the following values:

- $\pi_1 = 0.15; \pi_2 = 0.4; \pi_3 = 0.05; \pi_4 = 0.15; \pi_5 = 0.25;$
- $\nu_1 = 10, \nu_2 = 12, \nu_3 = 14, \nu_4 = 16, \nu_5 = 18.$
- $\boldsymbol{\mu}_1 = (0, 3)^\top; \boldsymbol{\mu}_2 = (7, 1)^\top; \boldsymbol{\mu}_3 = (5, 9)^\top; \boldsymbol{\mu}_4 = (-11, 11)^\top; \boldsymbol{\mu}_5 = (-7, 5)^\top;$
- $\boldsymbol{\Sigma}_1 = \begin{bmatrix} 1 & 0.5 \\ 0.5 & 1 \end{bmatrix}, \boldsymbol{\Sigma}_2 = \begin{bmatrix} 2 & -1.5 \\ -1.5 & 2 \end{bmatrix}, \boldsymbol{\Sigma}_3 = \begin{bmatrix} 2 & 1.3 \\ 1.3 & 2 \end{bmatrix}, \boldsymbol{\Sigma}_4 = \begin{bmatrix} 0.5 & 0 \\ 0 & 0.5 \end{bmatrix},$
 $\boldsymbol{\Sigma}_5 = \begin{bmatrix} 2.5 & 0 \\ 0 & 2.5 \end{bmatrix}.$

Given the strong separation, it makes sense to assume that each mixture component generates a cluster. Therefore, we can certainly argue that the true $K = 5$ in this case. However, with few data, the difficulty arises because of the clusters' varying shape, which causes problems for solutions with fixed-shape clusters. Moreover, with a small $n = 300$, this data set may cause trouble to the selection methods based on resampling. Indeed, the third component generates on average 15 points and may easily disappear in bootstrap samples or cross-validation folds.

T510D. The DGP is the same as T52D, except that we add 8 uninformative spherically distributed marginals. Let $\dot{\boldsymbol{\mu}}_k$ and $\dot{\boldsymbol{\Sigma}}_k$ the mean and covariance matrix parameters for the k -th component of the T510D sample design. Define

- $\dot{\boldsymbol{\mu}}_k = (\boldsymbol{\mu}_k^\top, 0, 0, 0, 0, 0, 0, 0)^\top;$
- $\dot{\boldsymbol{\Sigma}}_k = \begin{bmatrix} \boldsymbol{\Sigma}_k & \mathbf{0} \\ \mathbf{0} & \mathbf{I}_8 \end{bmatrix};$

where $\boldsymbol{\mu}_k$ and $\boldsymbol{\Sigma}_k$ are the mean and covariance matrix parameters in the previous T52D model. The addition of the 8 uninformative features do not provide clustering information, which is only defined along the first two dimensions. This DGP adds noise to the

previous DGP because it introduces some interaction between informative marginals and uninformative ones. Along some pair-wise scatter plot (see Figure 3-(PF)), it is possible to visualize 3 or 4 clusters rather than the true defined $K = 5$. With $n = 300$, the difficulty is also due to the small ratio n_k/p , where $n_k = \pi_k n$ is the expected number of points belonging to the k -th group. For example, for the third group, we expect 15 data points into $p = 10$ dimensions, which makes particularly difficult to jointly estimate the mean and the covariance parameter.

Flower2. The DGP is a mixture of 5 components with equal proportions. The density function is

$$f(\mathbf{x}) = \sum_{i=1}^2 \pi_i u_i(\mathbf{x}) + \sum_{l=3}^4 \pi_l t_l(\mathbf{x}; \boldsymbol{\mu}_l, \boldsymbol{\Sigma}_l) + \pi_5 \phi(\mathbf{x}; \boldsymbol{\mu}_\phi, \boldsymbol{\Sigma}_\phi);$$

where $u(\cdot)$, $t(\cdot)$ and $\phi(\cdot)$ are the uniform, Gaussian and Student-t densities respectively. The distribution used are obtained as follows:

- $\pi_i = 0.2$ for $i = 1, \dots, 5$;
- u_1 is a uniform distribution on the two-dimensional rectangle with vertices in $(-1, 1)$, $(-1, 10)$, $(1, 1)$, $(1, 10)$, rotated 45 degrees clockwise;
- u_2 is defined as u_1 , except that the rotation occurs counter-clockwise;
- t_3 is a Student-t distribution with 9 degrees of freedom, centered on $\boldsymbol{\mu}_t = (0, 5)^\top$, with covariance

$$\boldsymbol{\Sigma}_t = \begin{bmatrix} 1 & 0 \\ 0 & 10 \end{bmatrix}$$

and the overall scatter is rotated 135 degrees clockwise.

- t_4 is defined as t_3 , except that the rotation occurs counter-clockwise;
- ϕ_5 is a standard Gaussian distribution in dimension 2, that is $\boldsymbol{\mu}_\phi = (0, 0)^\top$ with covariance matrix $\boldsymbol{\Sigma}_\phi = \mathbf{I}_2$.

It may be challenging to identify 5 groups here because the DGP mixes elliptical shapes (Gaussian and Student-t) with non-elliptical ones (uniform distributions), and features strong overlap between the components.

Uniform. Provides a case of unclustered data in two dimensions. Points are sampled from a uniform distribution over the unit square with vertices on $(0, 0)$, $(0, 1)$, $(1, 0)$ and $(1, 1)$.

S5.7 Monte Carlo experiments

Figure S9 summarizes results of the Monte Carlo replicates for each of the five DGPs. Boxplots are already discussed in the PF. Here we add the frequencies plots for the selected number of clusters $K = 1, 2, \dots, 10$. In each replicate, each criterion selects the optimal clustering solution, of which we track the number of clusters.

Table S8: Summary results for the Monte Carlo experiments. Mean and median ARI and VIC are reported (standard errors in parentheses). Last two columns indicate the most and second most frequent selected number of clusters (frequency in parentheses). First two rows show the best feasible solutions with respect to the ARI and the VIC criteria (BEST ARI and BEST VIC).

(a) Pentagon5						
Criterion	Mean ARI	Mean VIC	Med. ARI	Med. VIC	1st K	2nd K
BEST ARI	$0.92 \pm (0.02)$		0.92		5 (0.83)	4 (0.1)
BEST VIC		$-0.36 \pm (0.07)$		-0.36	4 (0.52)	5 (0.34)
AIC	$0.82 \pm (0.11)$	$-0.66 \pm (0.31)$	0.87	-0.57	5 (0.59)	6 (0.11)
BIC	$0.88 \pm (0.04)$	$-0.43 \pm (0.09)$	0.89	-0.43	5 (0.45)	4 (0.3)
ICL	$0.85 \pm (0.03)$	$-0.42 \pm (0.06)$	0.84	-0.43	3 (0.88)	4 (0.08)
QH	$0.76 \pm (0.12)$	$-0.89 \pm (0.36)$	0.80	-0.83	10 (0.31)	7 (0.16)
QS	$0.84 \pm (0.07)$	$-0.57 \pm (0.25)$	0.86	-0.48	4 (0.39)	3 (0.16)
CH	$0.84 \pm (0.02)$	$-0.43 \pm (0.05)$	0.84	-0.44	3 (1)	
ASW	$0.84 \pm (0.03)$	$-0.43 \pm (0.06)$	0.84	-0.43	3 (1)	4 (0)
FW	$0.84 \pm (0.06)$	$-0.43 \pm (0.1)$	0.84	-0.43	3 (0.99)	2 (0.01)
CVLK	$0.73 \pm (0.13)$	$-0.85 \pm (0.33)$	0.75	-0.82	6 (0.32)	5 (0.23)
CVQH	$0.82 \pm (0.09)$	$-0.58 \pm (0.25)$	0.85	-0.50	4 (0.42)	3 (0.32)
CVQS	$0.84 \pm (0.05)$	$-0.48 \pm (0.13)$	0.85	-0.45	3 (0.61)	4 (0.31)
BQH	$0.85 \pm (0.03)$	$-0.43 \pm (0.06)$	0.84	-0.44	3 (0.9)	4 (0.08)
BQS	$0.84 \pm (0.03)$	$-0.43 \pm (0.06)$	0.84	-0.44	3 (0.98)	4 (0.02)

(b) T52D						
Criterion	Mean ARI	Mean VIC	Med. ARI	Med. VIC	1st K	2nd K
BEST ARI	$0.99 \pm (0.01)$		0.99		5 (0.99)	4 (0.01)
BEST VIC		$-0.06 \pm (0.05)$		-0.05	5 (0.97)	4 (0.01)
AIC	$0.84 \pm (0.13)$	$-0.5 \pm (0.32)$	0.86	-0.48	6 (0.21)	9 (0.2)
BIC	$0.97 \pm (0.04)$	$-0.12 \pm (0.1)$	0.98	-0.10	5 (0.9)	6 (0.09)
ICL	$0.98 \pm (0.01)$	$-0.11 \pm (0.08)$	0.99	-0.09	5 (0.95)	4 (0.04)
QH	$0.85 \pm (0.1)$	$-0.55 \pm (0.26)$	0.86	-0.58	10 (0.41)	9 (0.19)
QS	$0.91 \pm (0.08)$	$-0.35 \pm (0.25)$	0.93	-0.29	10 (0.21)	5 (0.2)
CH	$0.7 \pm (0.1)$	$-0.7 \pm (0.26)$	0.68	-0.71	7 (0.4)	6 (0.31)
ASW	$0.92 \pm (0.15)$	$-0.26 \pm (0.32)$	0.97	-0.16	5 (0.86)	2 (0.13)
FW	$0.59 \pm (0.18)$	$-0.93 \pm (0.36)$	0.51	-1.08	2 (0.81)	4 (0.13)
CVLK	$0.84 \pm (0.13)$	$-0.44 \pm (0.27)$	0.89	-0.34	6 (0.41)	7 (0.24)
CVQH	$0.9 \pm (0.11)$	$-0.32 \pm (0.23)$	0.95	-0.26	4 (0.43)	5 (0.31)
CVQS	$0.93 \pm (0.08)$	$-0.27 \pm (0.19)$	0.95	-0.24	4 (0.54)	5 (0.31)
BQH	$0.99 \pm (0.01)$	$-0.08 \pm (0.06)$	0.99	-0.07	5 (0.98)	4 (0.01)
BQS	$0.99 \pm (0.01)$	$-0.08 \pm (0.06)$	0.99	-0.07	5 (0.98)	4 (0.01)

Table S8 reports the average ARI and VIC \pm one Monte Carlo standard error in parentheses. We also report median values and the most and second most frequent selected number of clusters with their frequencies in parentheses. Note that we report the negative of VIC so that higher values correspond to better clusterings. The first two rows show the same results for the BEST ARI and BEST VIC selected solutions. The best performances, excluding that of BEST ARI and BEST VIC, are highlighted in bold.

Table S8

(c) T510D

Criterion	Mean ARI	Mean VIC	Med. ARI	Med. VIC	1st K	2nd K
BEST ARI	0.99 \pm (0.01)		0.99		5 (0.99)	4 (0.01)
BEST VIC		-0.09 \pm (0.06)		-0.09	5 (0.99)	4 (0.01)
AIC	0.7 \pm (0.13)	-1.06 \pm (0.43)	0.68	-1.03	9 (0.24)	10 (0.24)
BIC	0.86 \pm (0.1)	-0.35 \pm (0.18)	0.82	-0.41	6 (0.5)	5 (0.49)
ICL	0.94 \pm (0.08)	-0.23 \pm (0.15)	0.97	-0.19	5 (0.83)	6 (0.16)
QH	0.55 \pm (0.08)	-1.23 \pm (0.32)	0.53	-1.20	10 (0.98)	9 (0.02)
QS	0.55 \pm (0.07)	-1.2 \pm (0.23)	0.53	-1.19	10 (0.98)	9 (0.02)
CH	0.51 \pm (0.03)	-1.1 \pm (0.05)	0.50	-1.11	2 (1)	
ASW	0.51 \pm (0.03)	-1.1 \pm (0.05)	0.51	-1.11	2 (1)	
FW	0.53 \pm (0.11)	-1.05 \pm (0.21)	0.50	-1.10	2 (0.94)	5 (0.04)
CVLK	0.74 \pm (0.13)	-0.75 \pm (0.43)	0.74	-0.67	6 (0.45)	7 (0.38)
CVQH	0.79 \pm (0.13)	-0.62 \pm (0.33)	0.79	-0.58	5 (0.36)	6 (0.35)
CVQS	0.8 \pm (0.13)	-0.61 \pm (0.34)	0.79	-0.58	5 (0.38)	6 (0.29)
BQH	0.91 \pm (0.12)	-0.28 \pm (0.26)	0.97	-0.19	5 (0.69)	6 (0.19)
BQS	0.94 \pm (0.09)	-0.2 \pm (0.18)	0.98	-0.15	5 (0.85)	6 (0.1)

(d) Flower2

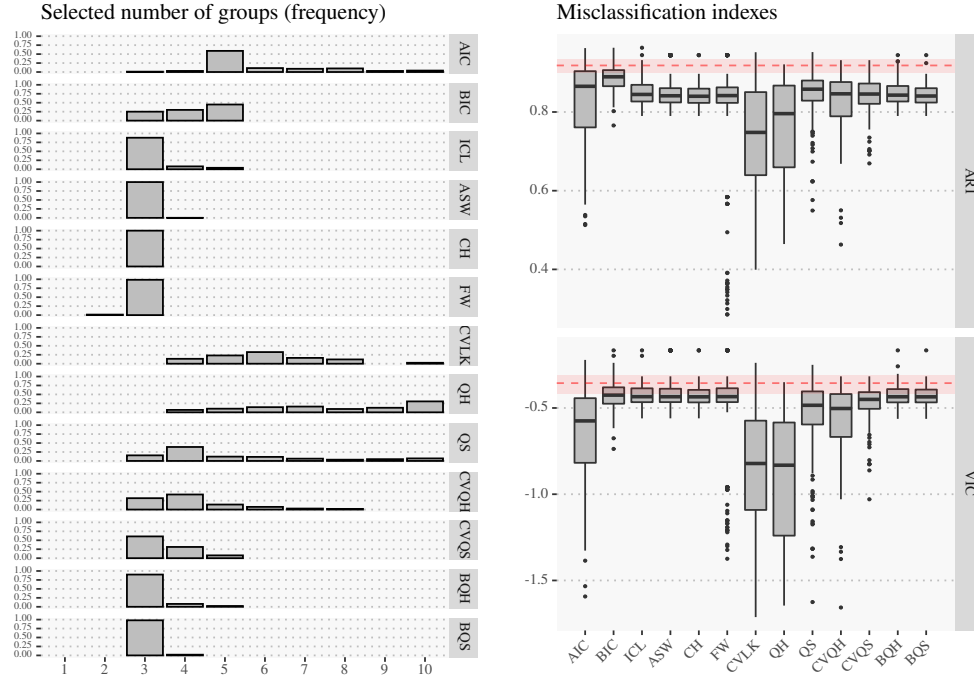
Criterion	Mean ARI	Mean VIC	Med. ARI	Med. VIC	1st K	2nd K
BEST ARI	0.68 \pm (0.06)		0.69		5 (0.73)	6 (0.11)
BEST VIC		-1.21 \pm (0.17)		-1.21	5 (0.77)	4 (0.18)
AIC	0.48 \pm (0.1)	-1.91 \pm (0.34)	0.48	-1.89	8 (0.24)	9 (0.22)
BIC	0.32 \pm (0.1)	-1.88 \pm (0.22)	0.29	-1.92	2 (0.58)	3 (0.33)
ICL	0.35 \pm (0.12)	-1.8 \pm (0.26)	0.30	-1.90	2 (0.65)	3 (0.2)
QH	0.47 \pm (0.07)	-1.96 \pm (0.21)	0.47	-1.97	10 (0.85)	9 (0.13)
QS	0.46 \pm (0.08)	-1.88 \pm (0.22)	0.46	-1.89	10 (0.59)	9 (0.21)
CH	0.44 \pm (0.04)	-1.98 \pm (0.17)	0.44	-1.98	10 (0.87)	9 (0.08)
ASW	0.45 \pm (0.17)	-1.58 \pm (0.29)	0.50	-1.50	5 (0.85)	2 (0.1)
FW	0.45 \pm (0.1)	-1.6 \pm (0.21)	0.46	-1.60	5 (0.86)	2 (0.09)
CVLK	0.49 \pm (0.11)	-1.8 \pm (0.27)	0.51	-1.79	7 (0.43)	8 (0.23)
CVQH	0.47 \pm (0.13)	-1.73 \pm (0.27)	0.48	-1.73	6 (0.27)	7 (0.27)
CVQS	0.43 \pm (0.14)	-1.74 \pm (0.27)	0.46	-1.80	5 (0.23)	6 (0.22)
BQH	0.53 \pm (0.09)	-1.51 \pm (0.25)	0.52	-1.49	5 (0.74)	9 (0.08)
BQS	0.46 \pm (0.11)	-1.58 \pm (0.24)	0.49	-1.52	5 (0.72)	2 (0.23)

(e) Uniform

Criterion	Mean ARI	Mean VIC	Med. ARI	Med. VIC	1st K	2nd K
BEST ARI	1 \pm (0)		1		1 (1)	
BEST VIC		0 \pm (0)		0	1 (1)	
AIC	0 \pm (0)	-3.01 \pm (0.22)	0	-3.03	10 (0.51)	9 (0.27)
BIC	0 \pm (0)	-1.94 \pm (0.4)	0	-1.98	4 (0.65)	5 (0.13)
ICL	0.77 \pm (0.42)	-0.22 \pm (0.45)	1	0.00	1 (0.77)	2 (0.18)
QH	0 \pm (0)	-3.1 \pm (0.11)	0	-3.12	10 (0.9)	9 (0.08)
QS	0.16 \pm (0.37)	-2.61 \pm (1.14)	0	-3.10	10 (0.71)	1 (0.16)
CH	0 \pm (0)	-3.06 \pm (0.41)	0	-3.16	10 (0.46)	9 (0.38)
ASW	0 \pm (0)	-2.1 \pm (0.37)	0	-1.99	4 (0.74)	3 (0.07)
FW	0 \pm (0)	-2.38 \pm (0.59)	0	-1.99	4 (0.64)	10 (0.18)
CVLK	0 \pm (0)	-2.84 \pm (0.28)	0	-2.84	8 (0.3)	9 (0.24)
CVQH	0.06 \pm (0.24)	-2.3 \pm (0.81)	0	-2.55	7 (0.22)	6 (0.19)
CVQS	0.85 \pm (0.35)	-0.25 \pm (0.73)	1	0.00	1 (0.85)	2 (0.07)
BQH	0 \pm (0)	-3.14 \pm (0.31)	0	-3.21	10 (0.82)	9 (0.1)
BQS	0.96 \pm (0.19)	-0.1 \pm (0.54)	1	0.00	1 (0.96)	10 (0.03)

Figure S9: Results on artificial data sets. In each panel: (left) frequencies for the selected number of clusters for $K = 1, 2, \dots, 10$; (right) boxplots of the Monte Carlo distribution of ARI and BIC.

(a) Pentagon5



(b) T52D

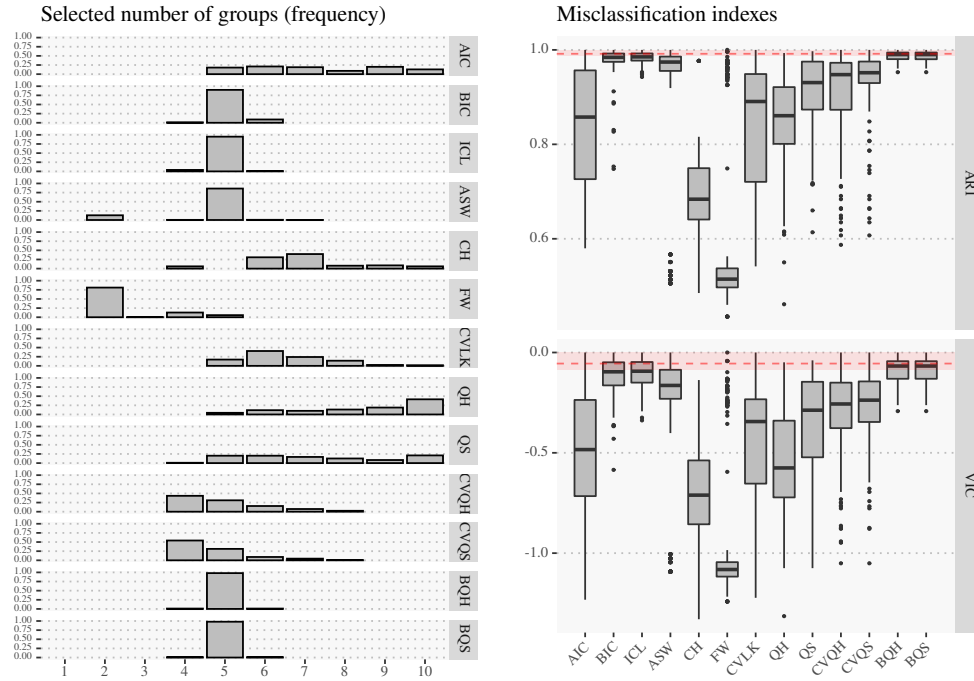
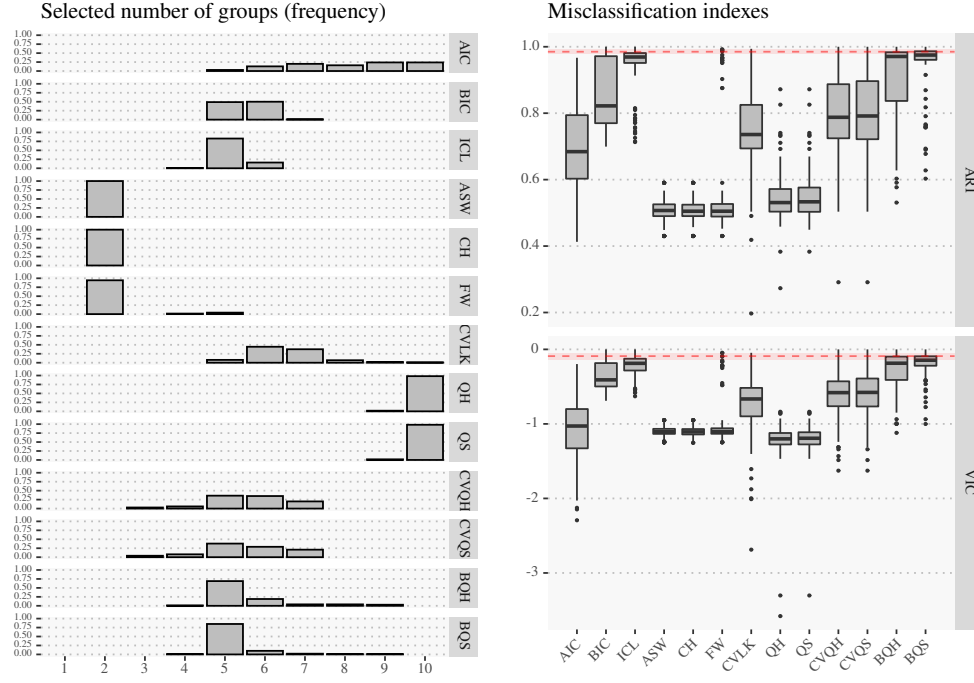


Figure S9

(c) T510D



(d) Flower2

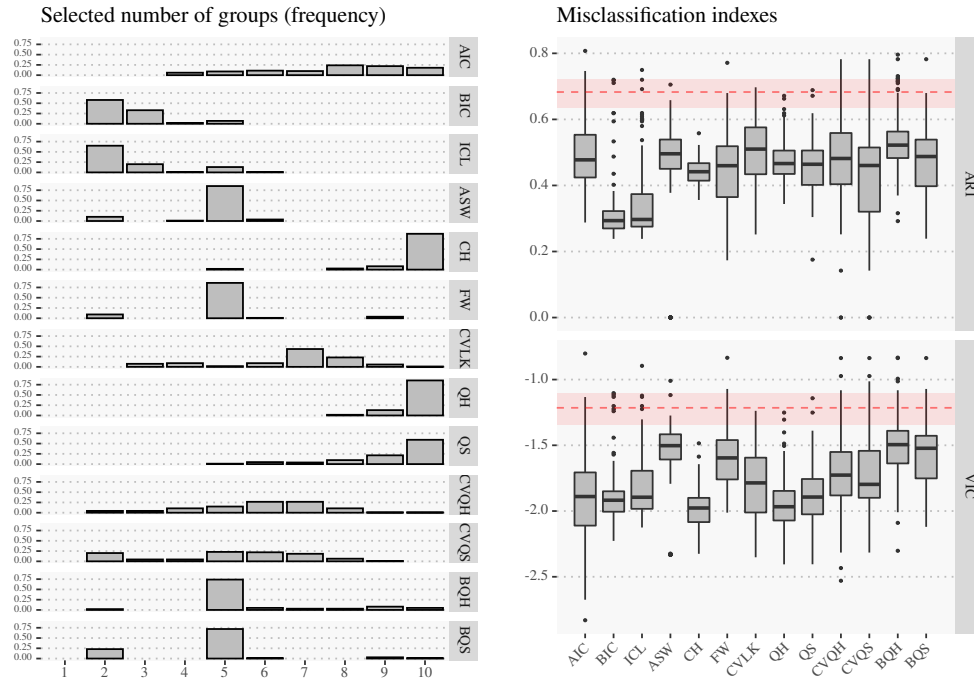
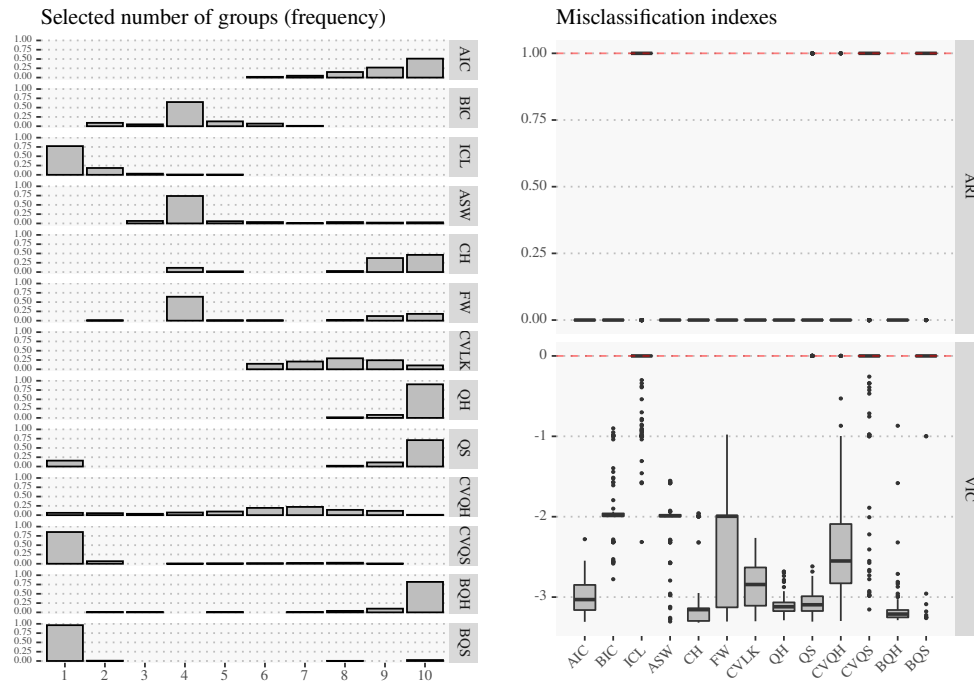


Figure S9

(e) Uniform



References

- Akaike, H. (1973). Information theory and an extension of the maximum likelihood principle. In *Second International Symposium on Information Theory (Tsahkadsor, 1971)*, pp. 267–281.
- Anderson, E. (1936). The Species Problem in Iris. *Annals of the Missouri Botanical Garden Vol. 23*(No. 3), 471–483.
- Baudry, J.-P. (2015). Estimation and model selection for model-based clustering with the conditional classification likelihood. *Electronic Journal of Statistics* 9(1), 1041–1077.
- Biernacki, C., G. Celeux, and G. Govaert (2000). Assessing a mixture model for clustering with the integrated completed likelihood. *IEEE transactions on pattern analysis and machine intelligence* 22(7), 719–725.
- Caliński, T. and J. Harabasz (1974). A dendrite method for cluster analysis. *Communications in Statistics-theory and Methods* 3(1), 1–27.
- Celeux, G. and G. Govaert (1995). Gaussian parsimonious clustering models. *Pattern recognition* 28(5), 781–793.
- Coretto, P. and C. Hennig (2016). Robust improper maximum likelihood: tuning, computation, and a comparison with other methods for robust gaussian clustering. *Journal of the American Statistical Association* 111(516), 1648–1659.
- Coretto, P. and C. Hennig (2017). Consistency, breakdown robustness, and algorithms for robust improper maximum likelihood clustering. *Journal of Machine Learning Research* 18(142), 1–39.
- Coretto, P. and C. Hennig (2021). *otrimle: Robust Model-Based Clustering*. R package version 2.0.
- Dempster, A. P., N. M. Laird, and D. B. Rubin (1977). Maximum likelihood from incomplete data via the em algorithm. *Journal of the Royal Statistical Society: Series B (Methodological)* 39(1), 1–22.
- Ester, M., H.-P. Kriegel, J. Sander, and X. Xu (1996). A density-based algorithm for discovering clusters in large spatial databases with noise. In *Proceedings of the 2nd International Conference on Knowledge Discovery and Data Mining (KDD-96)*, pp. 226–231. Institute for Computer Science, University of Munich.
- Fang, Y. and J. Wang (2012). Selection of the number of clusters via the bootstrap method. *Computational Statistics & Data Analysis* 56(3), 468–477.
- Fisher, R. A. (1936). The use of Multiple Measurements in Taxonomic Problems. *Annals of Eugenics*.
- Flury, B. and H. Riedwyl (1988). *Multivariate Statistics. A practical approach*. Chapman and Hall.
- Forina, M., C. Armanino, S. Lanteri, and E. Tiscornia (1983). Classification of olive oils from their fatty acid composition. *Food Research and Data Analysis* (January 1983), 189–214.

- Forina, M. and E. Tiscornia (1982). Pattern recognition methods in the prediction of {I}talian olive oil origin by their fatty acid content. *Annali di Chimica* 72(January 1982), 143–155.
- Fraley, C. (1998). Algorithms for model-based gaussian hierarchical clustering. *SIAM Journal on Scientific Computing* 20(1), 270–281.
- Fraley, C. and A. E. Raftery (2007). Bayesian regularization for normal mixture estimation and model-based clustering. *Journal of Classification* 24(2), 155–181.
- Frühwirth-Schnatter, S., G. Celeux, and C. P. Robert (Eds.) (2019). *Handbook of mixture analysis*. Chapman & Hall/CRC Handbooks of Modern Statistical Methods. CRC Press, Boca Raton, FL.
- García-Escudero, L. A., A. Gordaliza, F. Greselin, S. Ingrassia, and A. Mayo-Isar (2017). Eigenvalues and constraints in mixture modeling: geometric and computational issues. *Advances in Data Analysis and Classification* 12(2), 203–233.
- Hahsler, M., M. Piekenbrock, and D. Doran (2019). dbscan: Fast density-based clustering with R. *Journal of Statistical Software* 91(1), 1–30.
- Hartigan, J. A. and M. A. Wong (1979). Algorithm AS 136: A k-means clustering algorithm. *Applied Statistics* 28(1), 100.
- Hathaway, R. J. (1985). A constrained formulation of maximum-likelihood estimation for normal mixture distributions. *The Annals of Statistics* 13(2), 795–800.
- Kaufman, L. and P. J. Rousseeuw (1987). Clustering by means of medoids. In *Proceedings of the Statistical Data Analysis Based on the L1 Norm Conference, Neuchatel, Switzerland*, pp. 405–416.
- Kiefer, J. and J. Wolfowitz (1956). Consistency of the maximum likelihood estimator in the presence of infinitely many incidental parameters. *The Annals of Mathematical Statistics* 27(4), 887–906.
- Maechler, M., P. Rousseeuw, A. Struyf, M. Hubert, and K. Hornik (2019). *cluster: Cluster Analysis Basics and Extensions*. R package version 2.1.0 — For new features, see the ‘Changelog’ file (in the package source).
- McLachlan, G. J. and T. Krishnan (2007). *The EM algorithm and extensions*, Volume 382. John Wiley & Sons.
- Milligan, G. W. and M. C. Cooper (1985). An examination of procedures for determining the number of clusters in a data set. *Psychometrika* 50(2), 159–179.
- Pedersen, T. L., S. Hughes, and X. Qiu (2017). *densityClust: Clustering by Fast Search and Find of Density Peaks*. R package version 0.3.
- Peel, D. and G. J. McLachlan (2000). Robust mixture modelling using the t distribution. *Statistics and computing* 10(4), 339–348.
- Pollard, D. (1981). Strong consistency of \$ k \$-means clustering. *The Annals of Statistics* 9(1), 135–140.
- R Core Team (2021). *R: A Language and Environment for Statistical Computing*. Vienna, Austria: R Foundation for Statistical Computing.

- Rodriguez, A. and A. Laio (2014). Clustering by fast search and find of density peaks. *Science* 344(6191), 1492–1496.
- Rousseeuw, P. J. and L. Kaufman (1990). Finding groups in data. *Hoboken: Wiley Online Library*.
- Schwarz, G. (1978). Estimating the dimension of a model. *The Annals of Statistics* 6(2), 461–464.
- Scrucca, L., M. Fop, T. B. Murphy, and A. E. Raftery (2016). mclust 5: clustering, classification and density estimation using Gaussian finite mixture models. *The R Journal* 8(1), 205–233.
- Smyth, P. (2000). Model selection for probabilistic clustering using cross-validated likelihood. *Statistics and computing* 10(1), 63–72.
- Wang, K., A. Ng, and G. J. McLachlan (2018). *EMMIXskew: The EM Algorithm and Skew Mixture Distribution*. R package version 1.0.3.
- Wang, K., S.-K. Ng, and G. J. McLachlan (2009). Multivariate skew t mixture models: Applications to fluorescence-activated cell sorting data. In *2009 Digital Image Computing: Techniques and Applications*, pp. 526–531.